NACA RM L56J19

NACA

RESEARCH MEMORANDUM

EXPERIMENTAL INVESTIGATION OF FLOW FIELDS AT ZERO SIDESLIP NEAR SWEPT- AND UNSWEPT-WING—FUSELAGE COMBINATIONS AT LOW SPEED

By William J. Alford, Jr., and Thomas J. King, Jr.

Langley Aeronautical Laboratory
Langley Field, Va.

NATIONAL ADVISORY COMMITTEE
FOR AERONAUTICS

WASHINGTON
January 18, 1957
Declassified January 7, 1959

NATIONAL ADVISORY COMMITTEE FOR AERONAUTICS

RESEARCH MEMORANDUM

EXPERIMENTAL INVESTIGATION OF FLOW FIELDS AT ZERO SIDESLIP NEAR SWEPT- AND UNSWEPT-WING—FUSELAGE COMBINATIONS AT LOW SPEED

By William J. Alford, Jr., and Thomas J. King, Jr.

SUMMARY

The flow fields near swept- and unswept-wing—fuselage combinations at zero sideslip, as determined experimentally at low speed, are presented for various spanwise and vertical locations and angles of attack as variations with chordwise distance.

The results indicate that significant gradients in the flow parameters with chordwise and vertical distances are incurred by the finite thickness of the wings at zero angle of attack and that, when the angle of attack is increased, pronounced changes in the gradients occur. The effect of wing sweep (near zero angle of attack) is to increase the lateral flow angles. The results also indicate that the wing is the predominant factor in disturbing the field of flow for the conditions investigated.

INTRODUCTION

In order to estimate the aerodynamic loadings on objects such as tanks, bombs, or missiles and their pylons, which of practical necessity are located in close proximity to the airplane wing or fuselage, it is necessary to consider in detail the flow fields in which these objects are immersed.

An experimental investigation has therefore been made at low speed to determine in detail the flow-field characteristics near a model consisting of a fuselage and either a sweptback or an unswept wing. Part of the results obtained in this investigation have previously been presented in reference 1 where they were used in connection with first-order estimations of the forces and moments existing on a typical missile model located at various positions within the flow field. Additional parts of

these data have been presented in reference 2, where they were compared with theoretical calculations.

The purpose of the present paper is to present the complete experimental flow-field measurements for the condition of zero sideslip of the models. Only a brief analysis is included.

SYMBOLS

The directions of positive distances and angles for the body-axis system employed are presented in figure 1.

A	aspect ratio
b	wing span, ft
c	local wing chord, ft
$\bar{c}$	mean aerodynamic chord, ft
C_L	lift coefficient, $\frac{\text{Lift}}{q_o S}$
C_D	drag coefficient, $\frac{\text{Drag}}{q_o S}$
C_m	pitching-moment coefficient referred to $0.25\bar{c}$, $\frac{\text{Pitching moment}}{q_o S \bar{c}}$
V_o	free-stream velocity, ft/sec
V_l	local velocity, ft/sec
q_o	free-stream dynamic pressure, lb/sq ft
q_l	local dynamic pressure, lb/sq ft
S	wing area, sq ft
l	fuselage length, 7.61 ft
d_{max}	maximum fuselage diameter, 0.70 ft
λ	taper ratio

Λ sweep angle, deg

α angle of attack, deg

α_l resultant flow angularity induced by wing-fuselage combination, measured in XZ-plane, between local flow direction and airplane axis of symmetry, $\alpha - \epsilon$, deg (fig. 1)

β_l resultant flow angularity induced by wing-fuselage combination, measured in XY-plane, between local flow direction and airplane axis of symmetry (fig. 1)

ϵ downwash angle induced by wing-fuselage combination, measured in XZ-plane between free-stream flow direction and local flow direction, positive when local flow is inclined downward relative to free stream, deg

X,Y,Z right-hand Cartesian coordinate system (fig. 1)

x distance in direction of X-axis with origin at the leading edge of the local wing chord, positive rearward, ft

y distance in direction of Y-axis with origin at plane of symmetry of airplane model, positive to right when viewed from rear, ft

z distance in direction of Z-axis with origin at wing chord plane, positive up, ft

MODEL AND APPARATUS

The models about which the flow surveys were made consisted of a single fuselage equipped with either a sweptback wing or an unswept wing. Drawings of the wing-fuselage combinations are presented in figure 2. The sweptback wing had 45° sweep of the quarter-chord line, an aspect ratio of 4.0, a taper ratio of 0.30, and NACA 65A006 airfoil sections parallel to the plane of symmetry. The unswept wing had 0° sweep of the half-chord line, an aspect ratio of 3.0, a taper ratio of 0.50, and NACA 65A004 airfoil sections parallel to the plane of symmetry. The fuselage had an ogival nose section, a cylindrical center section, and a truncated tail cone. The fuselage ordinates are presented in table I.

The flow-field characteristics were measured by use of a rake of hemispherically headed probes which had both angle-of-attack and angle-of-sideslip orifices and pitot-static orifices to measure dynamic pressure in conjunction with a multitube manometer board. A drawing of the flow-survey rake and a photograph showing the rake installed on the swept-wing—fuselage combination are presented in figure 3. The locations at which the surveys were made are shown in figure 4.

TESTS, CORRECTIONS, AND ACCURACY

The tests were made in the Langley 300 MPH 7- by 10-foot tunnel at a velocity of 100 mph. Included in the tests were surveys of the flow angularity, in both the longitudinal and the lateral planes, and dynamic pressures at numerous chordwise and six vertical locations for the following lateral locations of the swept-wing—fuselage combination: $y/\frac{b}{2}$ = 0, -0.098, -0.25, -0.50, -0.75, and -1.01. For the model with the unswept wing, surveys were made only at $y/\frac{b}{2}$ = -0.50. Flow surveys were also made at $y/\frac{b}{2}$ = -0.25, -0.50, and -0.75 for the fuselage alone. The angle-of-attack range generally extended from -8° to 24° for the swept-wing configuration and from -8° to 16° for the unswept-wing and fuselage-alone configurations. The surveys were made under the model center line and under the left wing.

Jet-boundary corrections were calculated by the method of reference 3. Blockage corrections calculated by the method of reference 4 have been applied to the free-stream dynamic pressure.

The small variations in jet-boundary and blockage corrections throughout the flow fields have been neglected since they were well within the estimated accuracy limits of the experimental data.

In order to expedite the data reduction, some relaxation of rigorous calibration procedures was found necessary. Accordingly, the calibrations of the survey rake were linearized, and the local dynamic pressures were considered to be the difference between free-stream total pressure and local static pressure; therefore the effects of local losses in total pressure were not included. Inasmuch as the majority of the survey locations were outside of the wing wake and boundary layer, to which the local losses in total pressure were confined, the error introduced because of neglecting the local total pressure was found to be negligible.

Additional possible sources of error were incurred by the local misalinement angles existing in the clear wind tunnel and by the adjustment accuracy in the model and rake supports. Consideration of all known sources of error indicated that the local angles of attack were accurate to ±1.0° below 16° local angle (in either plane) and could possibly be in error by as much as ±2.0° in regions where the local angle is 24° or greater. The local angles of sideslip are believed to be accurate to within ±1.5° below 16° local angle (in either plane) and could possibly be in error ±2.5° at 24° local angle. The local-dynamic-pressure ratios are believed accurate to within ±0.025 below 16° local angle (in either plane) and could possibly be in error by ±0.04 at 24° local angle.

RESULTS AND DISCUSSION

Presentation of Results

In analyzing the flow-field characteristics it is often desirable to have as a reference the force and moment characteristics of the models. These data for the models used in the present investigation are presented in figure 5.

The flow angularities are presented in terms of the local conditions α_l and β_l. For the sign convention adopted (fig. 1), positions where the local angle of attack α_l is more positive than the geometric angle of attack α are regions of upflow, and positions where α_l is less positive than α are regions of downflow. Since for the present investigation the geometric angle of sideslip β was zero and since the surveys were made under the left wing, positive values of the local angle of sideslip β_l indicate a flow inclination towards the left wing tip when viewed from the rear. Values of the local dynamic pressure ratio q_l/q_o greater than unity indicate regions of supervelocity relative to free-stream conditions.

The results are, in general, presented for constant angles of attack and for six vertical locations as variations of the local flow parameters α_l, β_l, and q_l/q_o with nondimensional chordwise distance x/c. The origin of measurements of x/c is the leading edge of the local wing chord with positive values in the downstream direction.

The flow-field characteristics of the swept-wing—fuselage combination are presented for lateral locations in which $y/\frac{b}{2} = 0$, -0.098, -0.25, -0.50, -0.75, and -1.01 in figures 6, 7, 8, 9, 10, and 11, respectively. The flow-field characteristics existing at the one-half semispan location of the unswept configuration are presented in figure 12. A comparison of the flow fields of the fuselage alone and the swept-wing—fuselage combination as a function of angle of attack for three spanwise locations and two chordwise locations are presented in figure 13.

Swept-Wing—Fuselage Flow Fields

The local angles of attack existing below the model in the plane of symmetry (fig. 6) have the greatest chordwise gradient at the negative angles of attack. As the angle of attack is increased positively these chordwise gradients are considerably diminished. The largest deflection of the airstream, that is, the smallest values of α_l, occur for the

vertical locations closest to the fuselage surface, and the flow angles are seen to approach the free-stream angle as the vertical distance from the fuselage is increased. The local angles of sideslip are essentially zero, in the plane of symmetry, and are unaffected by either chordwise position, vertical location, or angle of attack, except at the highest angle of attack where some small variations are in evidence. The dynamic pressures are slightly increased for negative angles of attack and correspondingly decreased for positive angles of attack.

The local angles of attack existing slightly outboard of the plane of symmetry $\left(y/\frac{b}{2} = -0.098, \text{ fig. } 7\right)$ have slightly more severe chordwise gradients than at the plane of symmetry, although the magnitudes of the airstream deflections appear less for the small vertical heights than was indicated at the center-line location. The effect of the small change in spanwise location is to cause an increase in the local angles of sideslip. The effect of increasing the model angle of attack is to cause increases in both the downflow and sideflow. The variations in the local-dynamic-pressure ratios with chordwise position and angle of attack is essentially the same as for the center-line location.

For more outboard spanwise locations, that is, $y/\frac{b}{2} = -0.25$, -0.50, and -0.75 (figs. 8, 9, and 10), the effects of the swept-wing—fuselage combination are to cause severe gradients in all the flow parameters with changes in both chordwise and vertical distances. The most severe gradients below the wing are, of course, for the negative angles of attack of the model inasmuch as the flow conditions are those for the suction side of the wing. For the closest vertical positions, the chordwise gradients in the flow parameters due to finite-wing thickness (parts (c) of figs. 8, 9, and 10) are seen to be significant. The effects of increasing the model angle of attack are to increase the variation of the local flow angles and dynamic pressures with chordwise location. In general, the variations of the flow parameters appear qualitatively similar for the one-quarter, one-half, and three-quarter semispan locations, although the conditions at the more inboard location $\left(y/\frac{b}{2} = -0.25, \text{ fig. } 8\right)$ and outboard location $\left(y/\frac{b}{2} = -0.75, \text{ fig. } 10\right)$ are somewhat more severe than for the one-half semispan location (fig. 9). This is presumed to be due to the additional effects of the fuselage for the inboard location and to the proximity of the wing-tip vortex for the outboard location.

The flow conditions existing slightly outboard of the wing tip $\left(y/\frac{b}{2} = -1.01, \text{ fig. } 11\right)$ are seen to be critically dependent on vertical position. The largest variations in the flow parameters with chordwise

distance and angle of attack occur for the closest vertical distance. The direction of the local angle of sideslip is seen to change sign abruptly above the wing-chord plane with the lateral flow, in general, being in an outboard direction below the wing-chord plane and in an inboard direction above the wing-chord plane for positive angles of attack. It should be noted that free-stream conditions are approached more rapidly as the vertical distance from the wing-chord plane is increased at the tip location than for the more inboard locations. The chordwise gradients in the flow parameters at the tip location (fig. 11) appear, in general, to be less severe than for the inboard locations. As is shown in references 5, 6, and 7, however, an object situated at the wing-tip in the wing-chord plane would be subject to a large rolling couple due to the abrupt change in the lateral flow angles incurred by the wing-tip vortex.

Unswept-Wing—Fuselage Flow Fields

The flow-field characteristics beneath the midsemispan location of the unswept-wing—fuselage combination (fig. 12) are, in general, subject to the same remarks as for the swept-wing—fuselage combination at the comparable lateral location (fig. 9), in that there are severe gradients in all the flow parameters with chordwise and vertical distances and with increases in model angle of attack causing significantly large changes in the flow parameters.

A direct comparison of the effects of wing sweep is not permissible since the wings of the present investigation had different plan-form characteristics other than the sweep angle. Some insight as to the effect of sweep is possible, however, at the lowest angle of attack (parts (c) of figs. 9 and 12). The chordwise variation in the local angles of sideslip is seen to be considerably larger for the swept wing than for the unswept wing for the nearest vertical locations. This characteristic would be expected from consideration of simple sweep theory (ref. 2).

Comparison of Wing-Fuselage and Fuselage-Alone Flow Fields

A comparison of the effects of the fuselage alone with the effects of the swept-wing—fuselage combination on the flow-field characteristics is presented in figure 13. An examination of these data indicates for both chordwise locations that for the fuselage alone only slight changes in the local angles of attack are induced at the most inboard location $\left(y/\frac{b}{2} = -0.25\right)$ with these effects diminishing rapidly as the lateral distance from the plane of symmetry is increased. The same is true in the case of the local angles of sideslip and the local dynamic pressures

appear to be unaffected for any of the lateral locations. Comparison of the fuselage-alone data with the wing-fuselage characteristics readily indicates that the effects of wing and wing-fuselage interference produce the predominant changes in the flow fields with changes in angle of attack and chordwise position.

CONCLUDING REMARKS

An experimental investigation of the flow fields beneath swept- and unswept-wing—fuselage combinations made at low speed indicated that significant gradients in the flow parameters with chordwise and vertical distances were incurred by the finite thickness of the wings at zero angle of attack and that, when the angle of attack was increased, pronounced changes in the gradients occurred. The effect of wing sweep (near zero angle of attack) was to increase the lateral flow angles. The results also indicated that the wing was the predominant factor in disturbing the field of flow for the conditions investigated.

Langley Aeronautical Laboratory,
National Advisory Committee for Aeronautics,
Langley Field, Va., October 3, 1956.

REFERENCES

1. Alford, William J., Jr., Silvers, H. Norman, and King, Thomas J., Jr.: Preliminary Low-Speed Wind-Tunnel Investigation of Some Aspects of the Aerodynamic Problems Associated With Missiles Carried Externally in Positions Near Airplane Wings. NACA RM L54J20, 1954.

2. Alford, William J., Jr.: Theoretical and Experimental Investigation of the Subsonic-Flow Fields Beneath Swept and Unswept Wings With Tables of Vortex-Induced Velocities. NACA TN 3738, 1956.

3. Gillis, Clarence L., Polhamus, Edward C., and Gray, Joseph L., Jr.: Charts for Determining Jet-Boundary Corrections for Complete Models in 7- by 10-Foot Closed Rectangular Wind Tunnels. NACA WR L-123, 1945. (Formerly NACA ARR L5G31.)

4. Herriot, John G.: Blockage Corrections for Three-Dimensional-Flow Closed-Throat Wind Tunnels, With Consideration of the Effect of Compressibility. NACA Rep. 995, 1950. (Supersedes NACA RM A7B28.)

5. Alford, William J., Jr., and Silvers, H. Norman: Investigation at High Subsonic Speeds of Finned and Unfinned Bodies Mounted at Various Locations From the Wings of Unswept- and Swept-Wing—Fuselage Models, Including Measurements of Body Loads. NACA RM L54B18, 1954.

6. Alford, William J., Jr., Silvers, H. Norman, and King, Thomas J., Jr.: Experimental Static Aerodynamic Forces and Moments at Low Speed on a Missile Model During Simulated Launching From the 25-Percent-Semispan and Wing-Tip Locations of a 45° Sweptback Wing-Fuselage Combination. NACA RM L55D20, 1955.

7. Alford, William J., Jr.: Experimental Static Aerodynamic Forces and Moments at Low Speed on a Canard Missile During Simulated Launching From the Midsemispan and Wing-Tip Locations of a 45° Sweptback Wing-Fuselage Combination. NACA RM L55A12, 1955.

TABLE I.- FUSELAGE ORDINATES

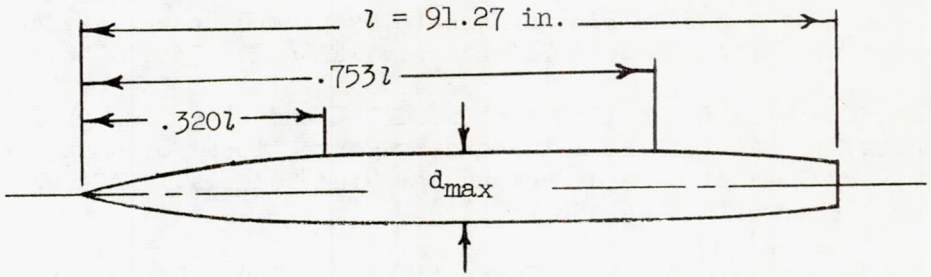

Ordinates, percent length	
Station	Radius
0	0
3.28	.91
6.57	1.71
9.86	2.41
13.15	3.00
16.43	3.50
19.72	3.90
23.01	4.21
26.29	4.43
29.58	4.53
32.00	4.57
75.34	4.57
76.69	4.54
79.98	4.38
83.26	4.18
86.55	3.95
89.84	3.72
93.13	3.49
96.41	3.26
100.00	3.02

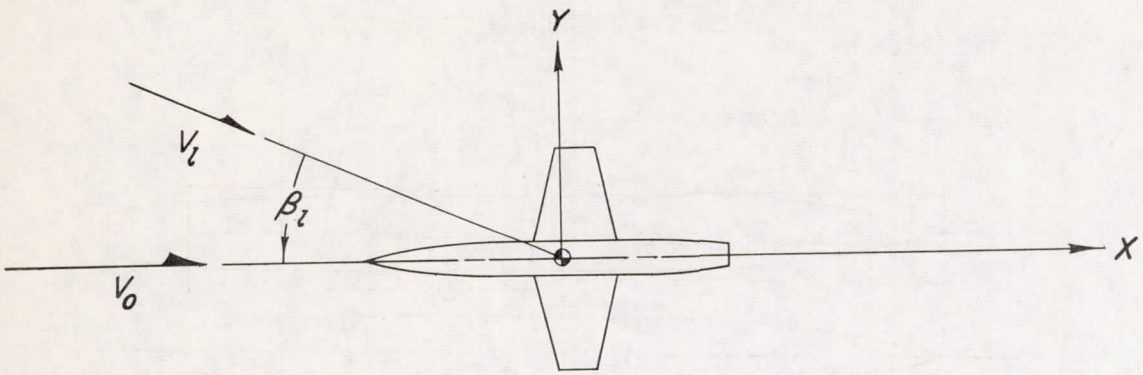

Lateral plane

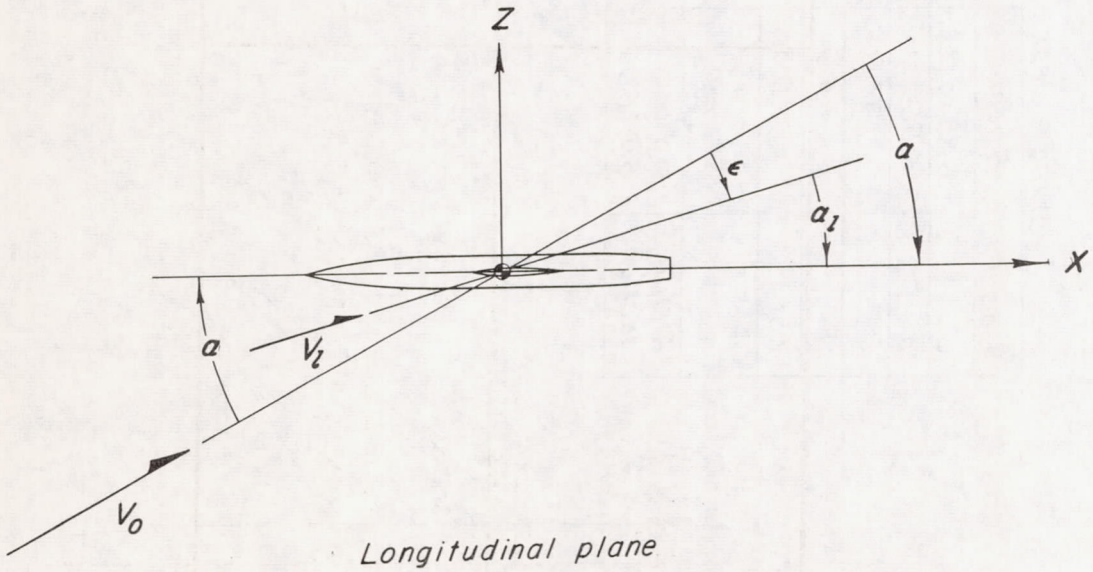

Longitudinal plane

Figure 1.- Positive directions of distances and angles for body-axis system.

Wing Geometry

Symbol	Swept	Unswept
S	6.25 sq ft	6.25 sq ft
b	5.00 ft	4.33 ft
$\bar{c}$	1.37 ft	1.49 ft
A	4.0	3.0
λ	0.3	0.5
Λ	45° @ $c/4$	0° @ $c/2$
Airfoil section	65A006	65A004

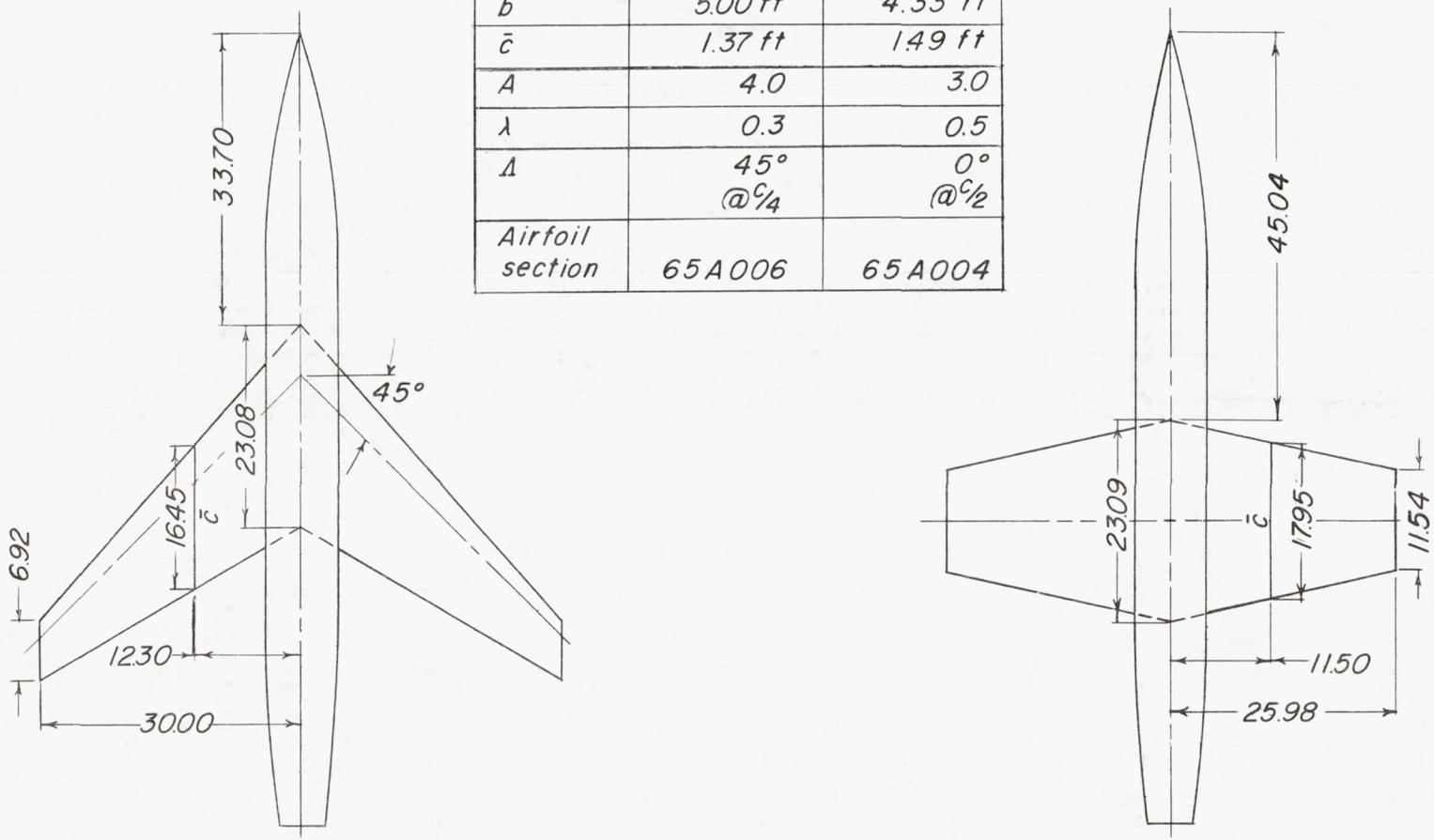

Figure 2.- Geometric characteristics of test models. All dimensions in inches.

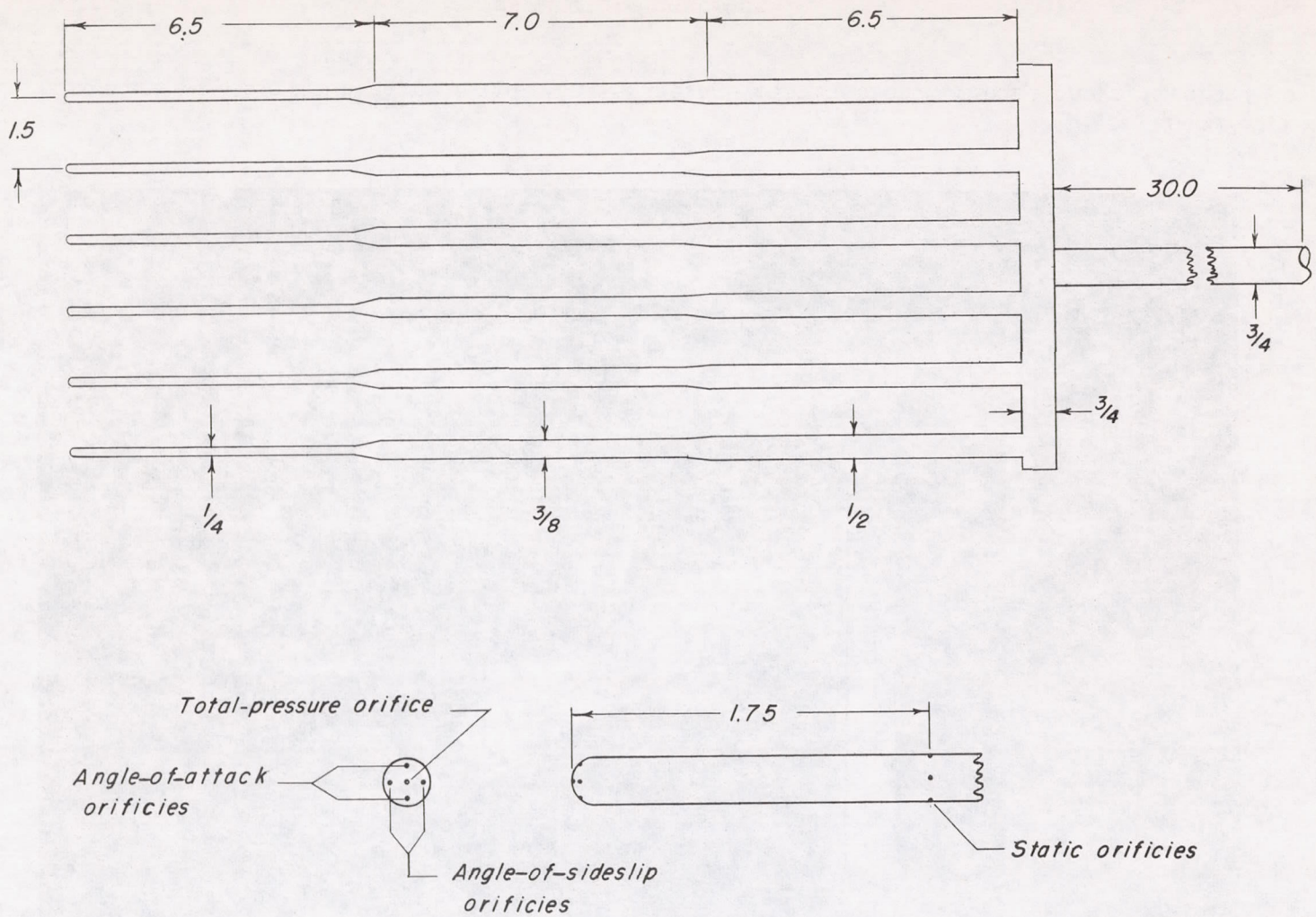

(a) General proportions. All dimensions in inches.

Figure 3.- Flow-survey rake.

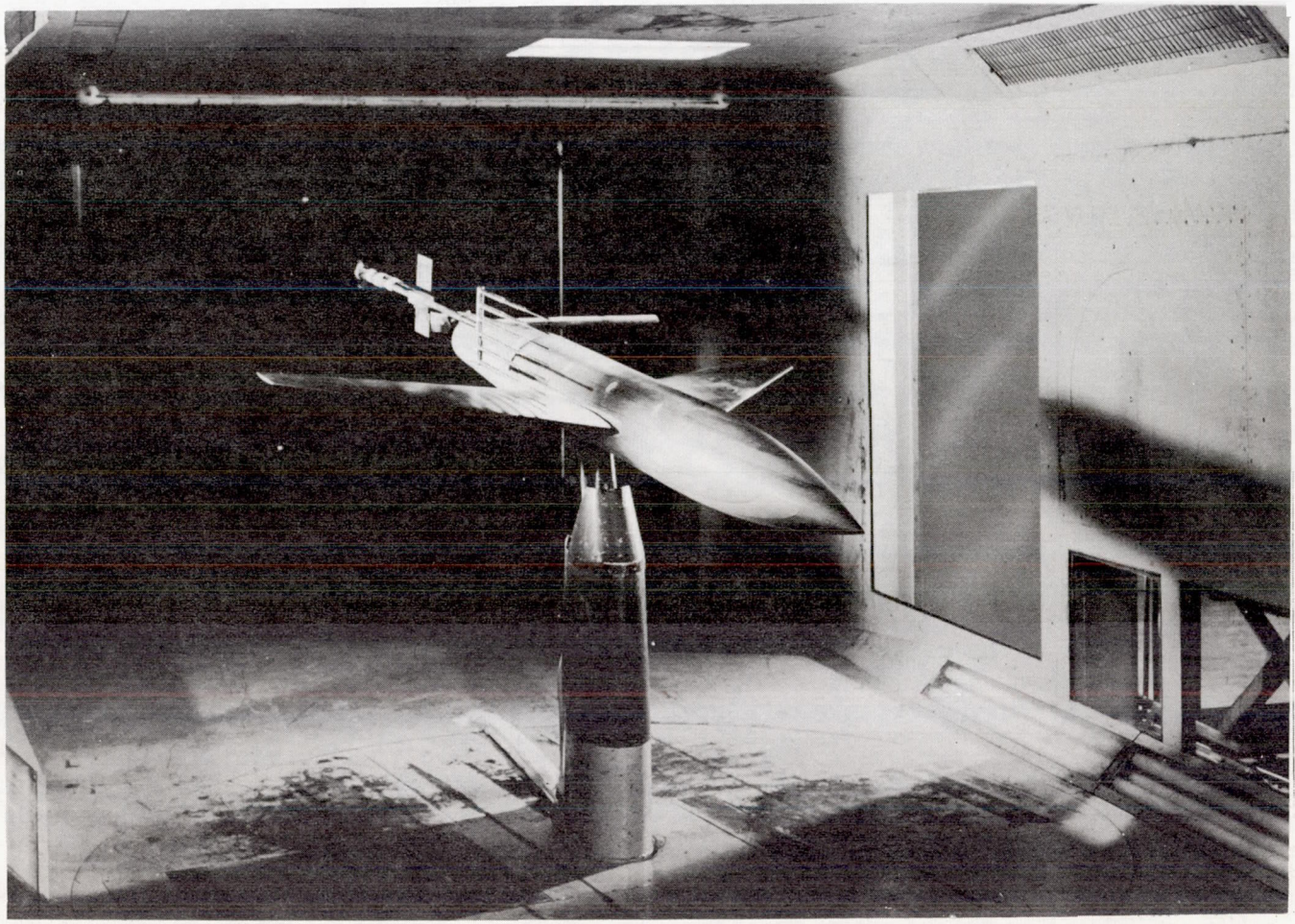

L-80760.1

(b) Photograph of rake mounted on swept-wing—fuselage combination. (Model shown inverted as tested.)

Figure 3.- Concluded.

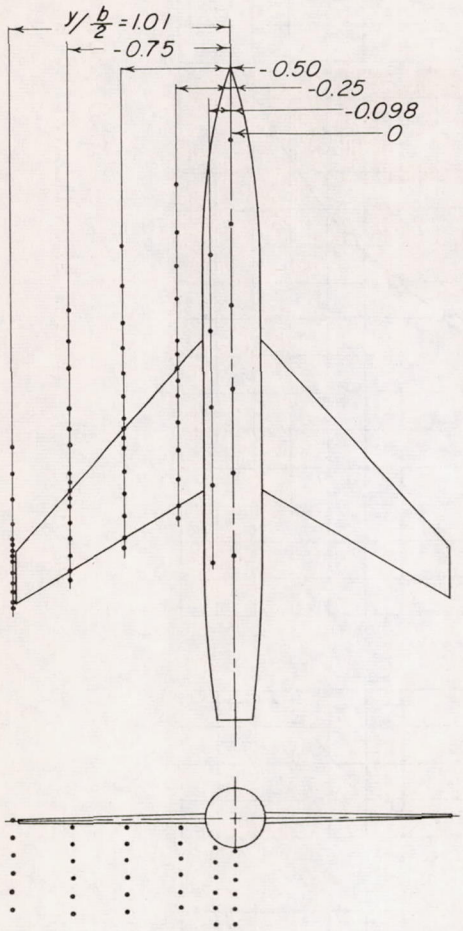

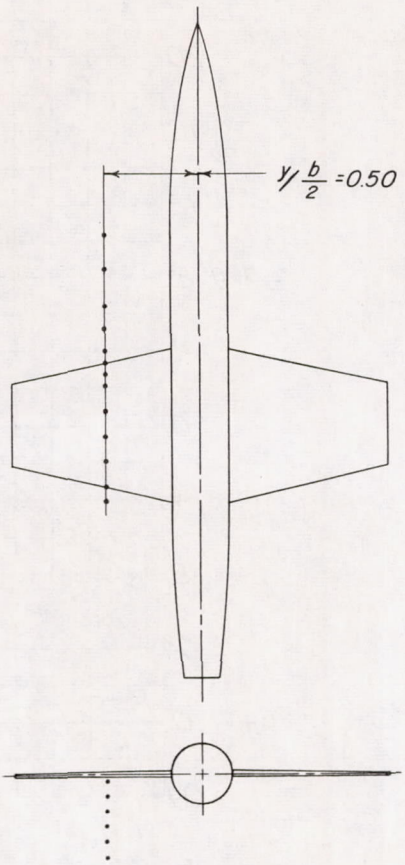

Swept wing - fuselage

$y/\frac{b}{2}$ =0		$y/\frac{b}{2}$ =-0.098		$y/\frac{b}{2}$ =-0.25		$y/\frac{b}{2}$ =-0.50		$y/\frac{b}{2}$ =-0.75		$y/\frac{b}{2}$ =-1.01	
x/c	z/c	x/c	z/c	x/c	z/c	x/c	z/c	x/c	z/c	x/c	z/c
1.50	-0.21	1.50	-0.17	1.10	-0.06	1.10	-0.07	1.10	-0.09	1.05	0.015
1.00	-0.28	1.00	-0.24	1.00	-0.14	1.00	-0.17	1.00	-0.23	0.95	-0.20
0.50	-0.34	0.50	-0.31	0.80	-0.22	0.80	-0.27	0.80	-0.37	0.75	-0.42
0	-0.40	0	-0.38	0.60	-0.30	0.60	-0.37	0.60	-0.51	0.60	-0.64
-0.50	-0.47	-0.50	-0.45	0.40	-0.38	0.40	-0.47	0.40	-0.65	0.40	-0.86
-1.00	-0.53		-0.51	0.20	-0.46	0.20	-0.57	0.20	-0.79	0.20	-1.08
				0.10		0.10		0.10		0.10	
				0		0		0		0	
				-0.10		-0.10		-0.10		-0.10	
				-0.20		-0.30		-0.20		-0.20	
				-0.50		-0.50		-0.55		-0.50	
				-0.75		-0.75		-0.75		-1.00	
				-1.00		-1.00		-1.00		-1.50	
				-1.35		-1.35		-1.50		-2.00	
						-1.70		-1.85			
								-2.20			

Unswept wing - fuselage

$y/\frac{b}{2}$ =-0.50	
x/c	z/c
1.10	-0.05
1.00	-0.14
0.80	-0.22
0.60	-0.31
0.40	-0.40
0.20	-0.48
0.10	
0	
-0.10	
-0.30	
-0.50	
-0.75	
-1.00	

Figure 4.- Locations at which flow surveys were made.

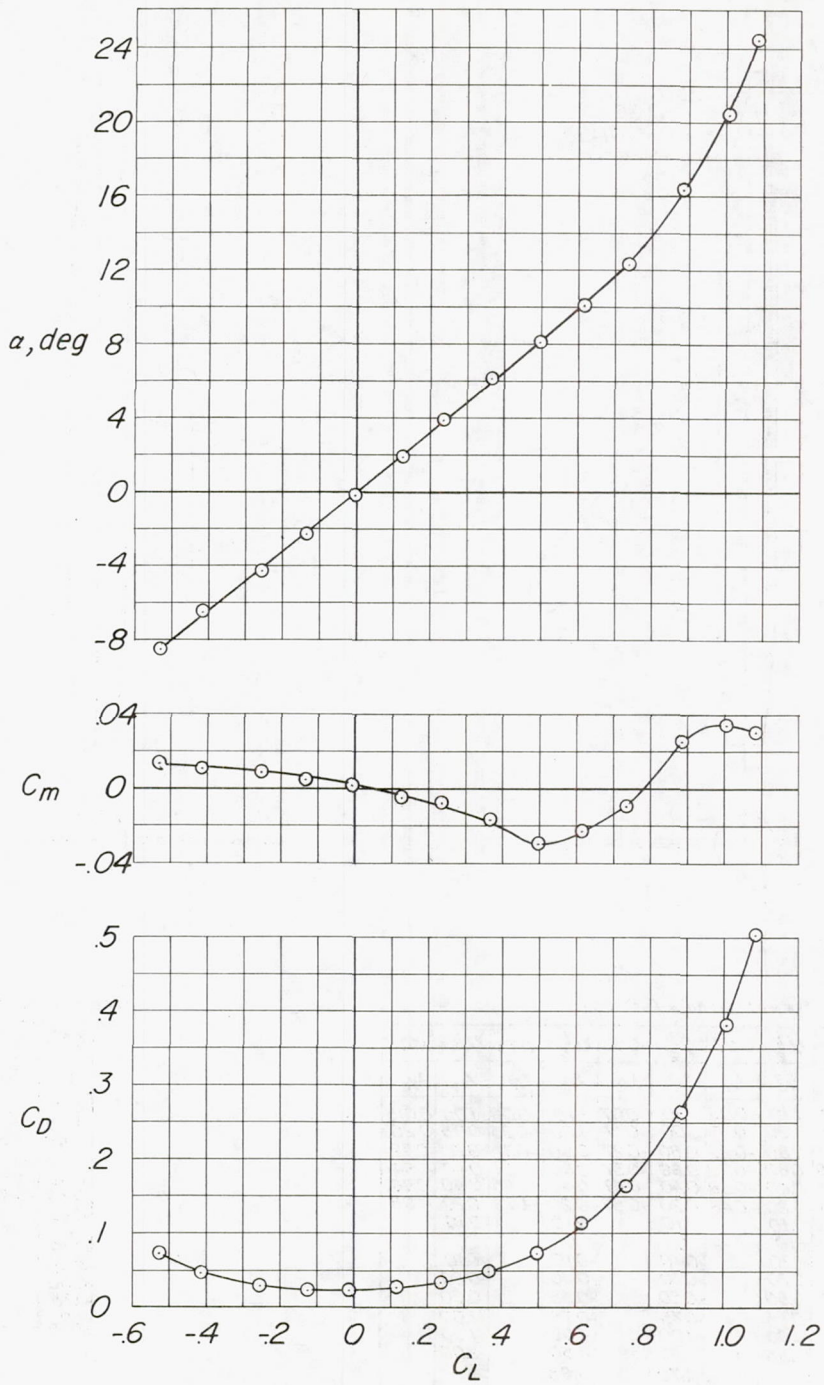

(a) Swept-wing—fuselage combination.

Figure 5.- Aerodynamic characteristics of test models.

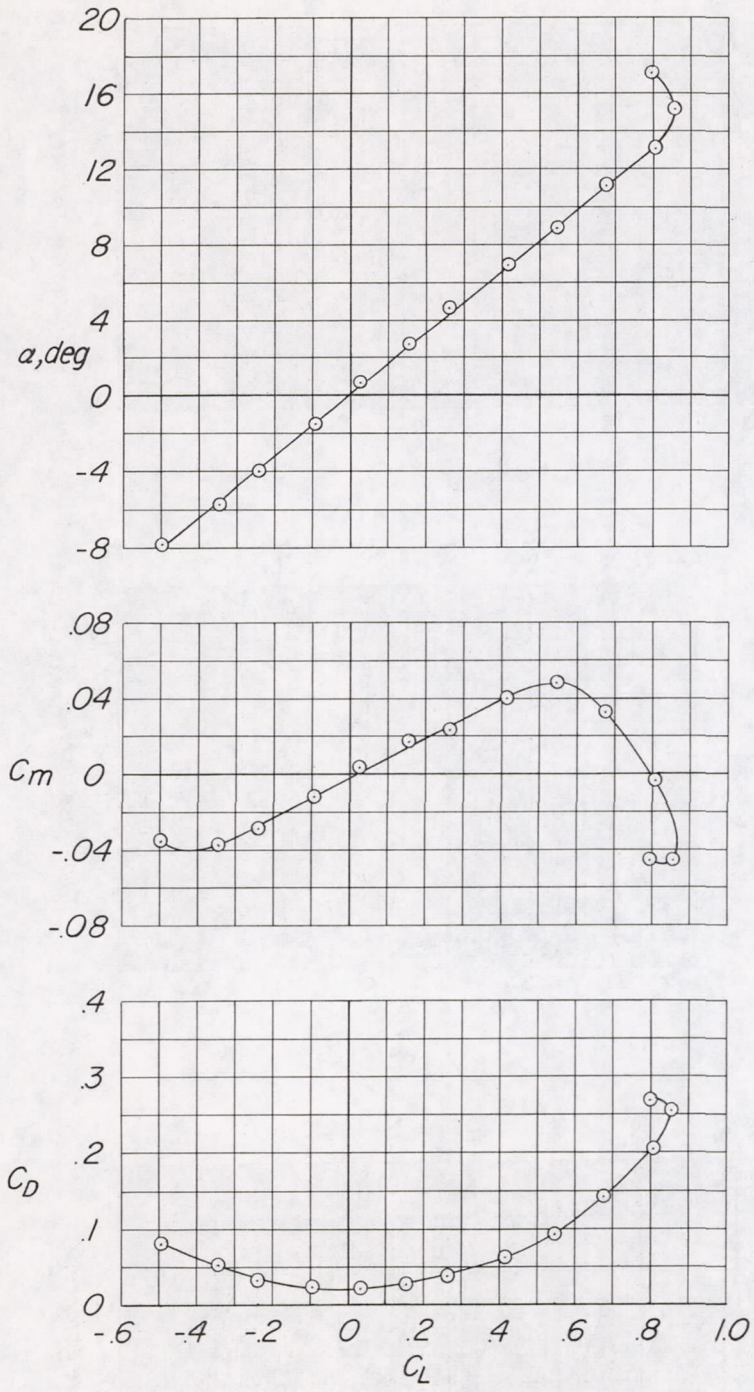

(b) Unswept-wing—fuselage combination.

Figure 5.- Concluded.

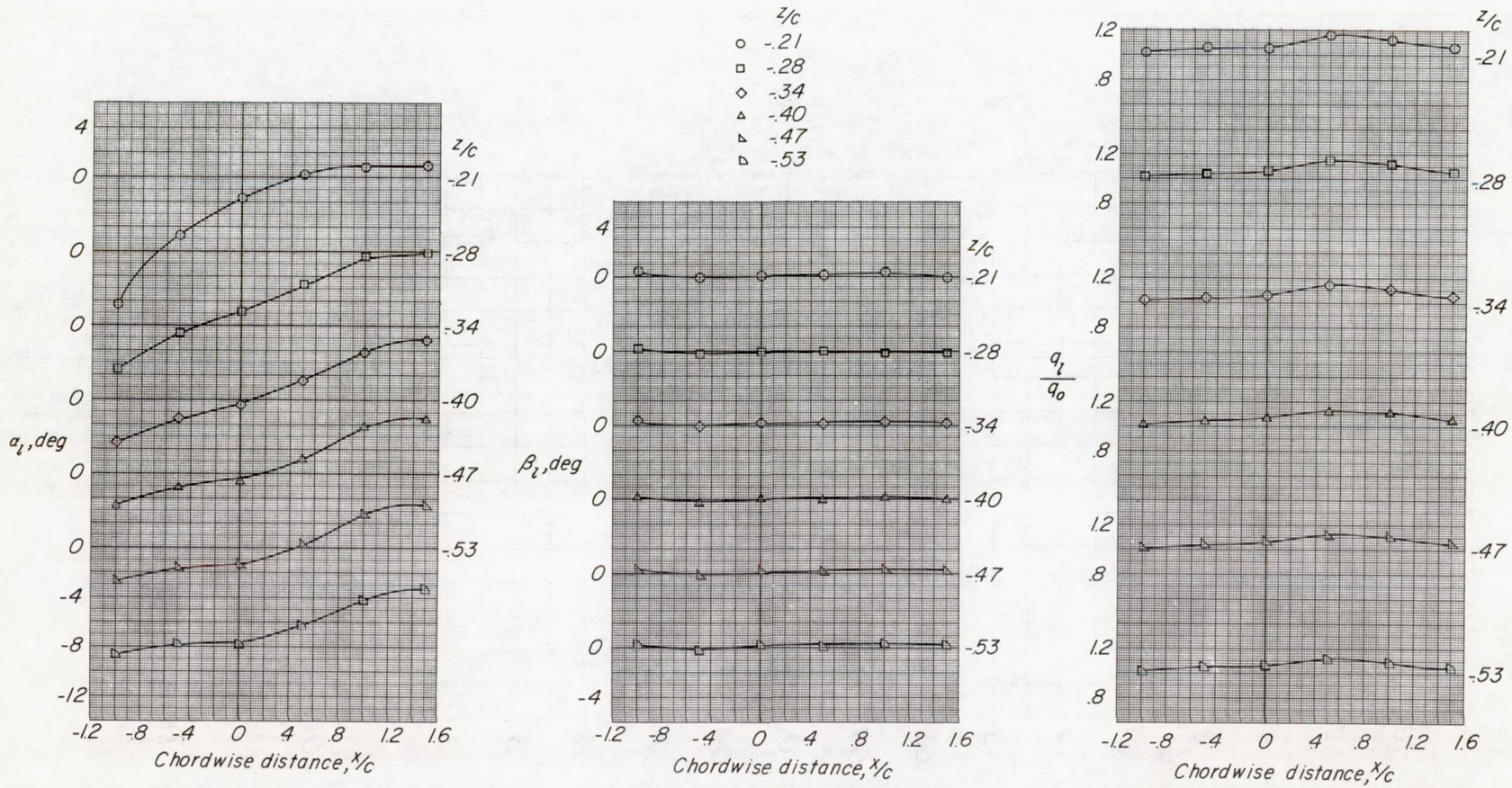

(a) $\alpha = -8.5^{\circ}$.

Figure 6.- Flow-field characteristics of swept-wing—fuselage combination at $y/\frac{b}{2} = 0$.

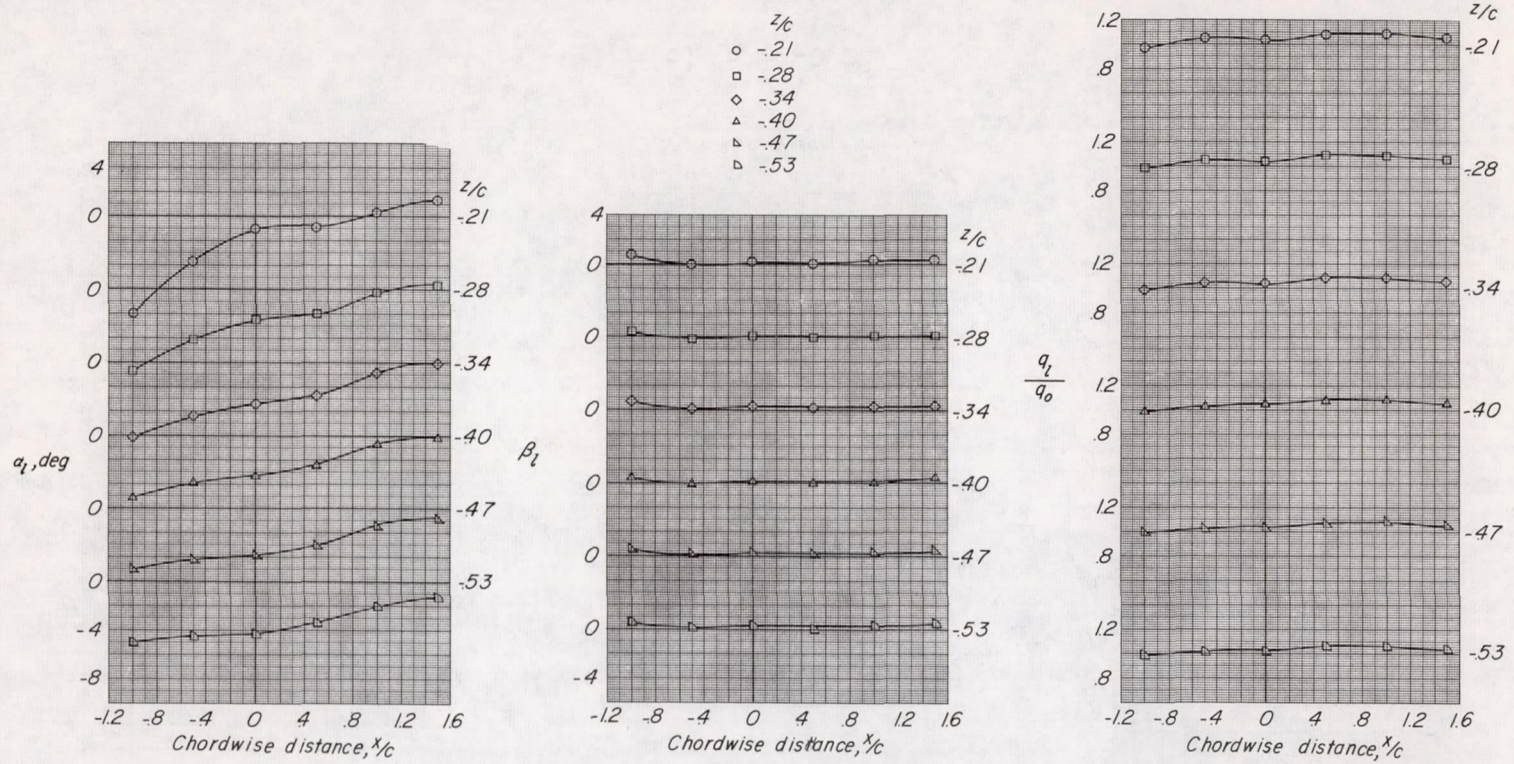

(b) $\alpha = -4.3°$.

Figure 6.- Continued.

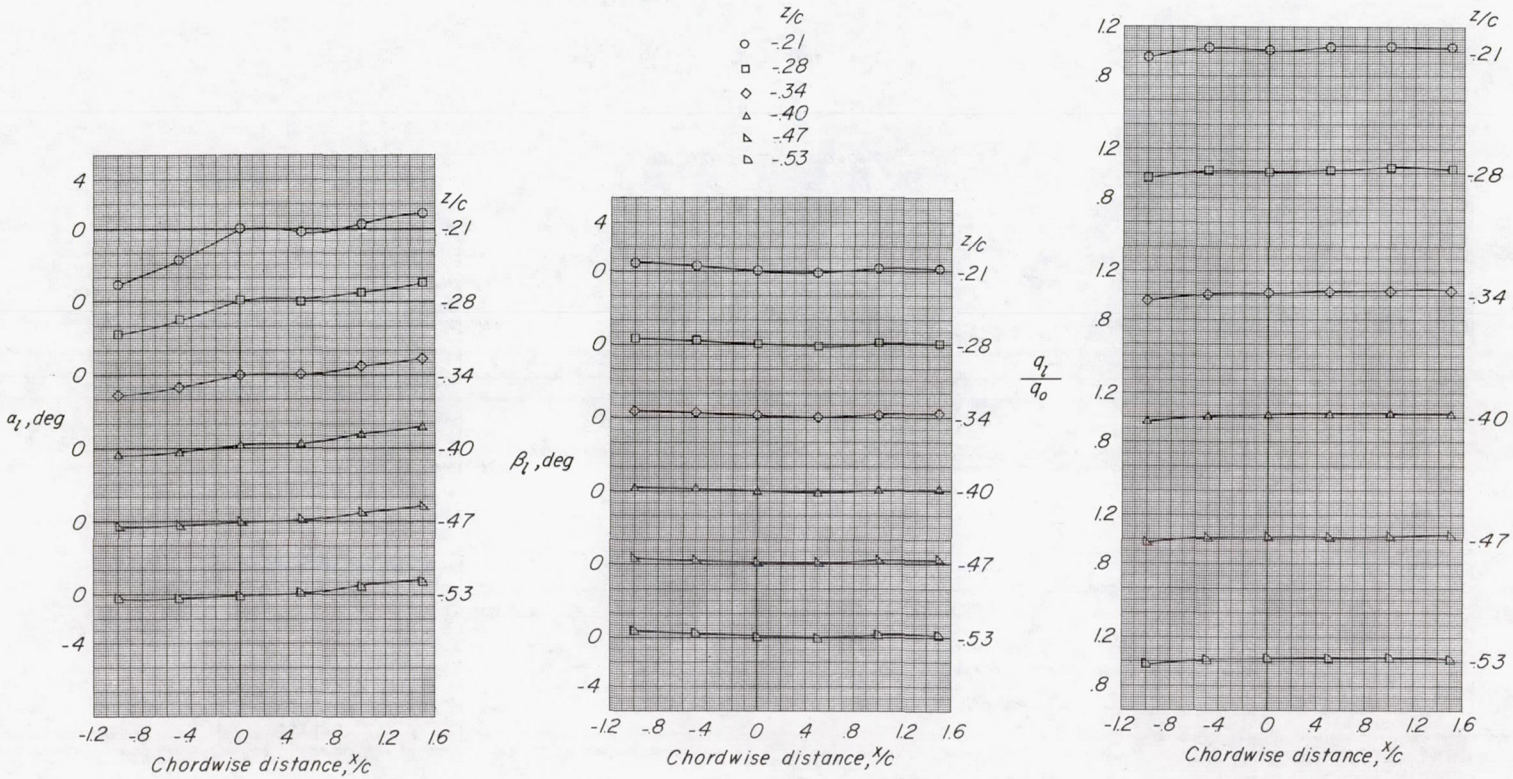

(c) $\alpha = -0.2^{\circ}$.

Figure 6.- Continued.

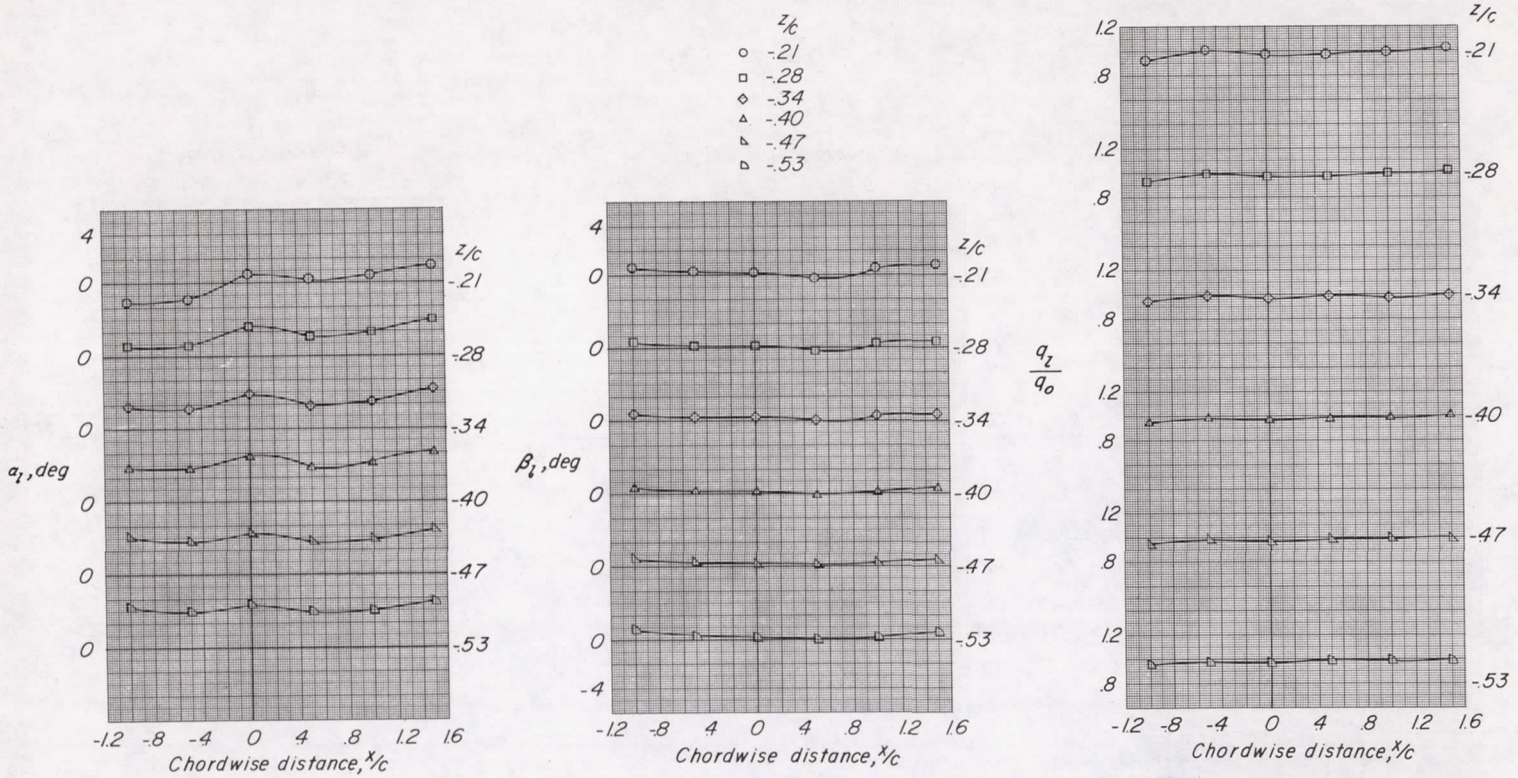

(d) $\alpha = 3.8^{\circ}$.

Figure 6.- Continued.

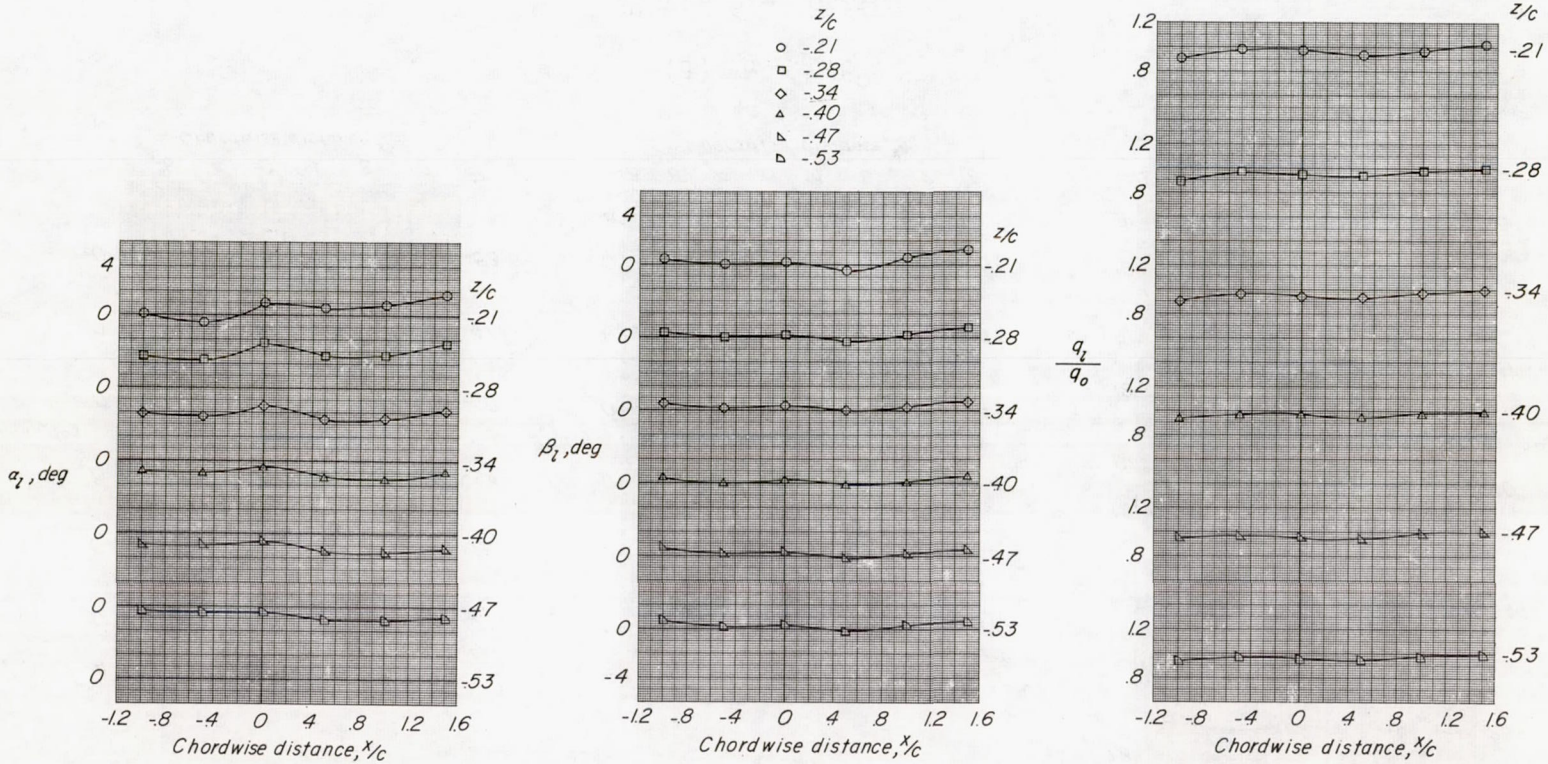

(e) $\alpha = 6.1^{\circ}$.

Figure 6.- Continued.

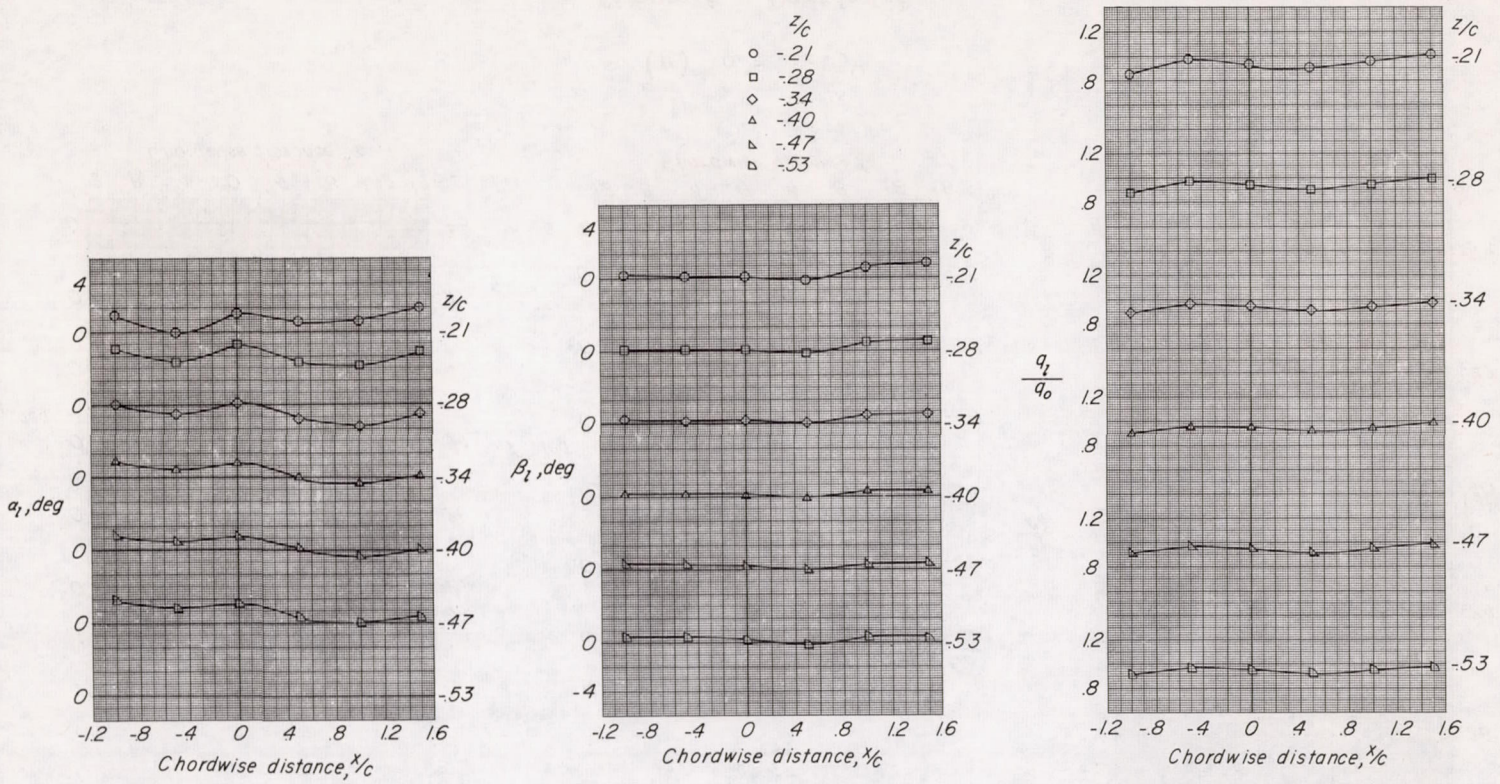

(f) $\alpha = 8.2^{\circ}$.

Figure 6.- Continued.

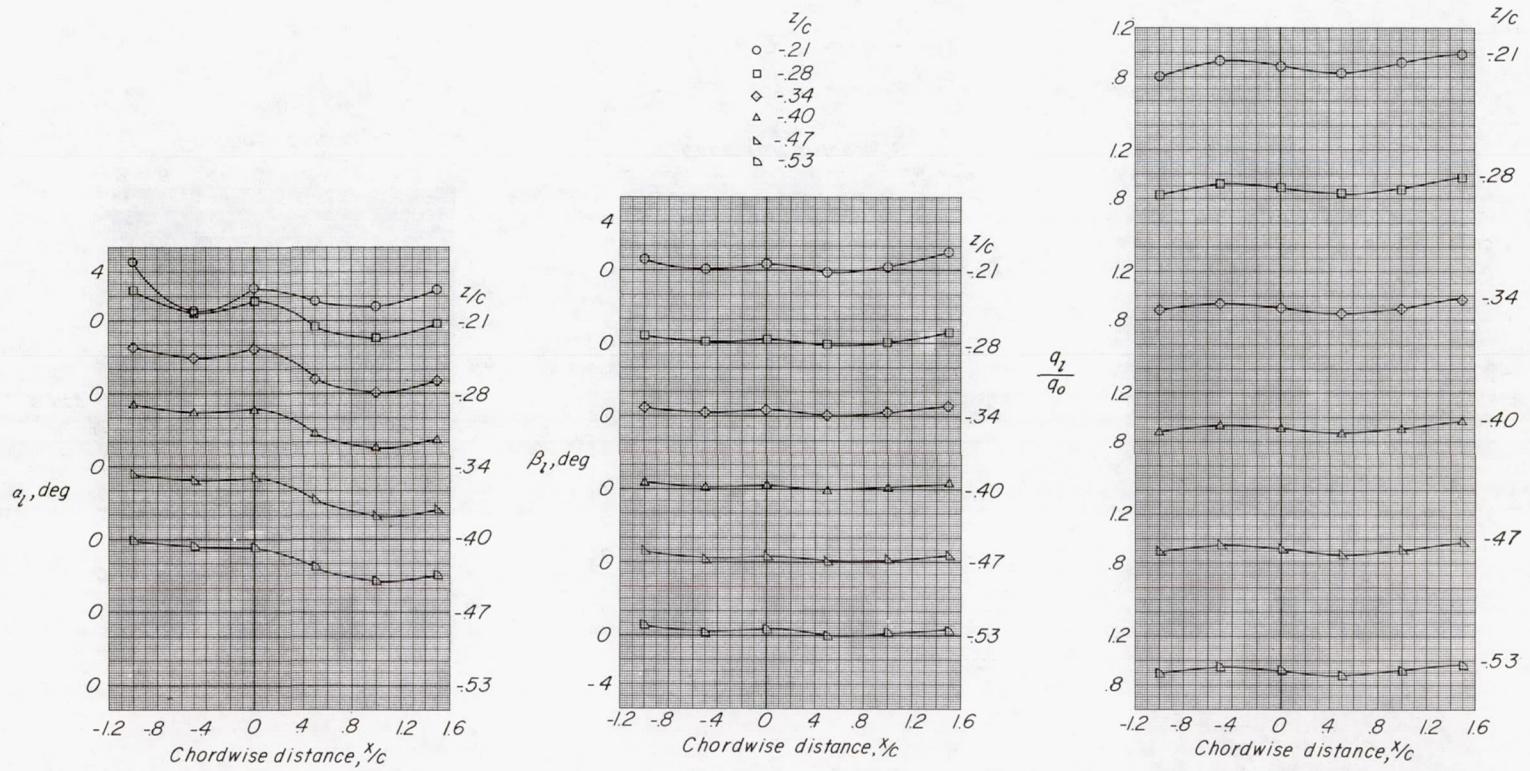

(g) $\alpha = 12.3^{\circ}$.

Figure 6.- Continued.

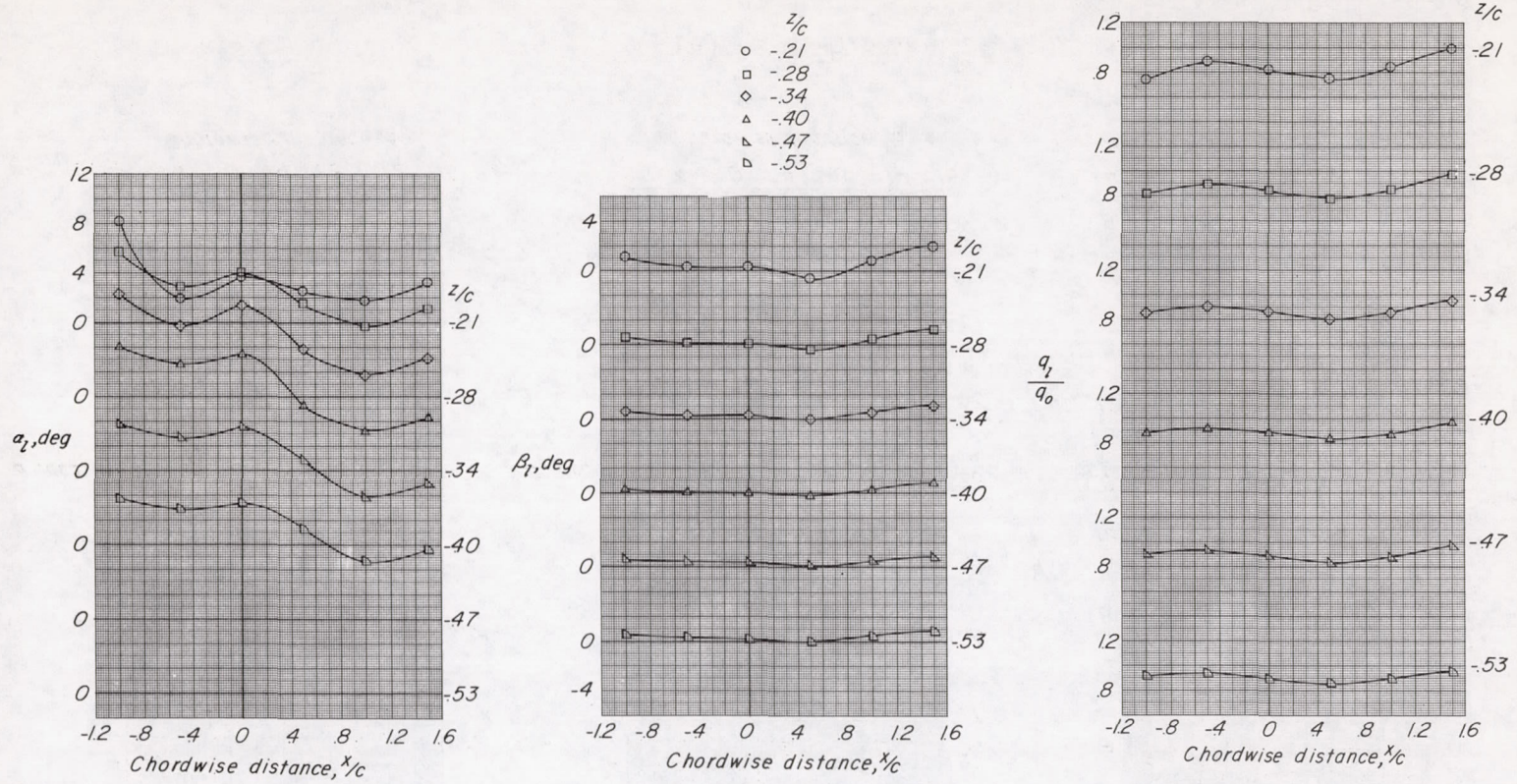

(h) $\alpha = 16.4^{\circ}$.

Figure 6.- Concluded.

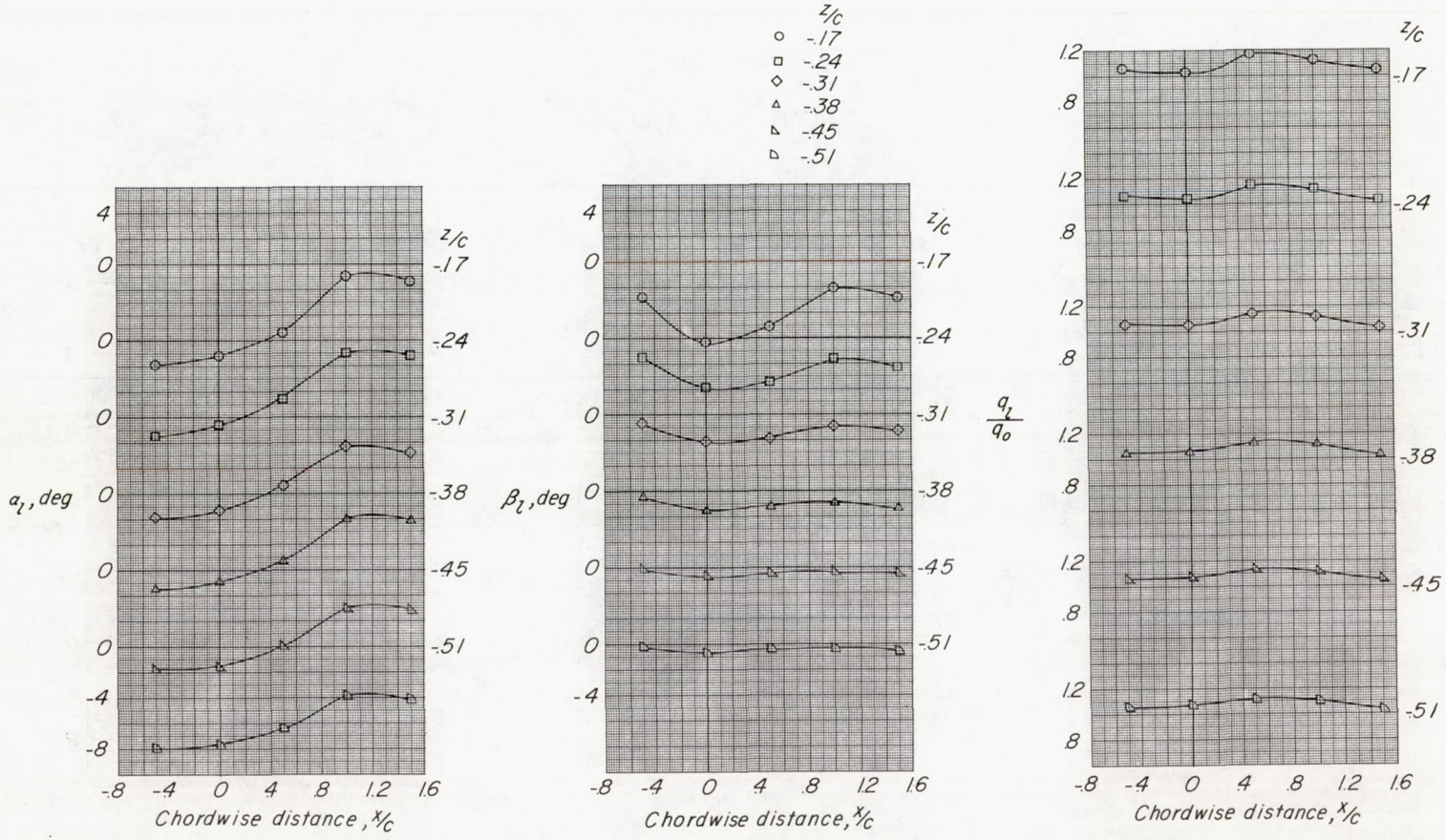

(a) $\alpha = -8.5^\circ$.

Figure 7.- Flow-field characteristics of swept-wing—fuselage combination at $y/\frac{b}{2} = -0.098$.

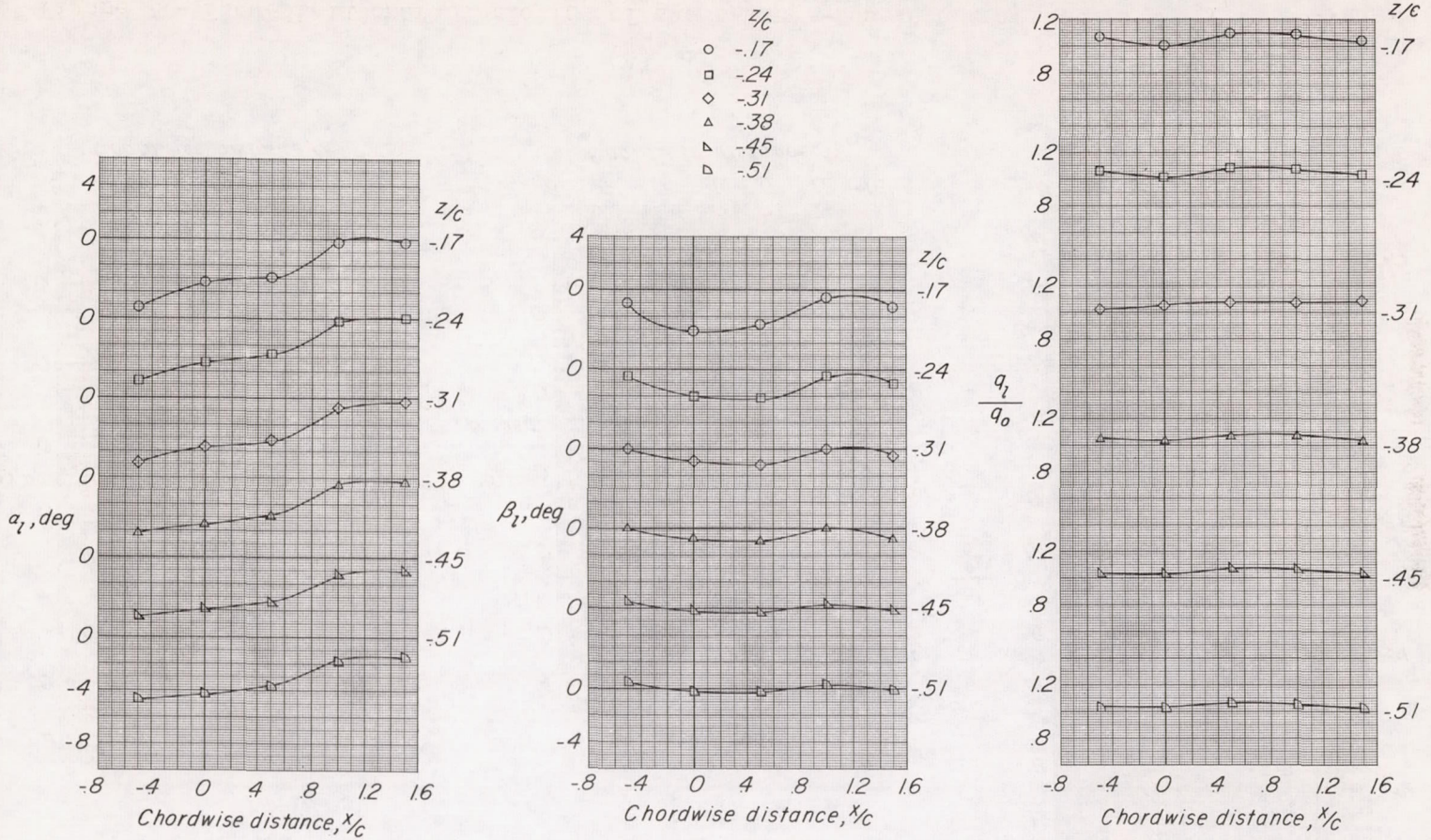

(b) $\alpha = -4.3^{\circ}$.

Figure 7.- Continued.

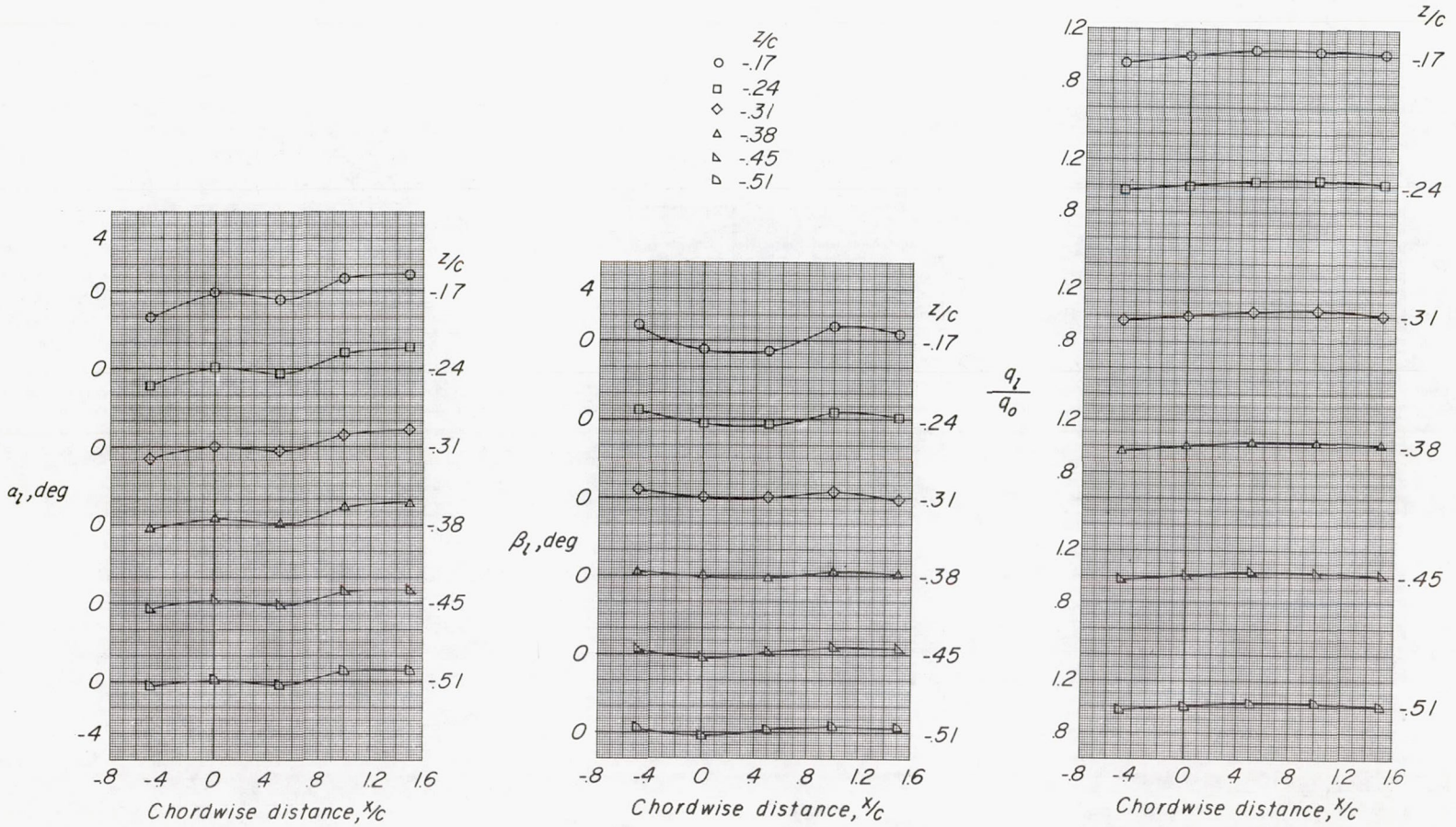

(c) $\alpha = -0.2^{\circ}$.

Figure 7.- Continued.

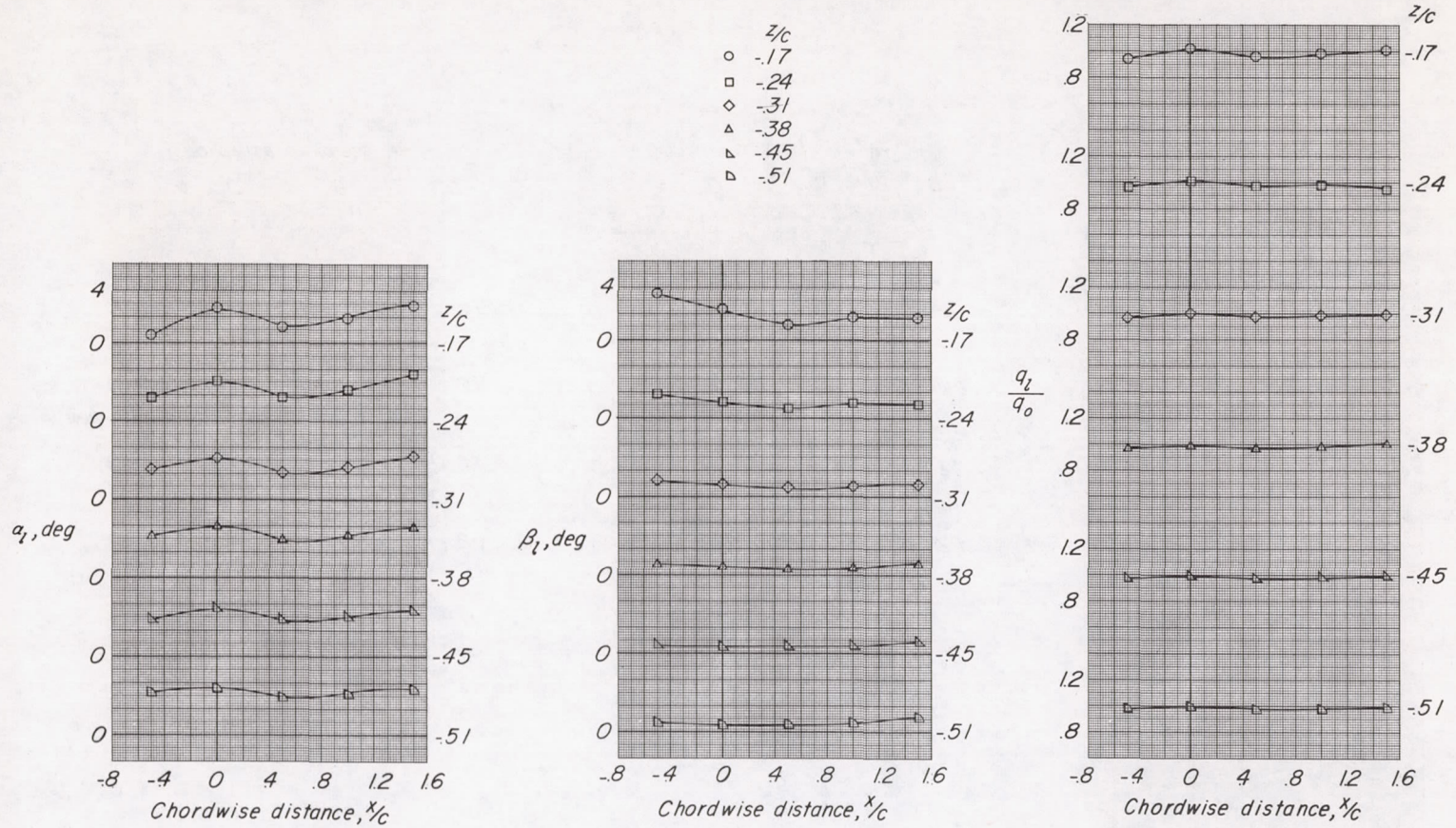

(d) $\alpha = 3.8^{\circ}$.

Figure 7.- Continued.

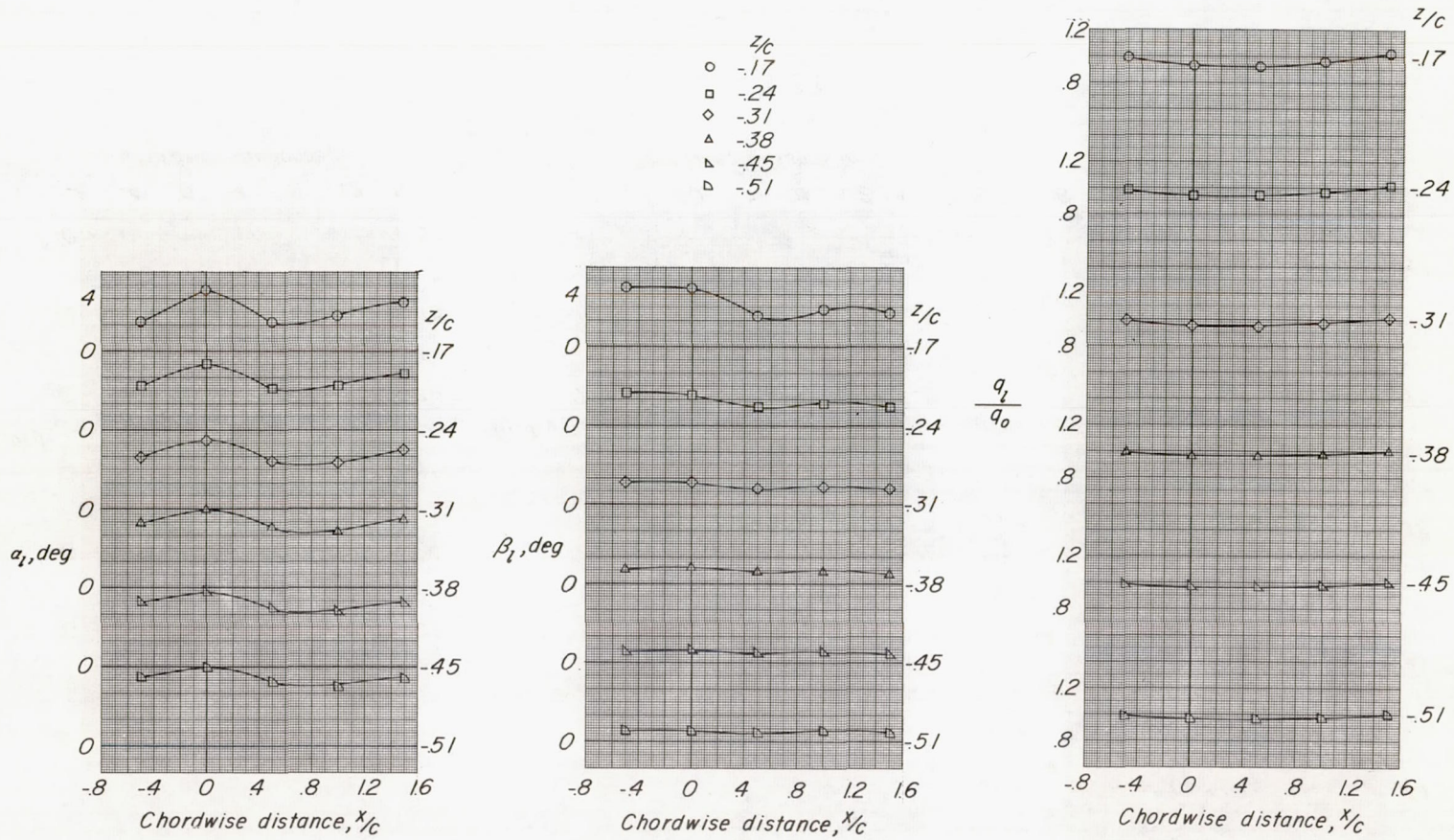

(e) $\alpha = 6.1^{\circ}$.

Figure 7.- Continued.

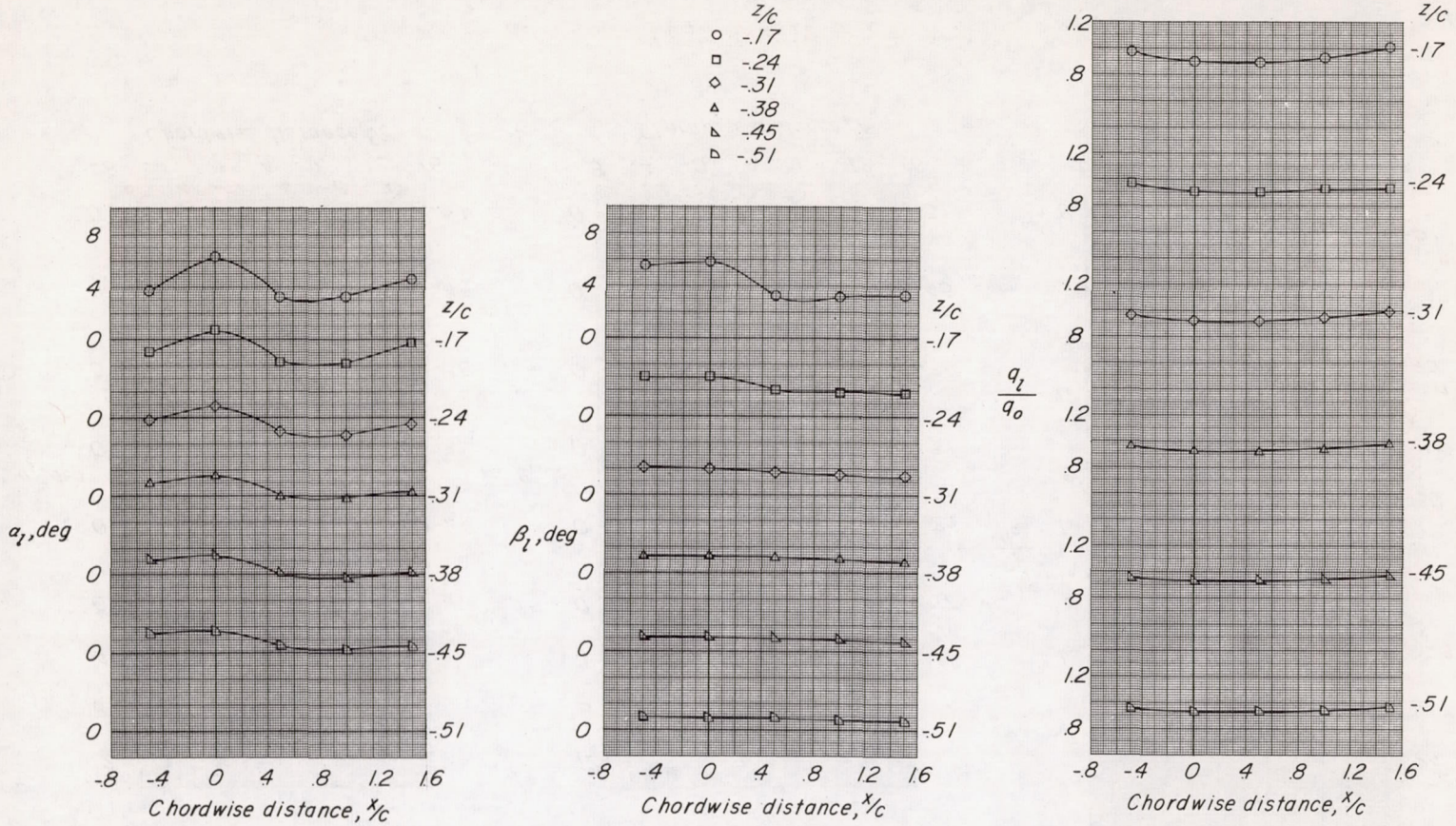

(f) $\alpha = 8.2^{\circ}$.

Figure 7.- Continued.

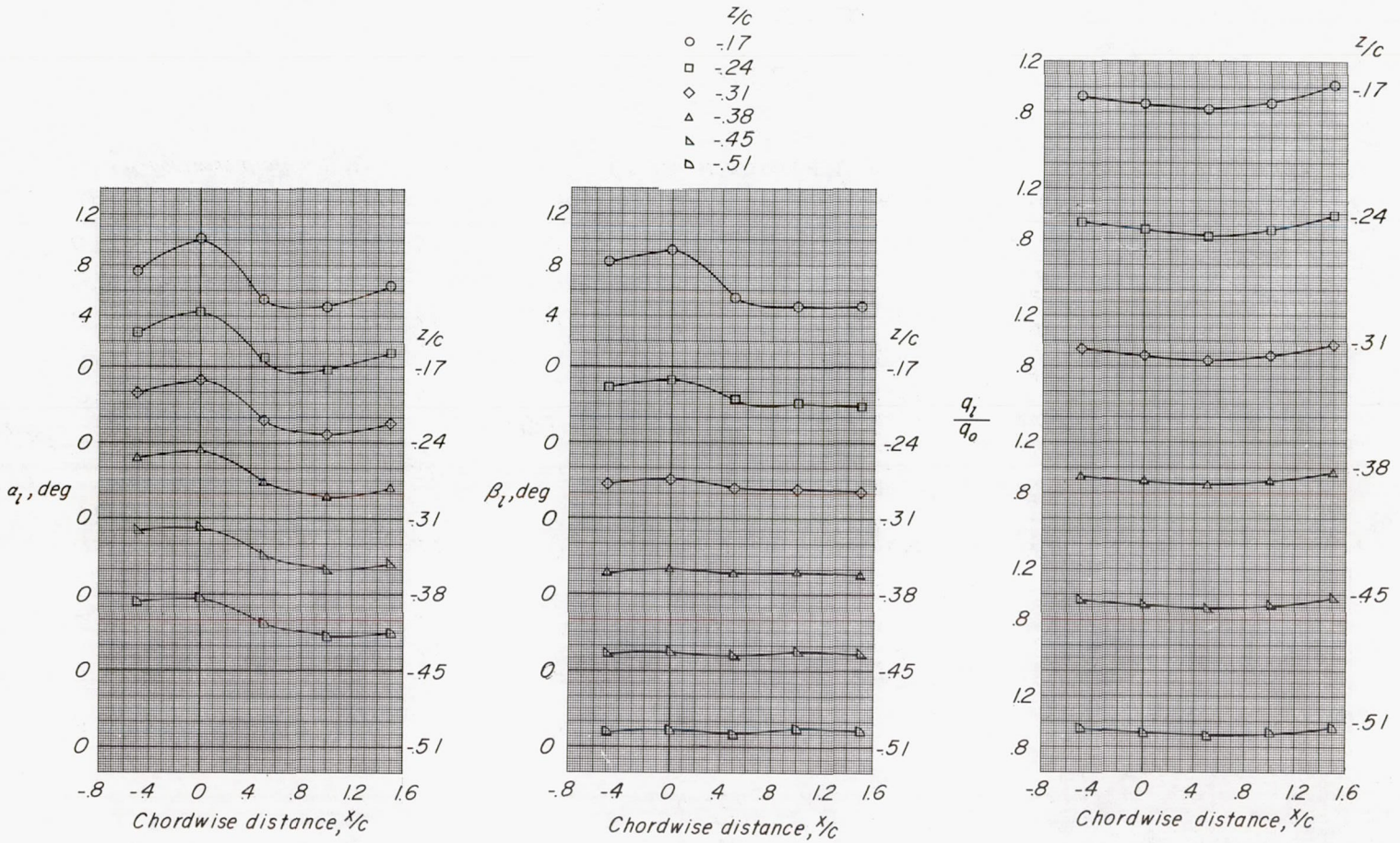

(g) $\alpha = 12.3^{\circ}$.

Figure 7.- Continued.

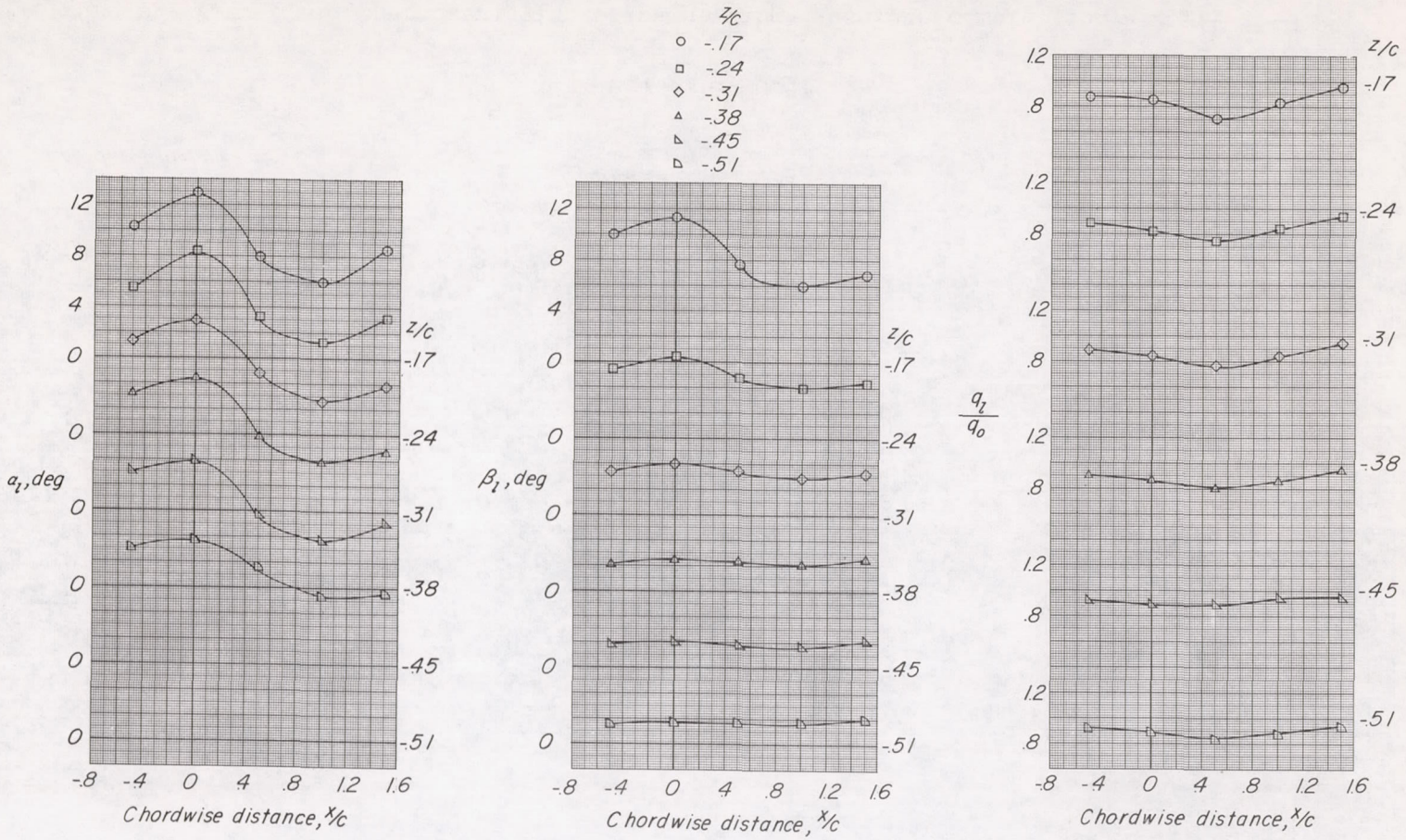

(h) $\alpha = 16.4^{\circ}$.

Figure 7.- Concluded.

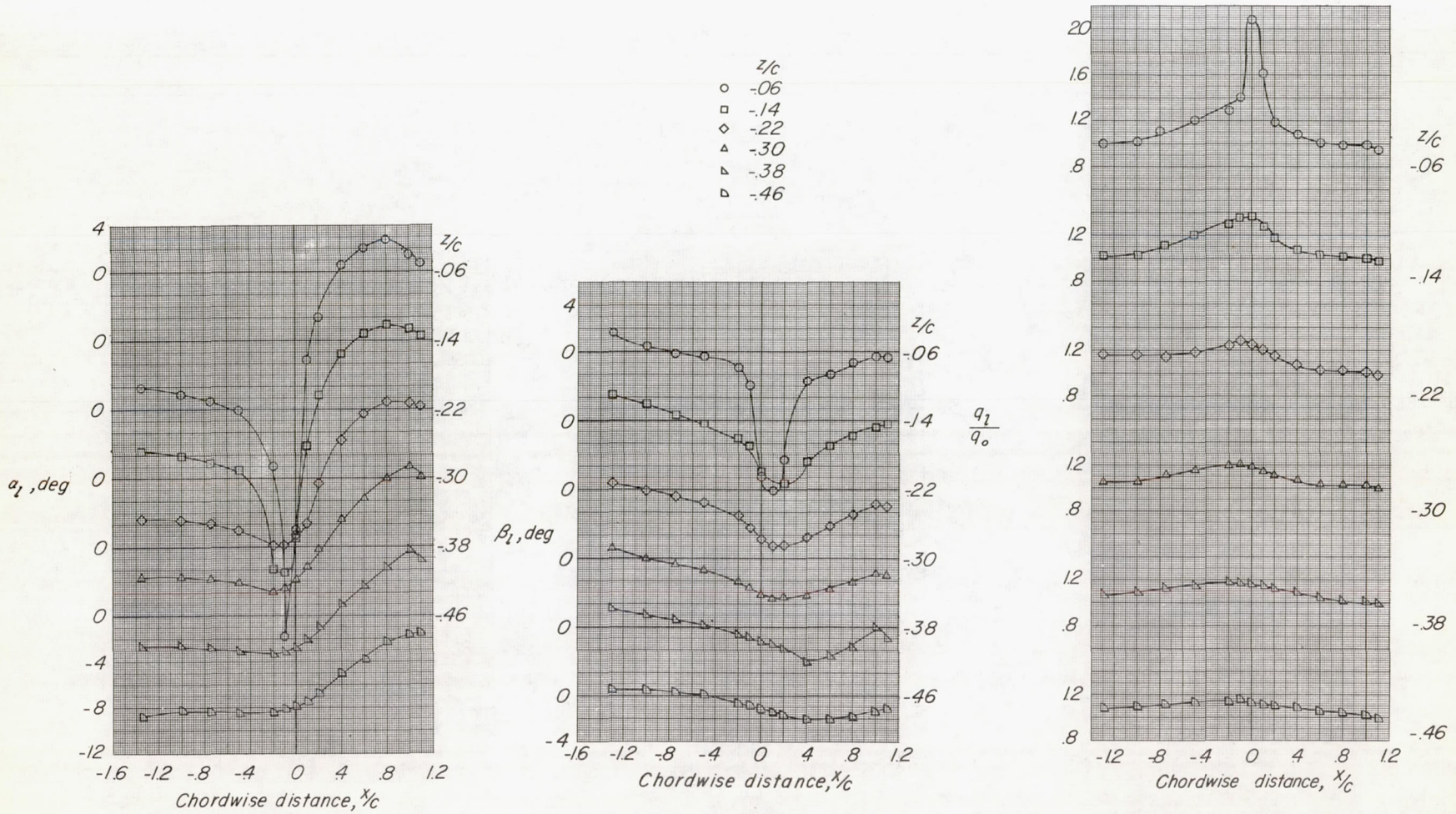

(a) $\alpha = -8.5^\circ$.

Figure 8.- Flow-field characteristics of swept-wing—fuselage combination at $y/\frac{b}{2} = -0.25$.

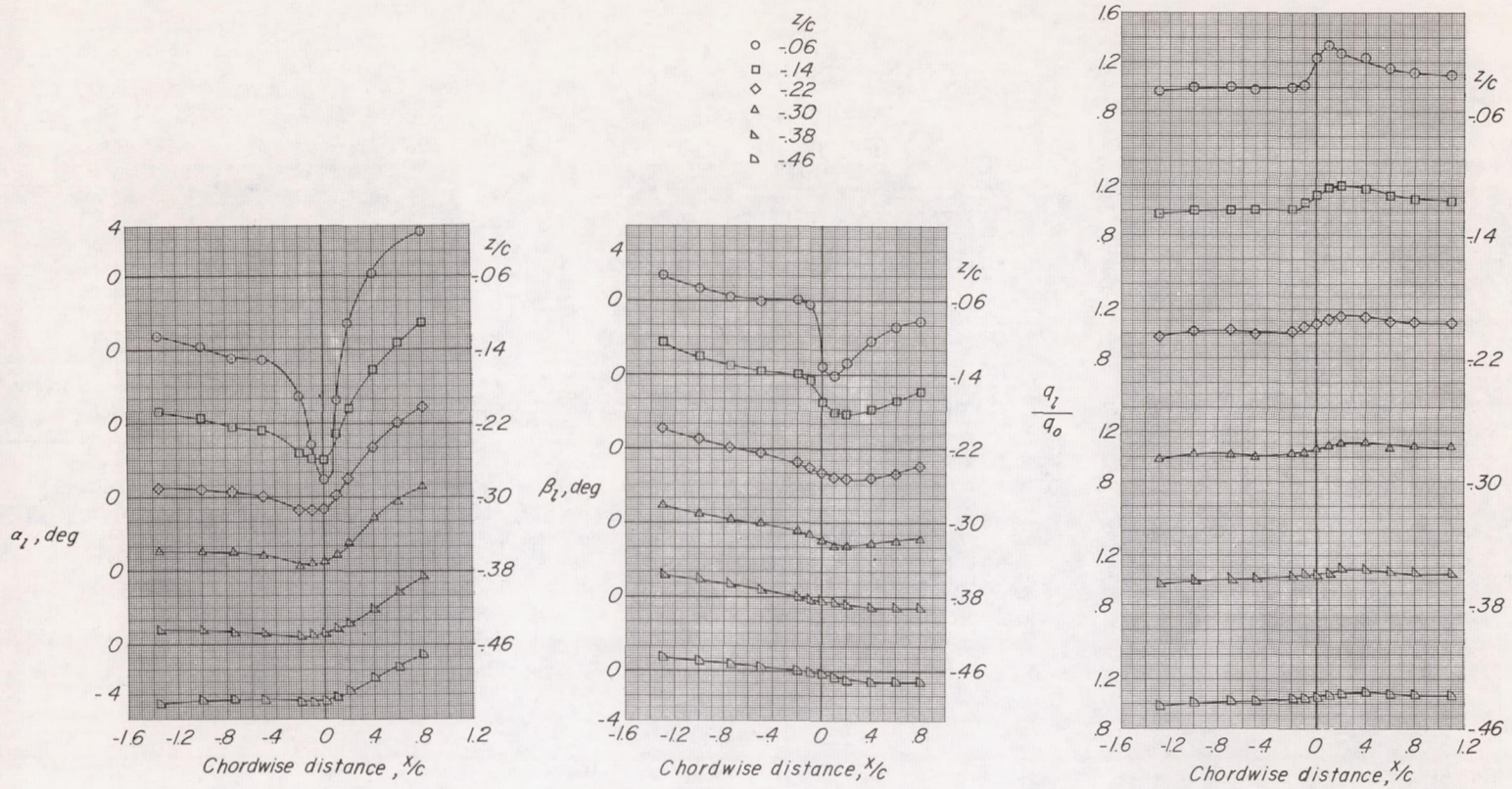

(b) $\alpha = -4.3^{\circ}$.

Figure 8.- Continued.

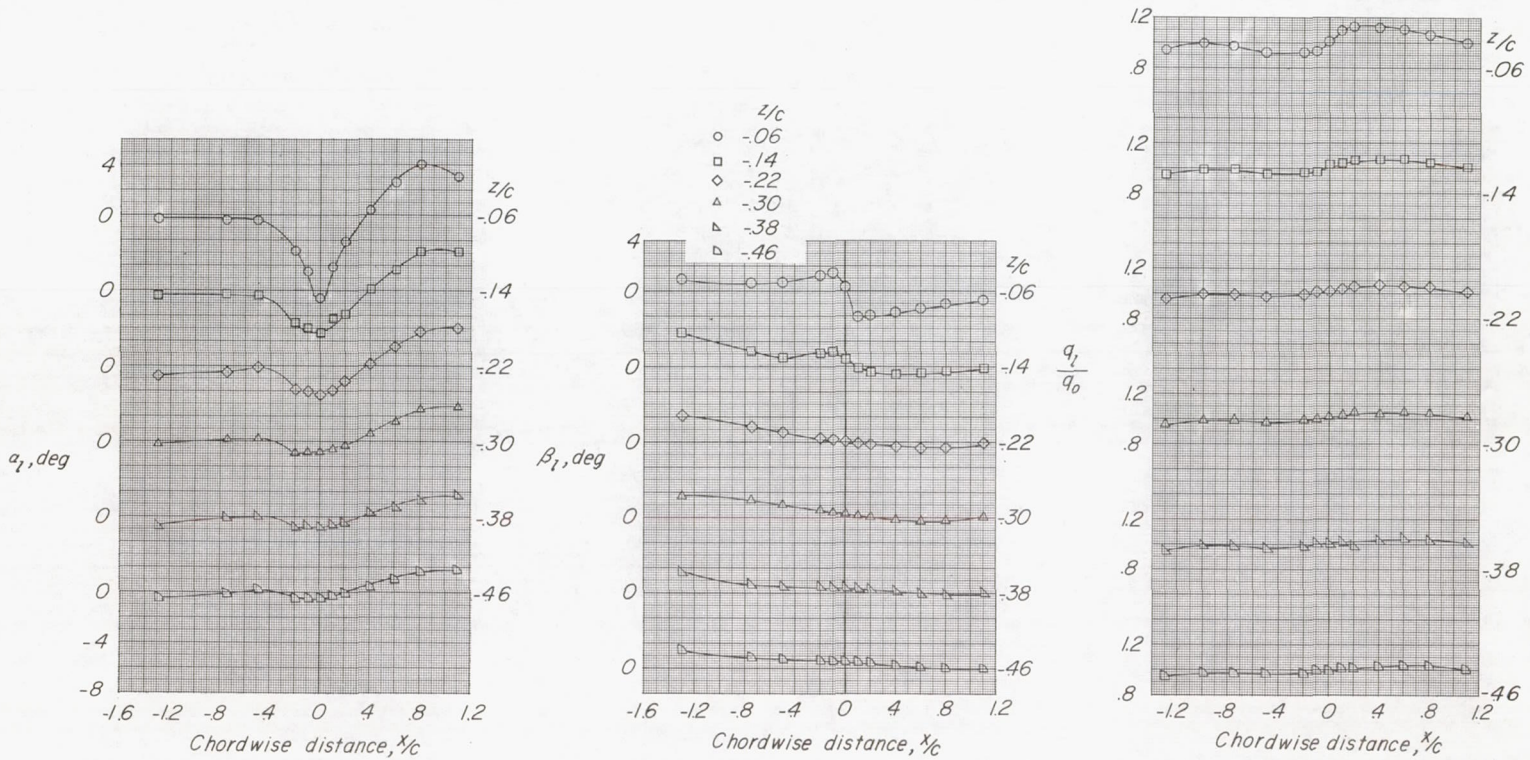

(c) $\alpha = -0.2^{\circ}$.

Figure 8.- Continued.

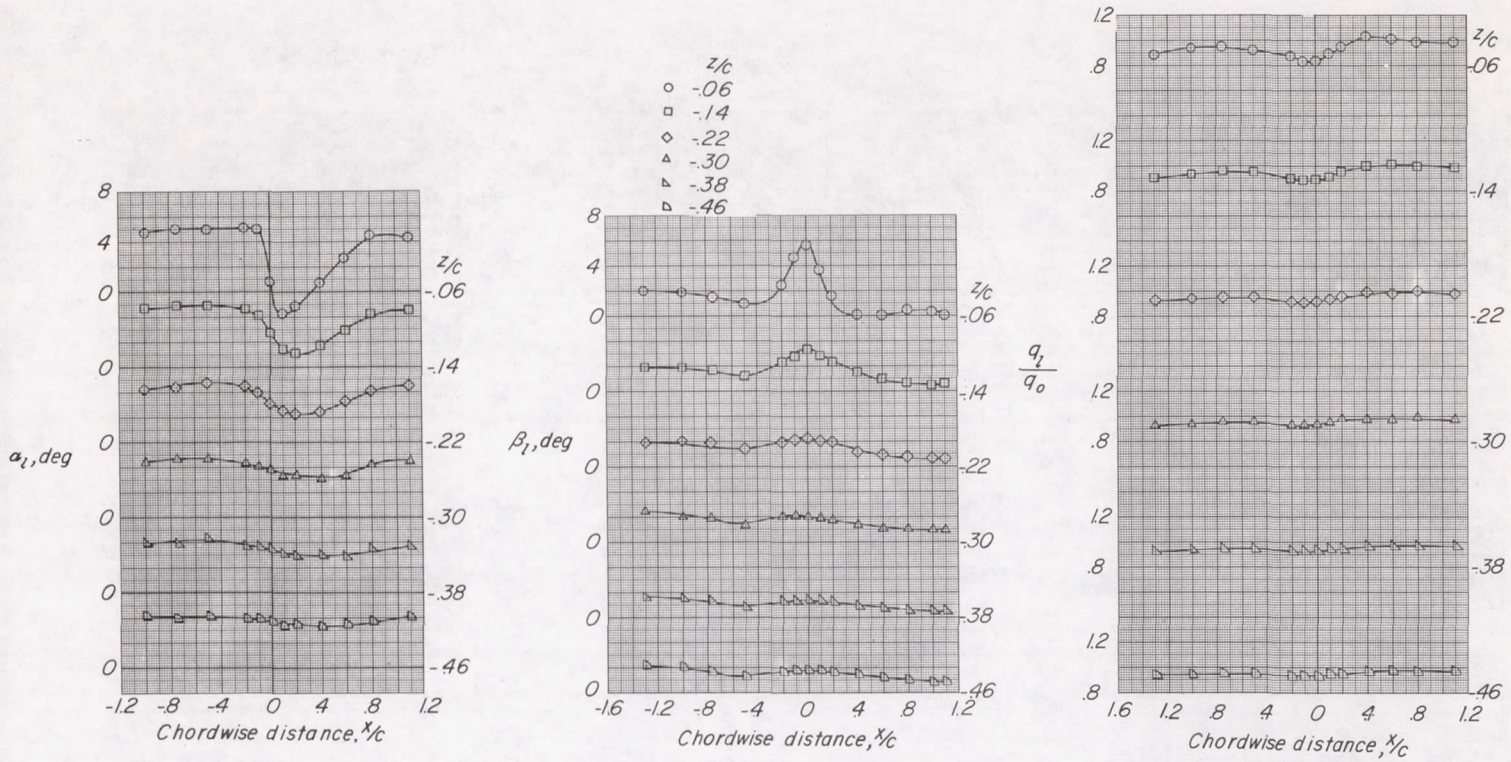

(d) $\alpha = 3.8^{\circ}$.

Figure 8.- Continued.

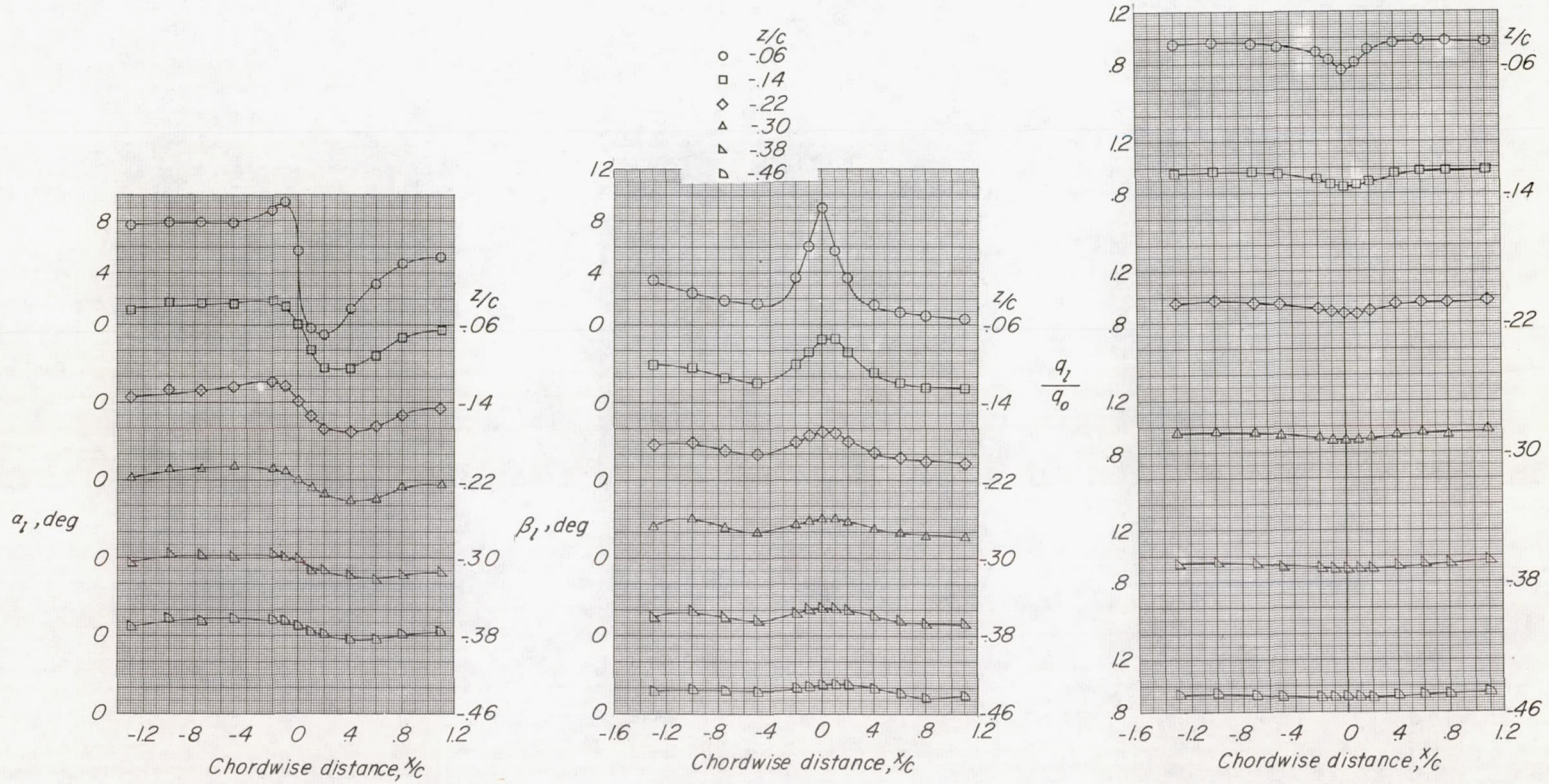

(e) $\alpha = 6.1^\circ$.

Figure 8.- Continued.

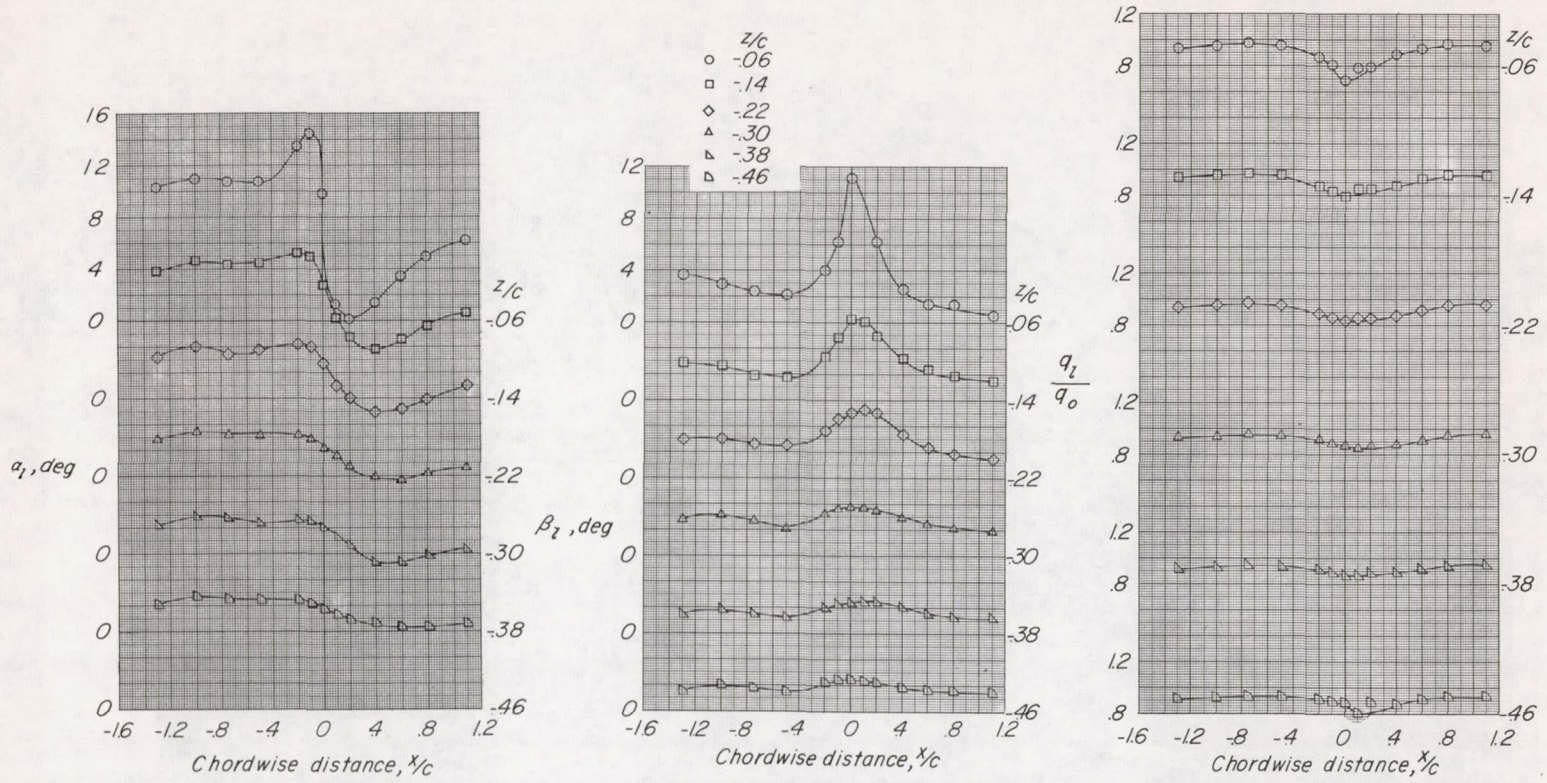

(f) $\alpha = 8.2^{\circ}$.

Figure 8.- Continued.

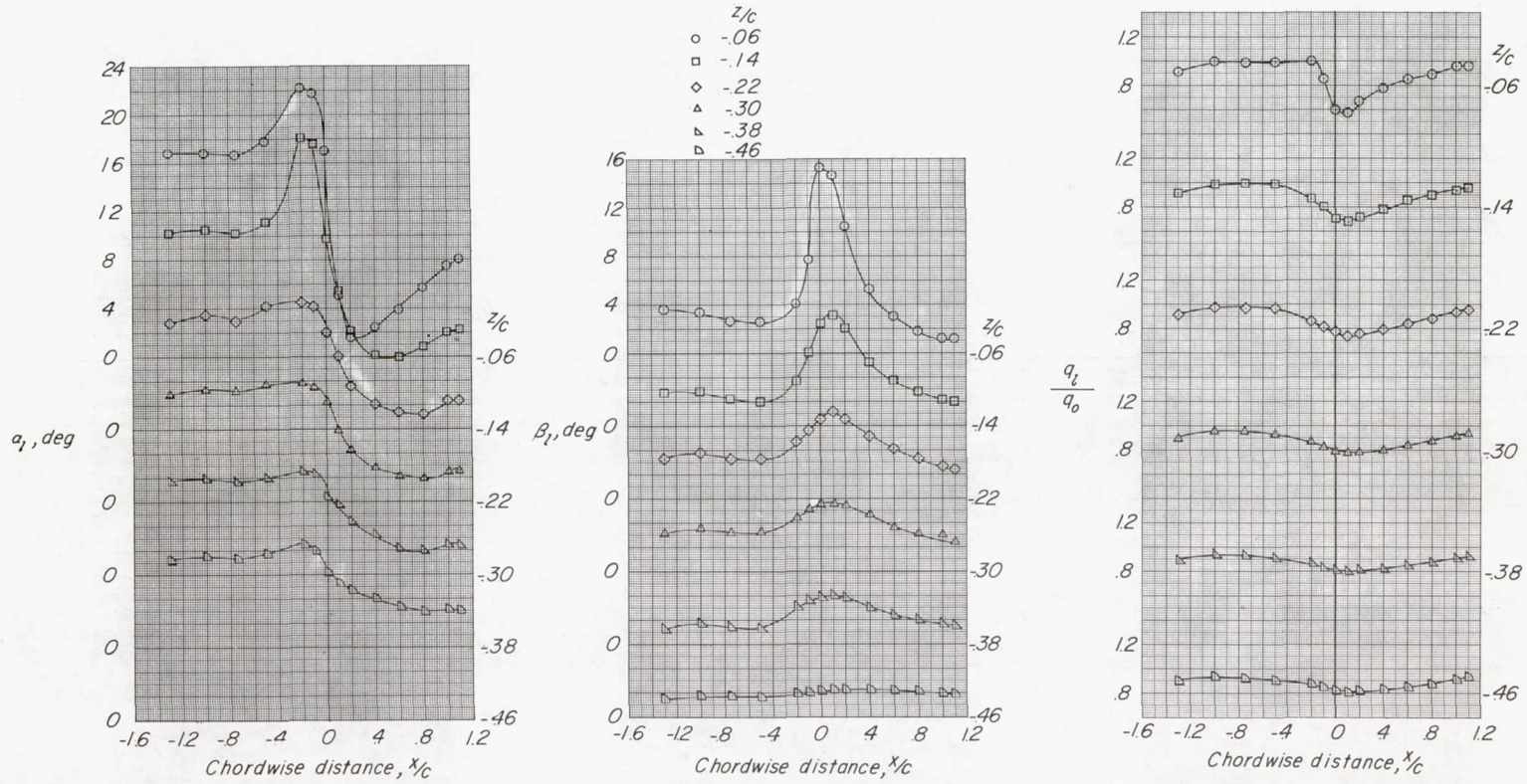

(g) $\alpha = 12.3^{\circ}$.

Figure 8.- Continued.

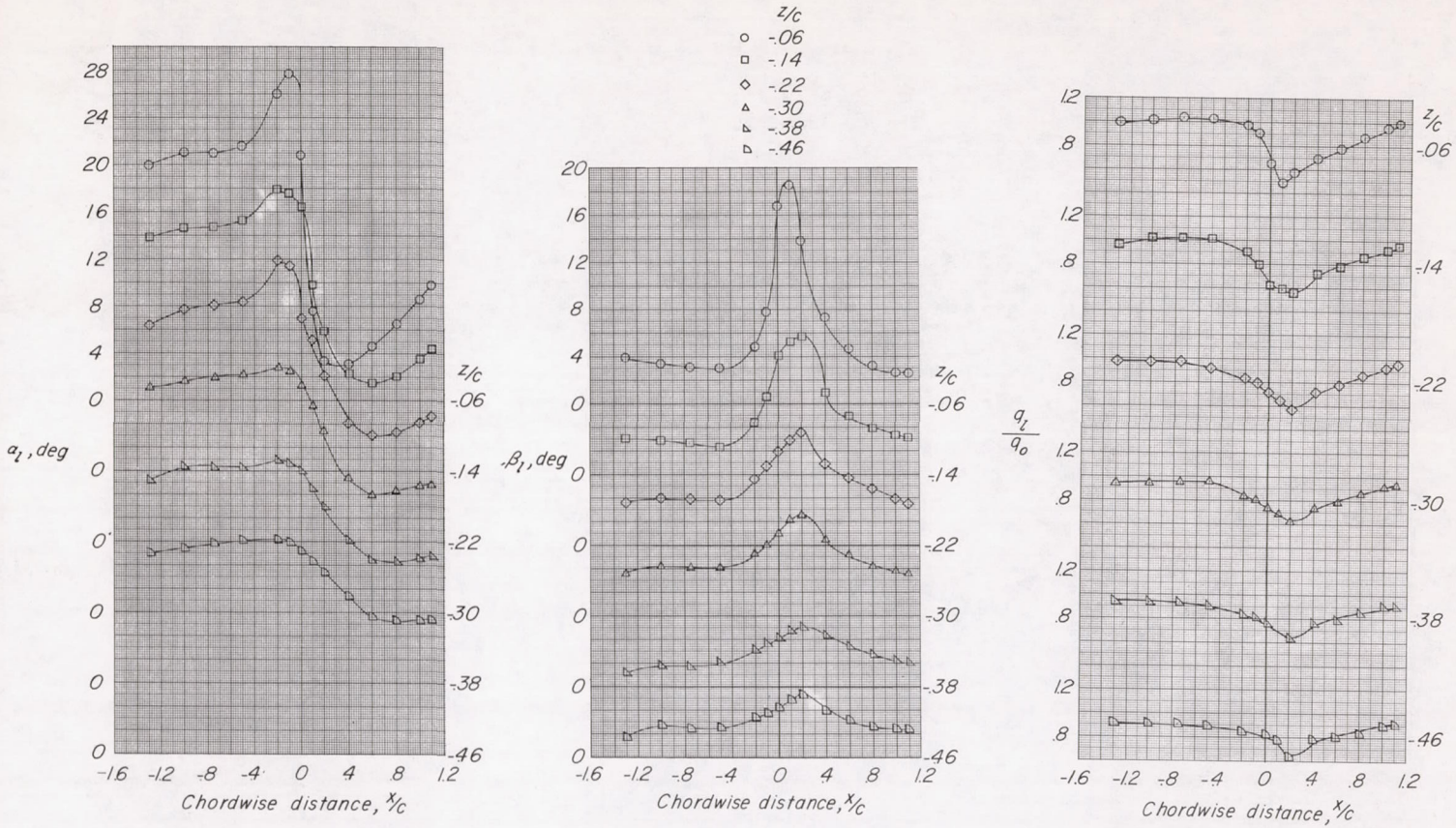

(h) $\alpha = 16.4°$.

Figure 8.- Continued.

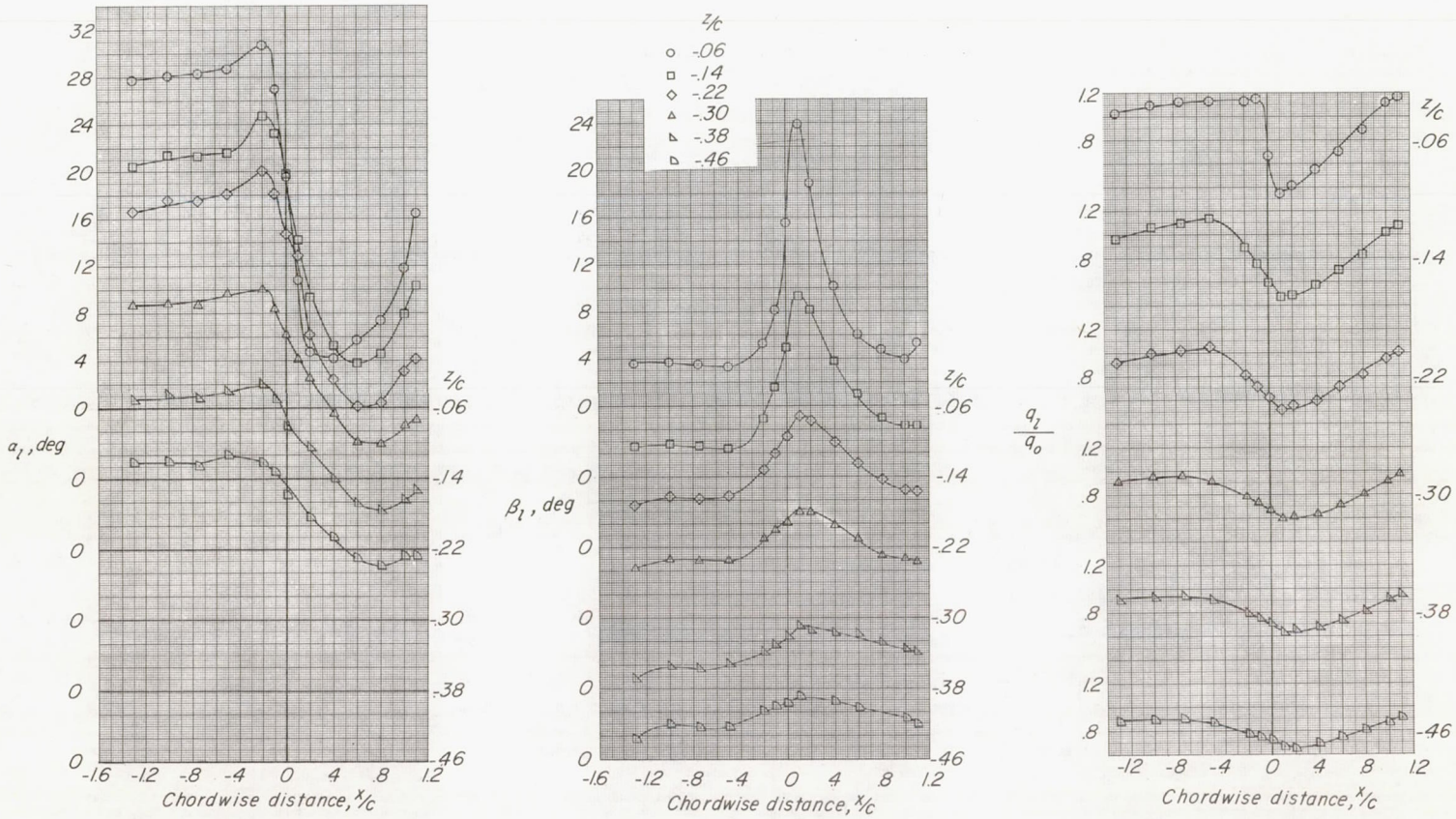

(i) $\alpha = 24.3^{\circ}$.

Figure 8.- Concluded.

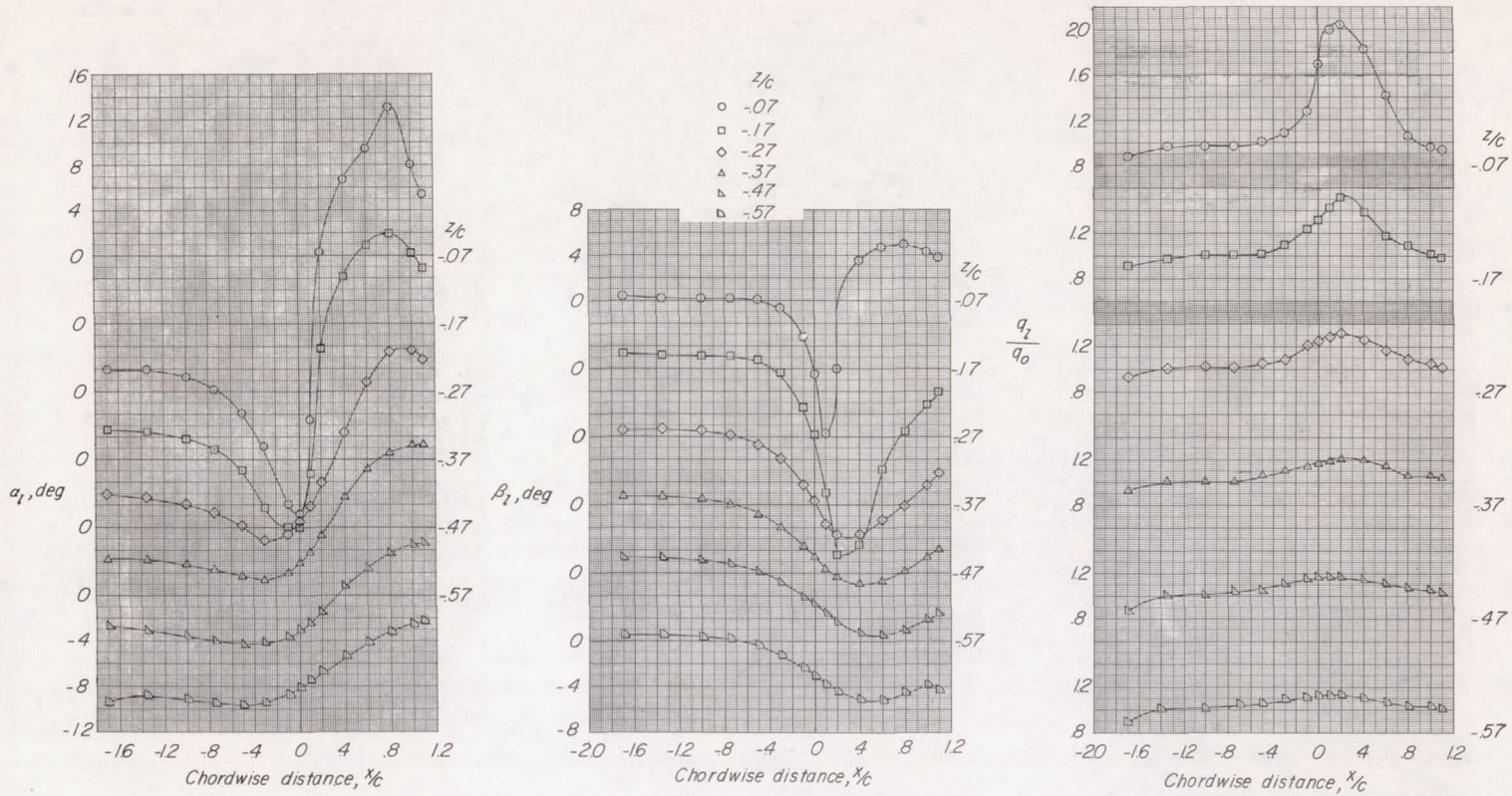

(a) $\alpha = -8.5^{\circ}$.

Figure 9.- Flow-field characteristics of swept-wing—fuselage combination at $y/\frac{b}{2} = -0.50$.

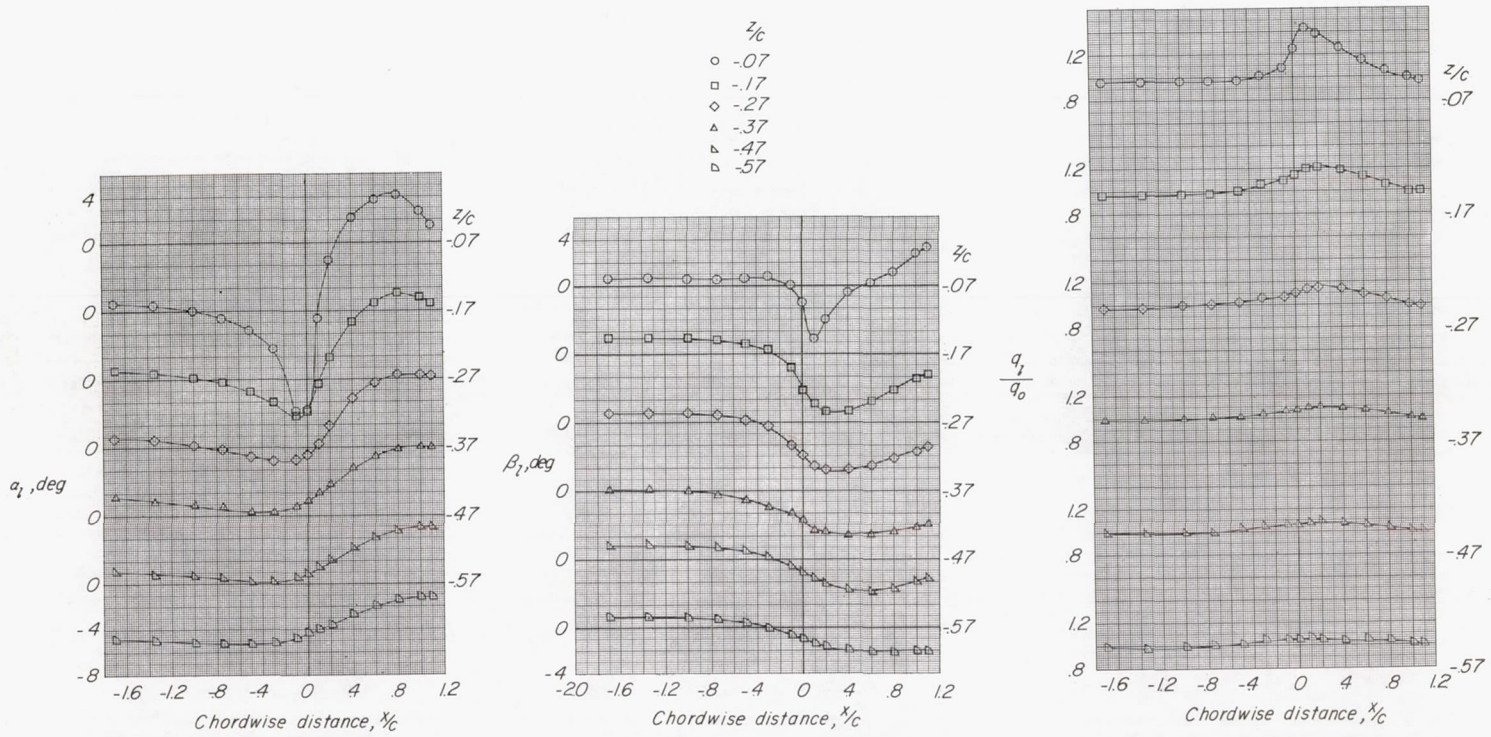

(b) $\alpha = -4.3^\circ$.

Figure 9.- Continued.

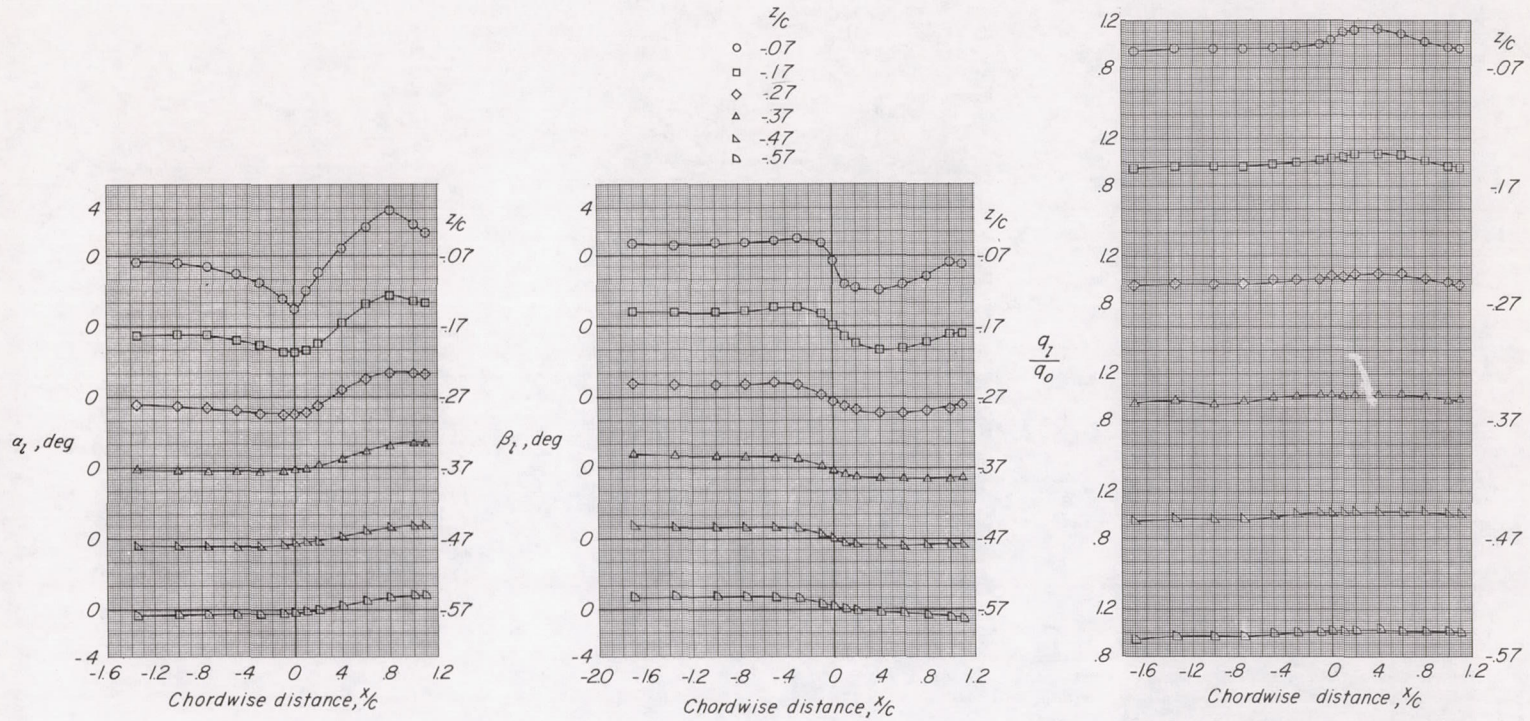

(c) $\alpha = -0.2^{\circ}$.

Figure 9.- Continued.

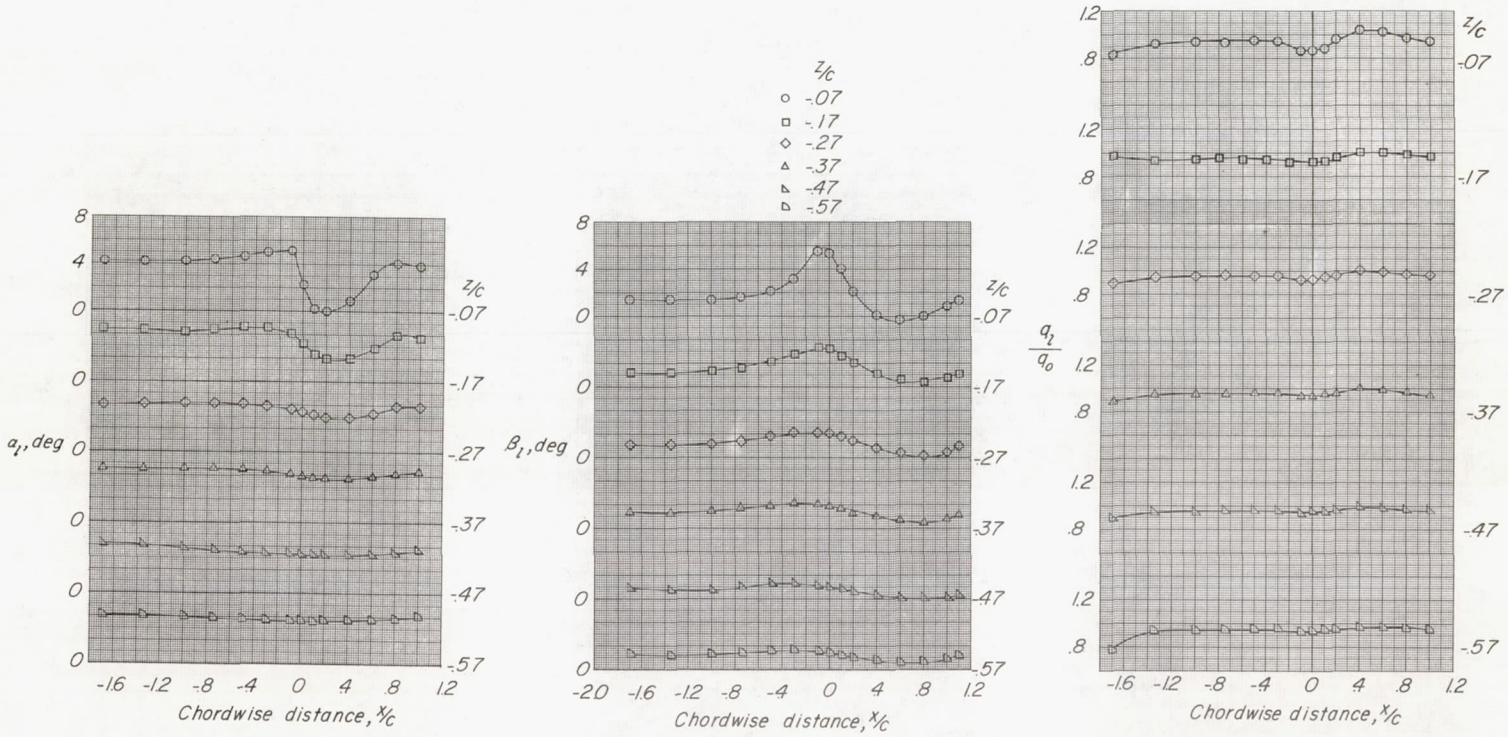

(d) $\alpha = 3.8^{\circ}$.

Figure 9.- Continued.

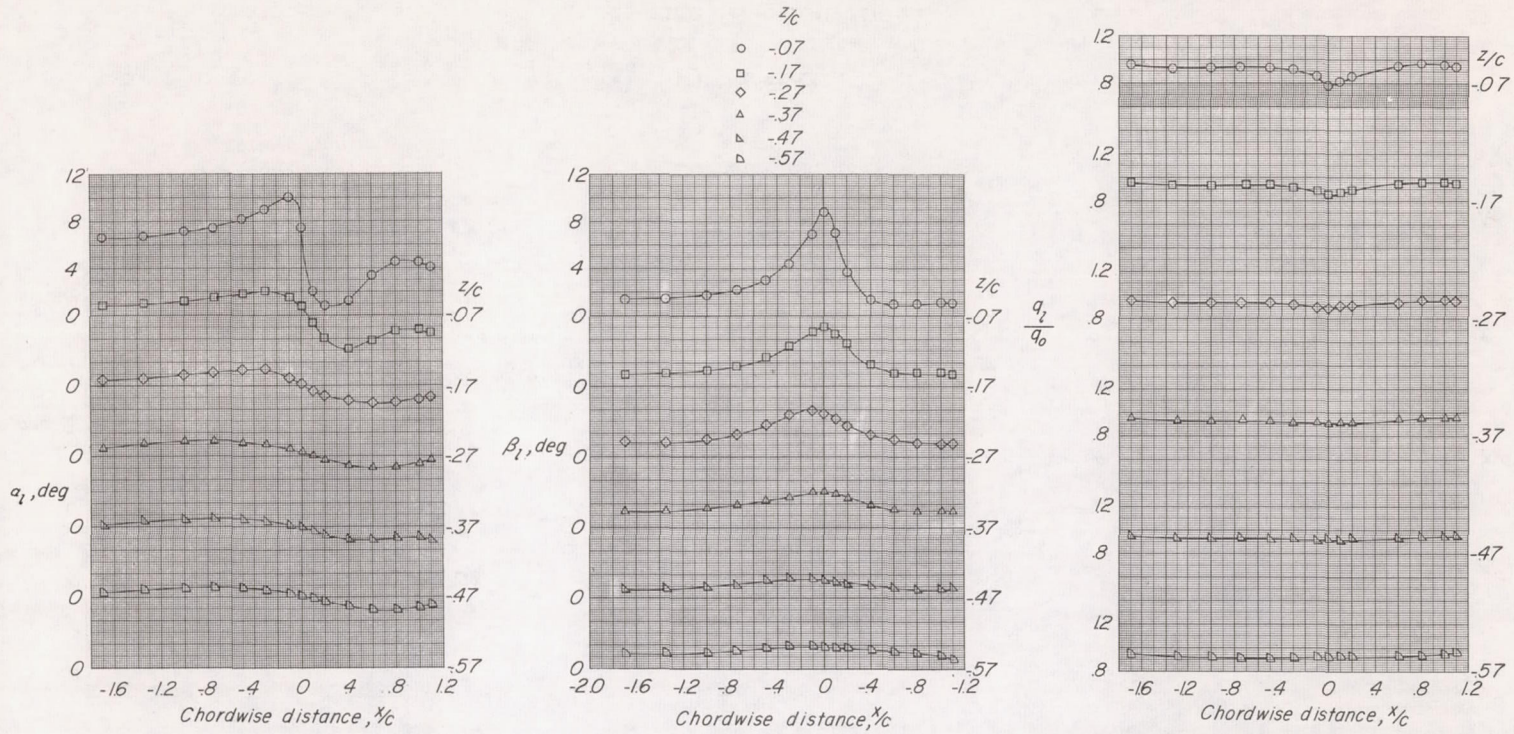

(e) $\alpha = 6.1^{\circ}$.

Figure 9.- Continued.

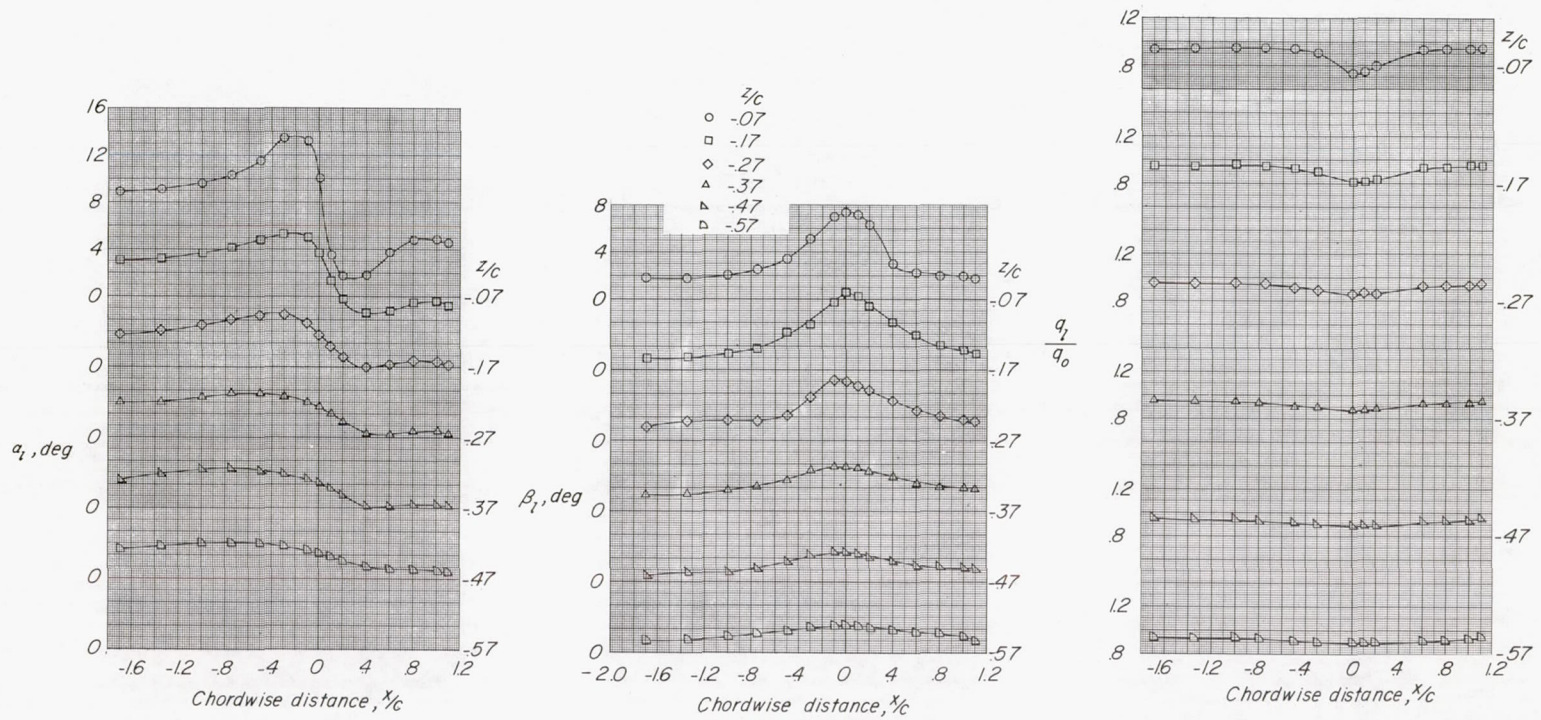

(f) $\alpha = 8.2^{\circ}$.

Figure 9.- Continued.

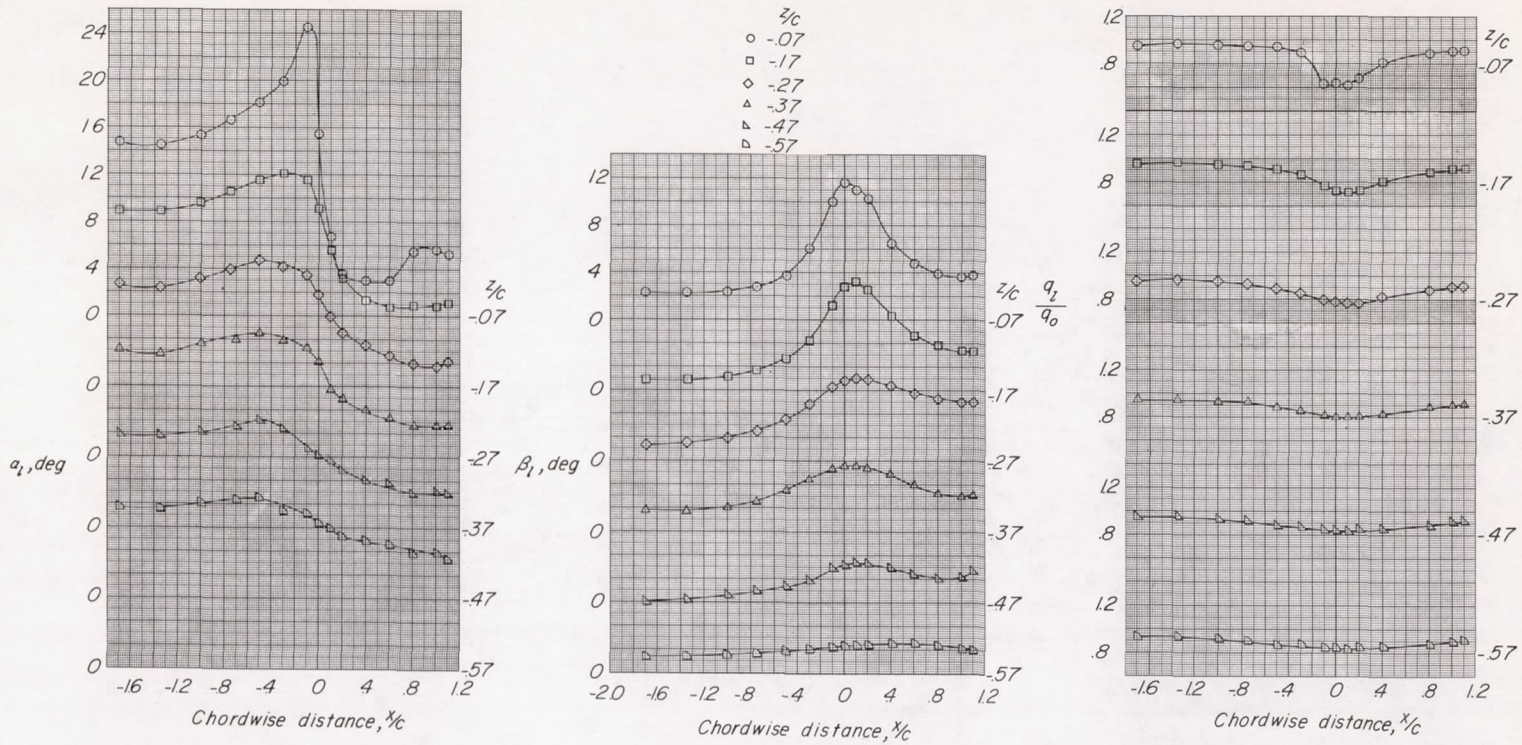

(g) $\alpha = 12.3^{\circ}$.

Figure 9.- Continued.

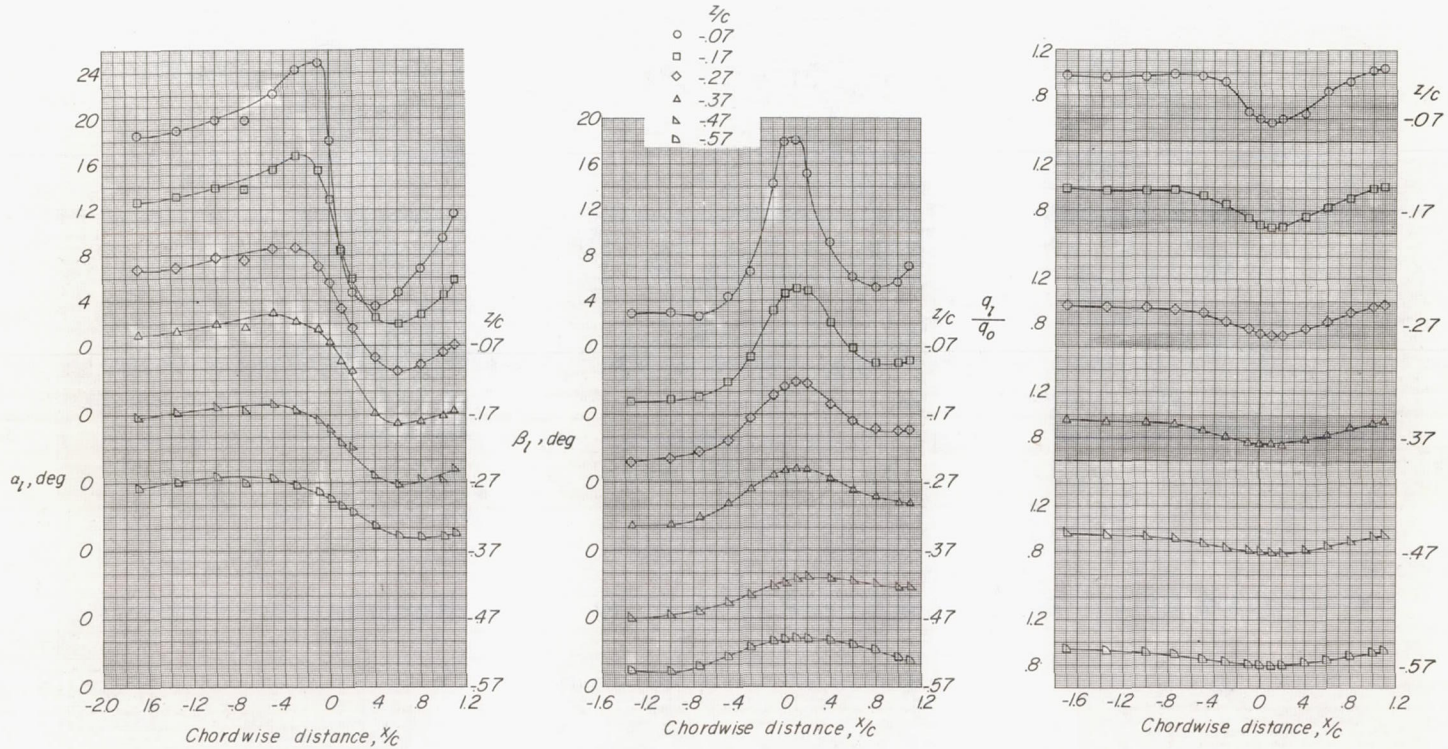

(h) $\alpha = 16.4^{\circ}$.

Figure 9.- Continued.

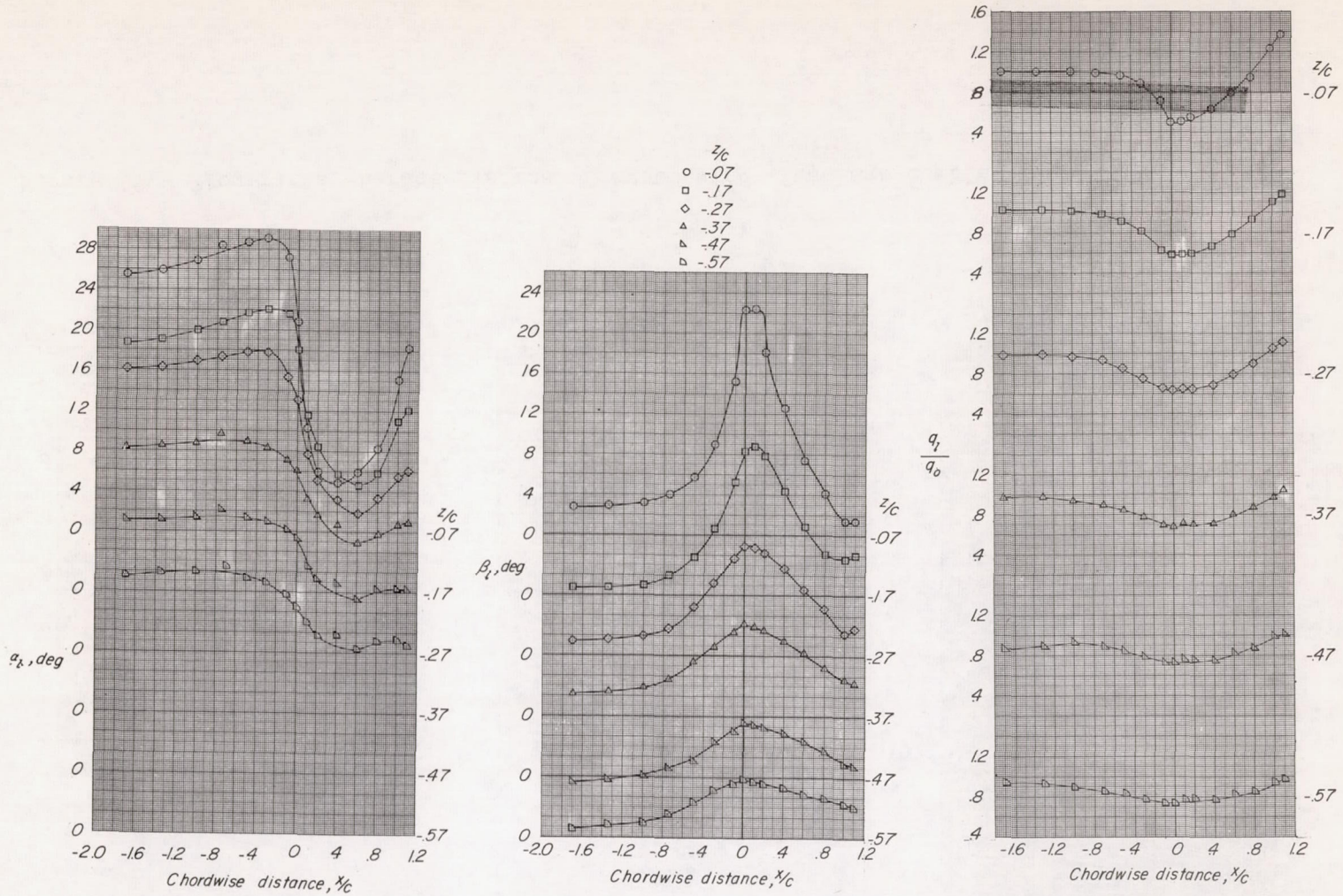

(i) $\alpha = 24.3^{\circ}$.

Figure 9.- Concluded.

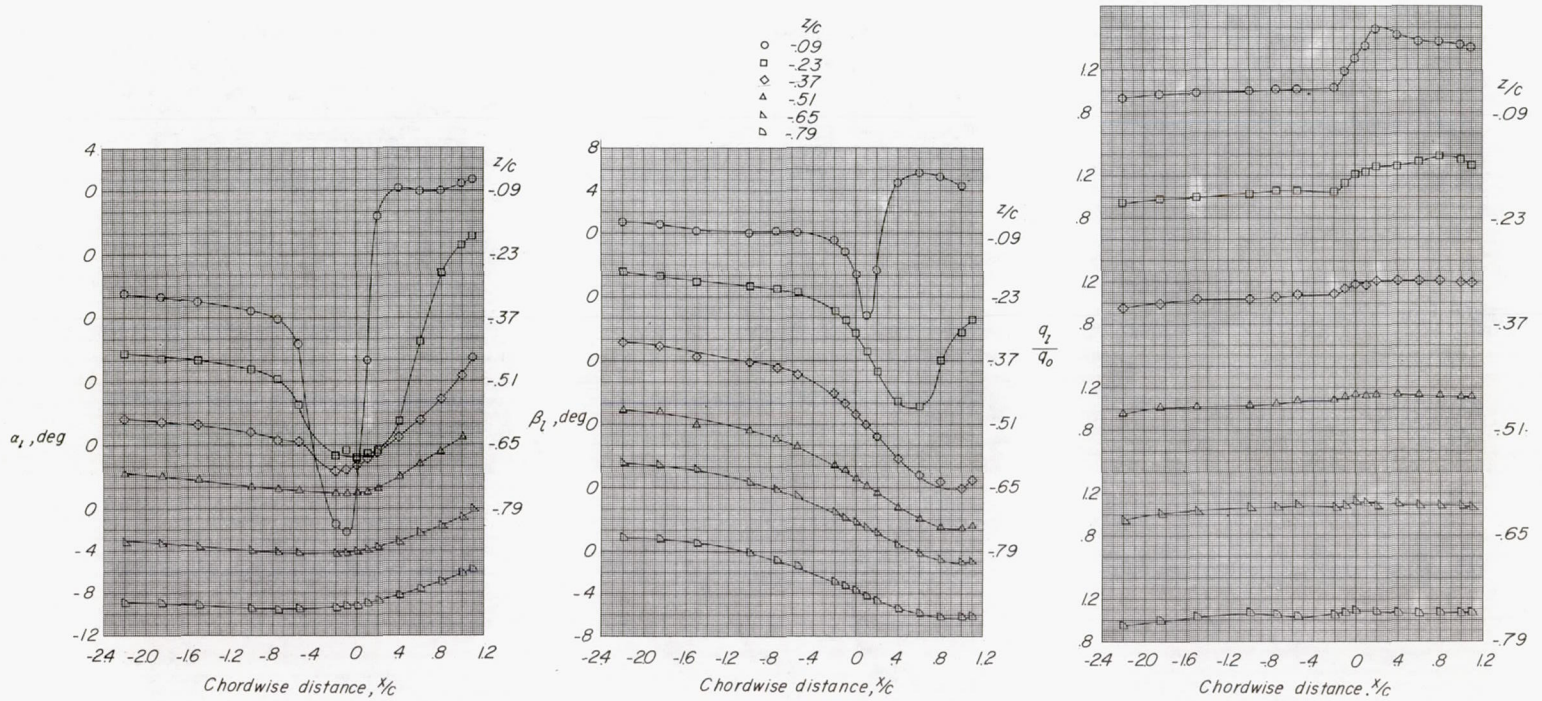

(a) $\alpha = -8.5^{\circ}$.

Figure 10.- Flow-field characteristics of swept-wing—fuselage combination at $y/\frac{b}{2} = -0.75$.

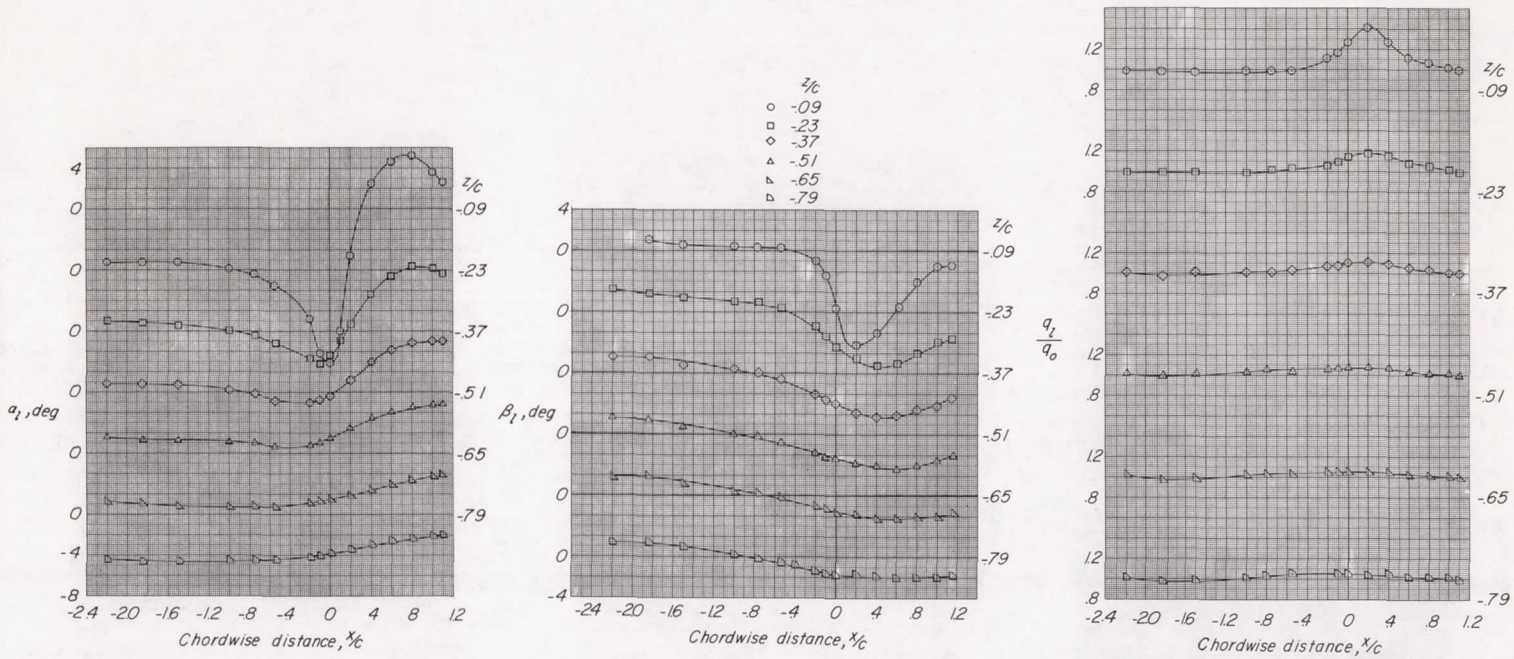

(b) $\alpha = -4.3^{\circ}$.

Figure 10.- Continued.

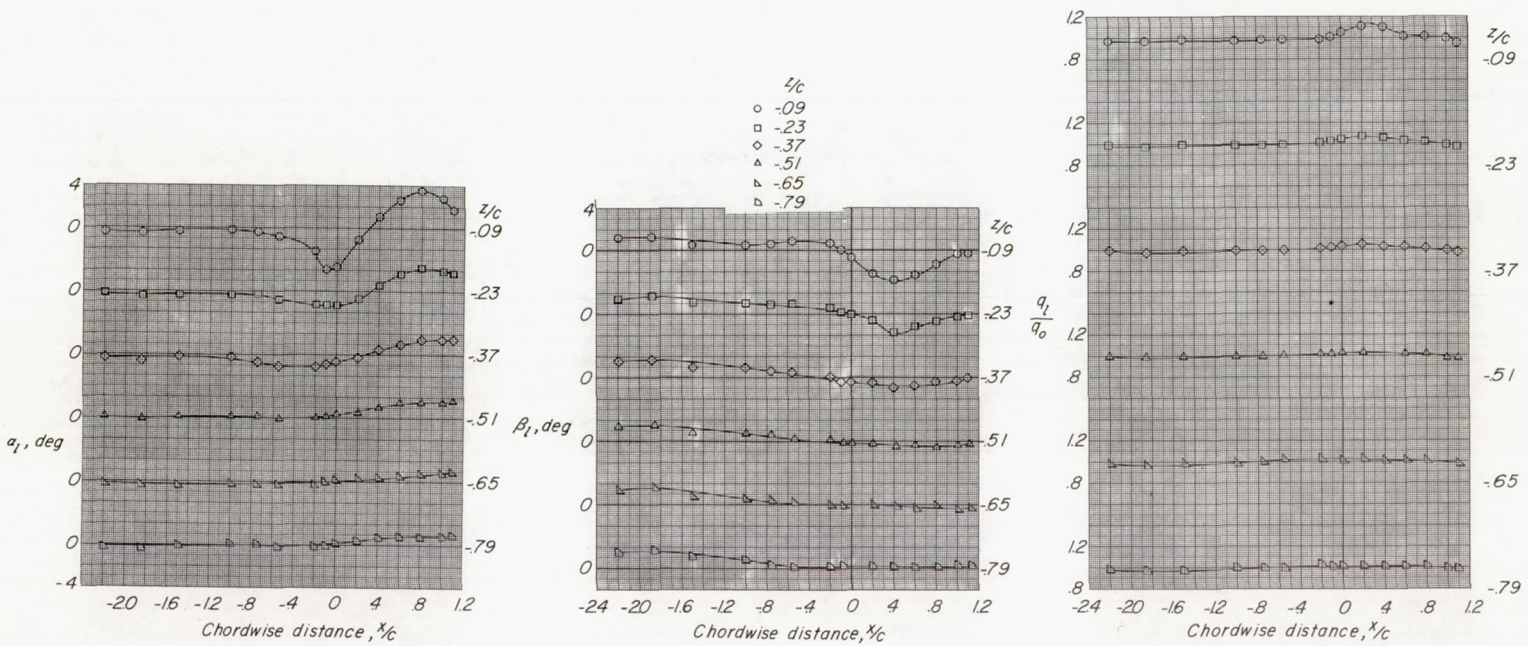

(c) $\alpha = -0.2^{\circ}$.

Figure 10.- Continued.

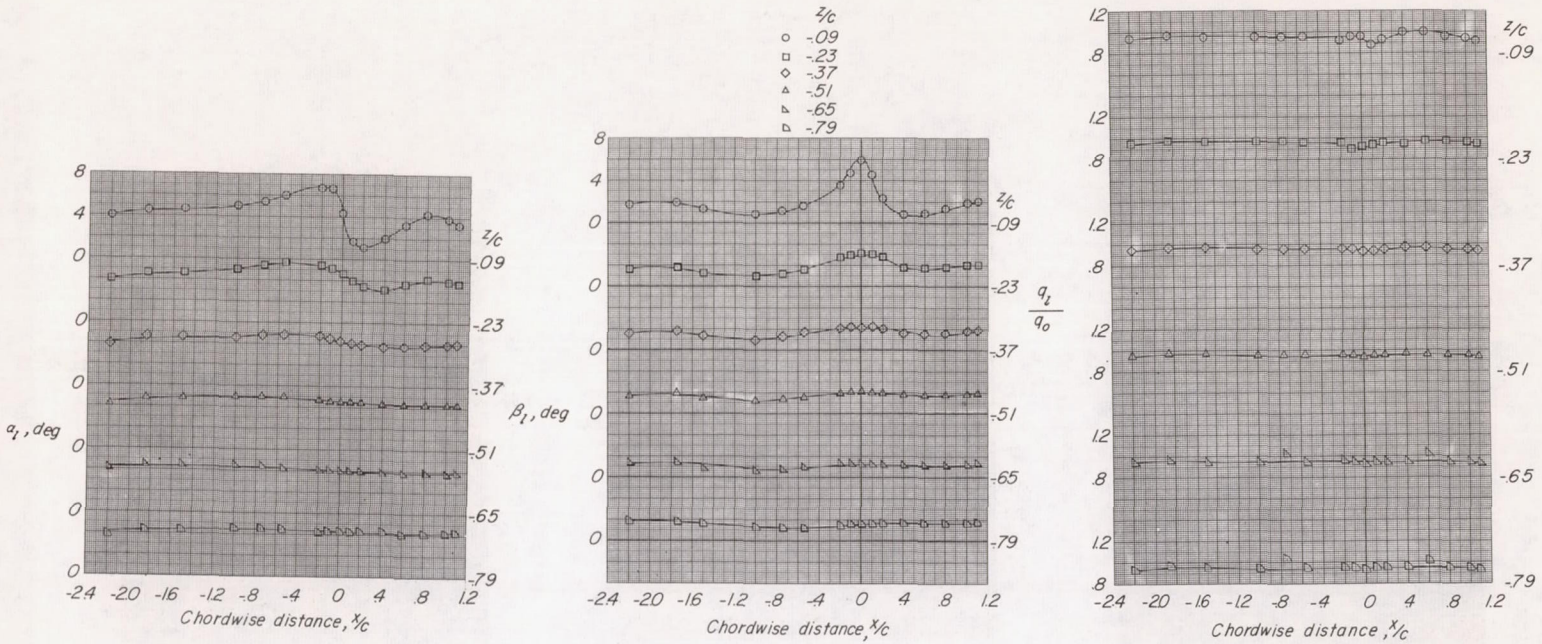

(d) $\alpha = 3.8^{\circ}$.

Figure 10.- Continued.

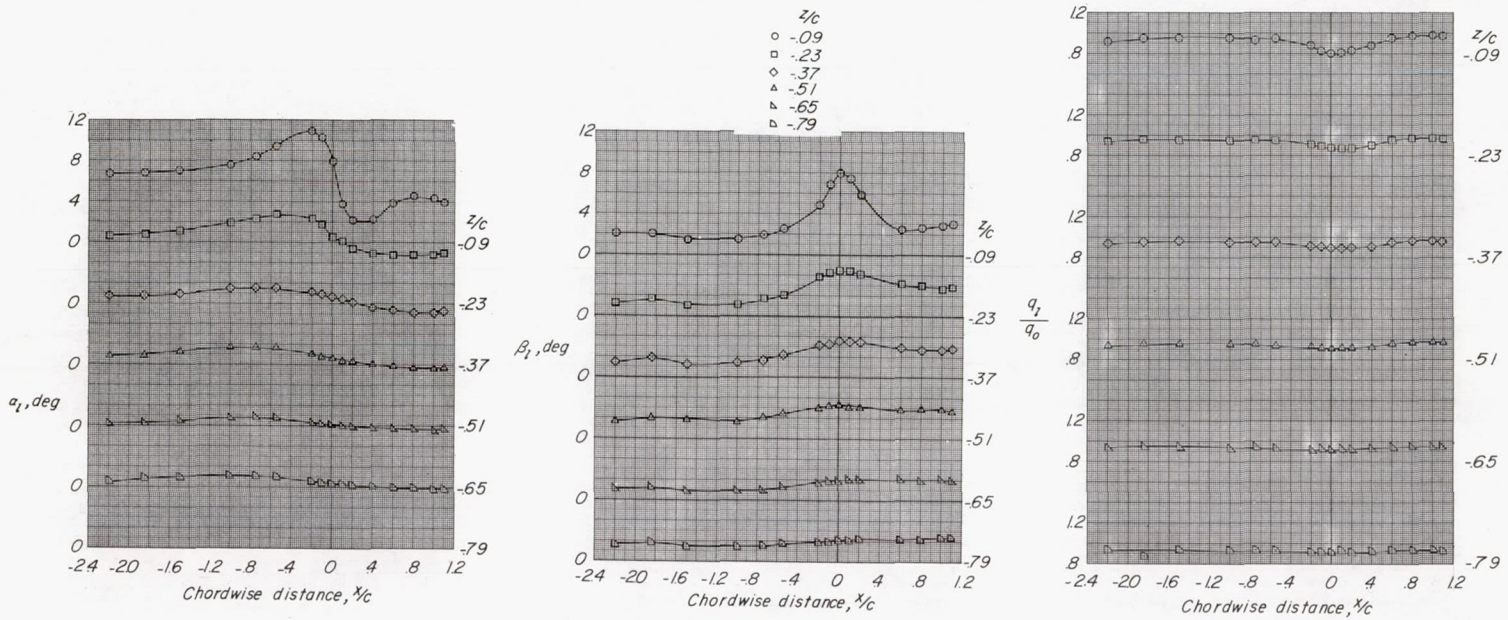

(e) $\alpha = 6.1^{\circ}$.

Figure 10.- Continued.

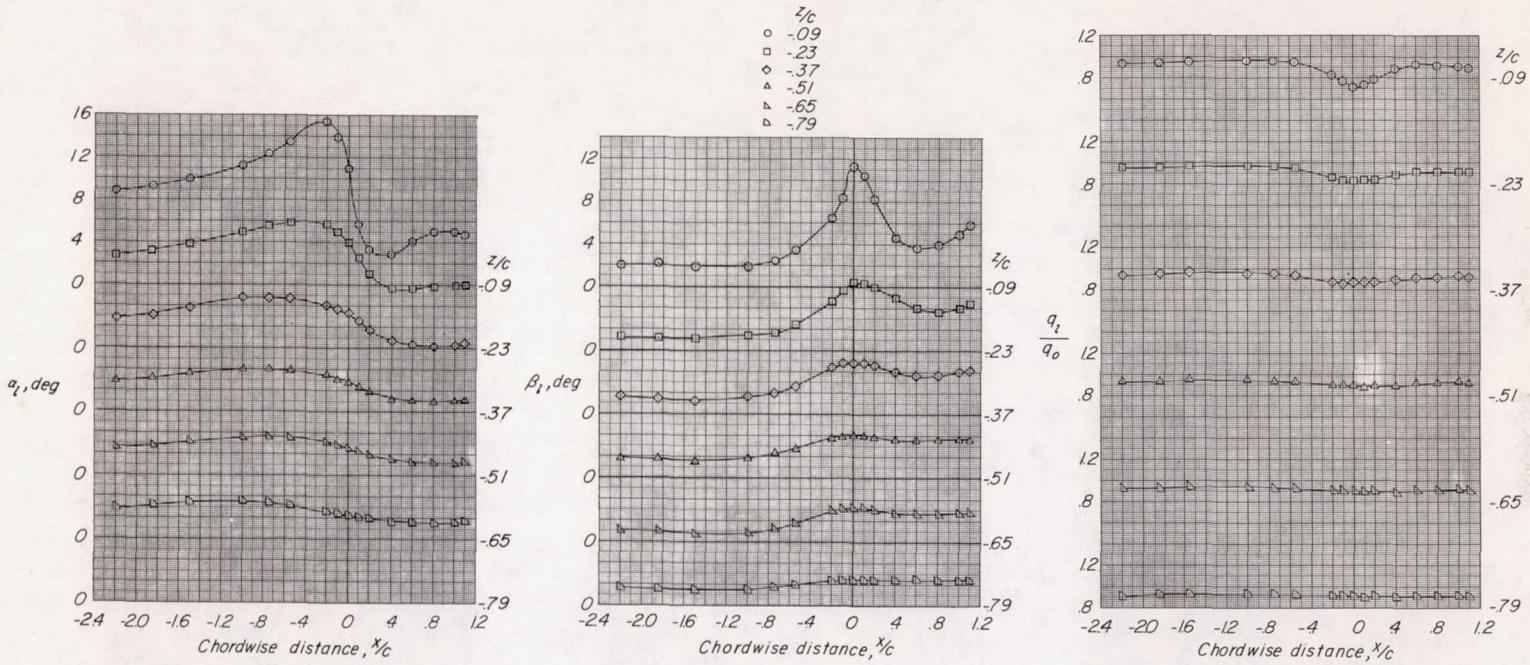

(f) $\alpha = 8.2^{\circ}$.

Figure 10.- Continued.

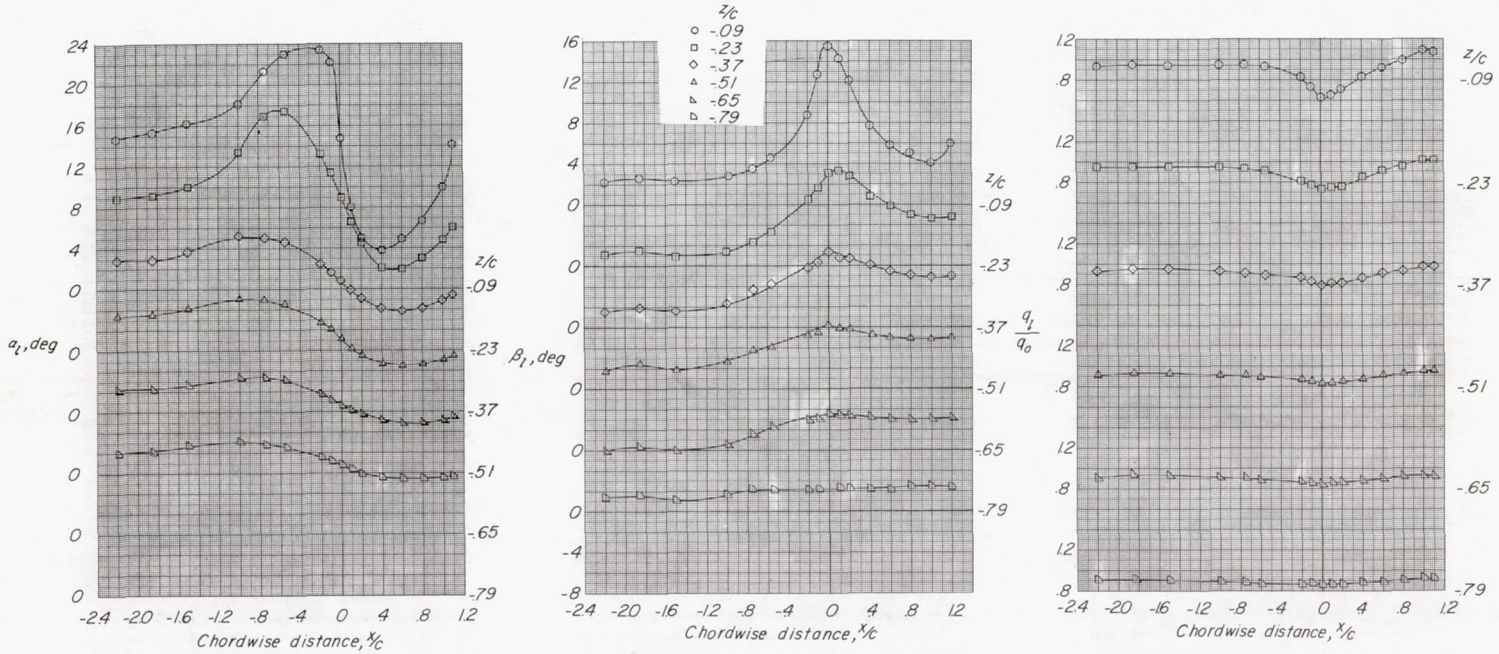

(g) $\alpha = 12.3^{\circ}$.

Figure 10.- Continued.

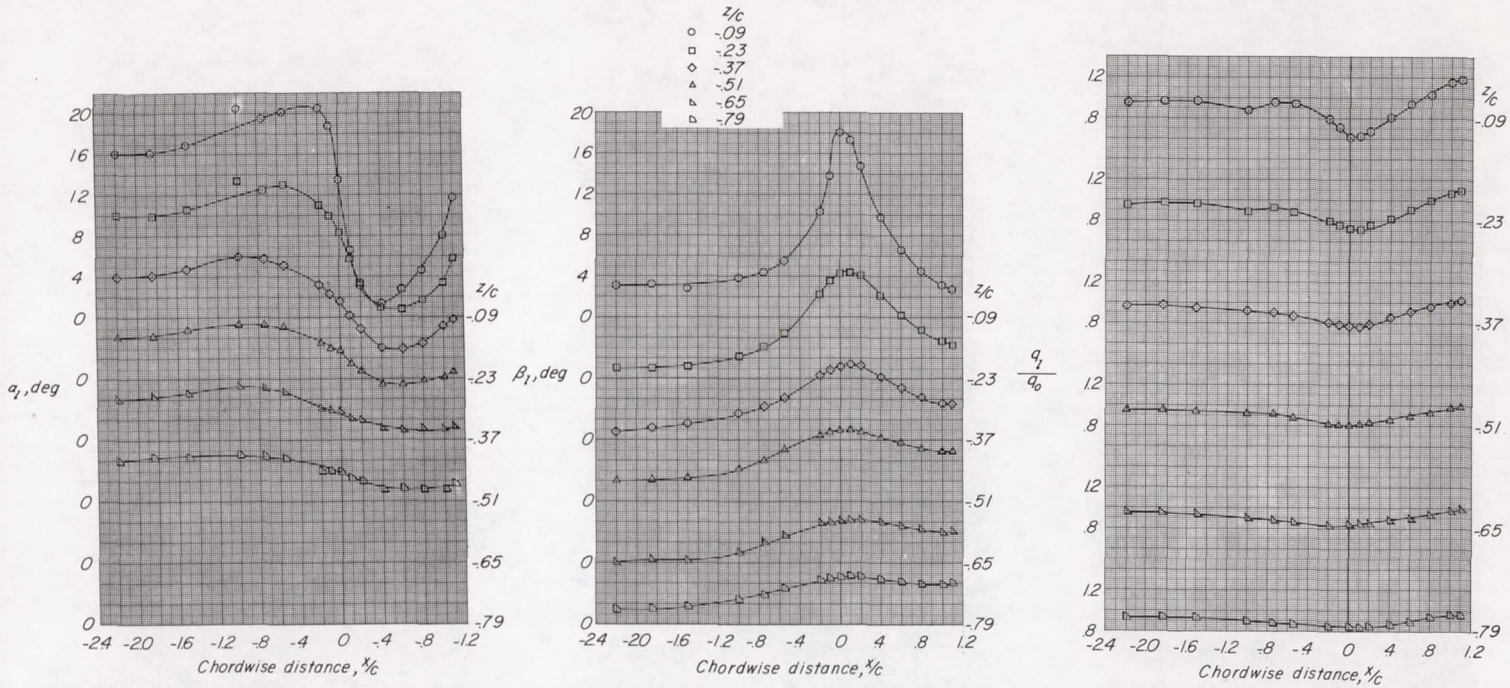

(h) $\alpha = 16.4^{\circ}$.

Figure 10.- Continued.

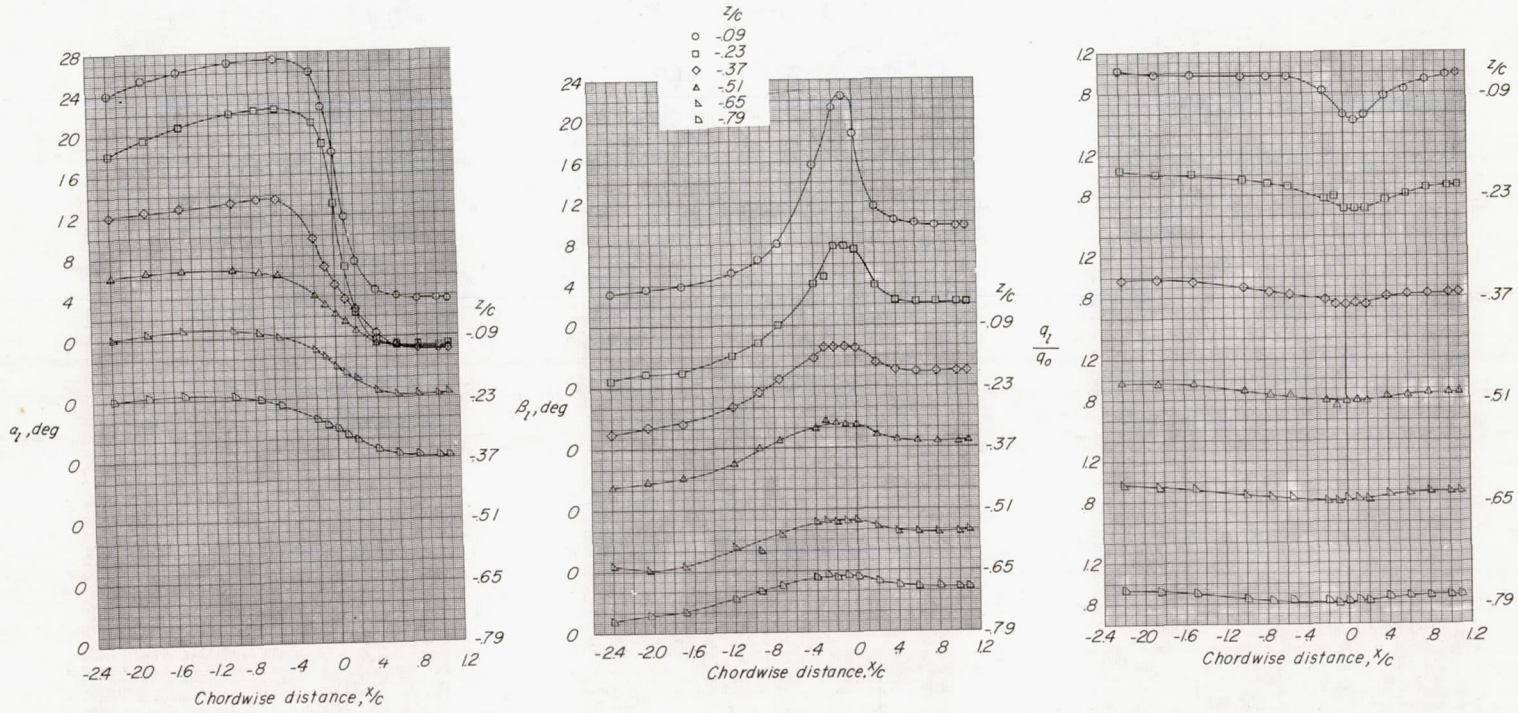

(i) $\alpha = 24.3^{\circ}$.

Figure 10.- Concluded.

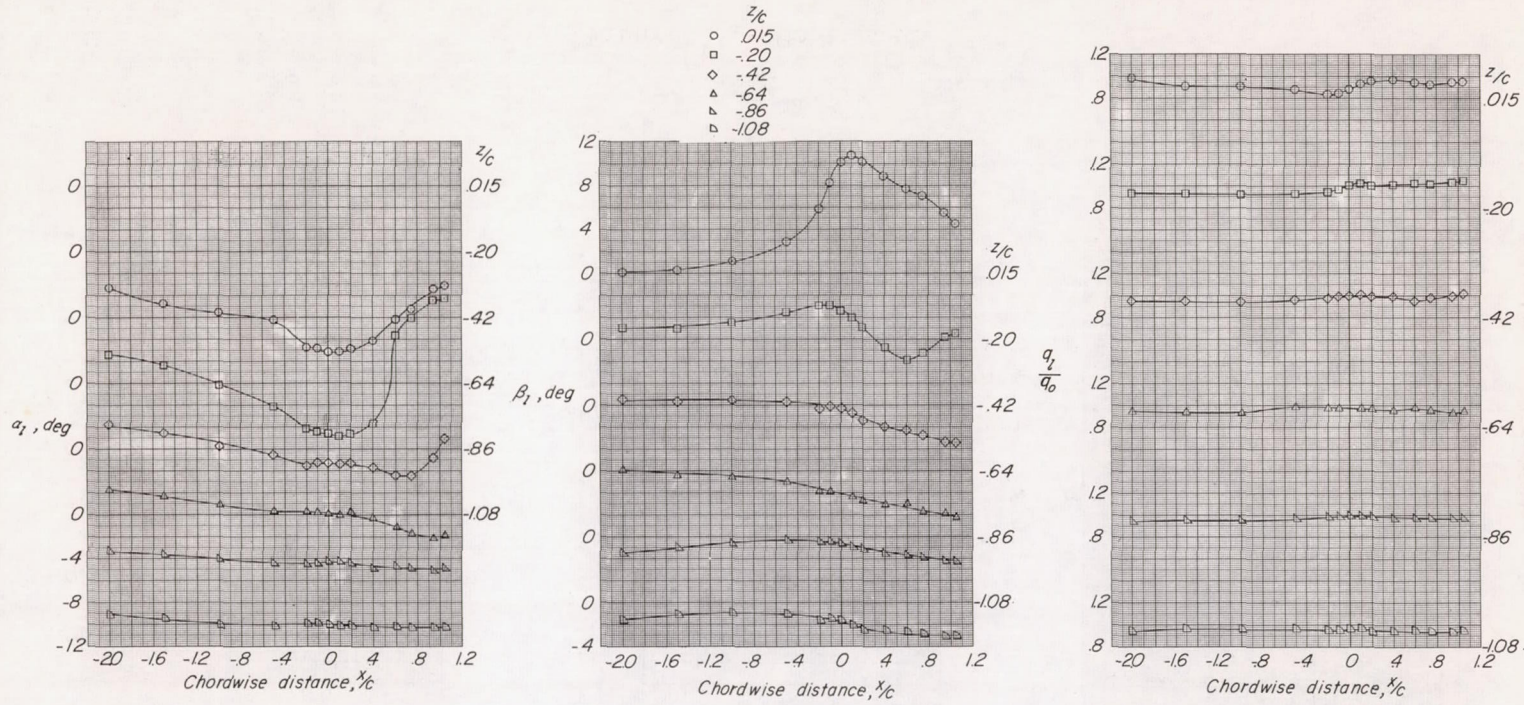

(a) $\alpha = -8.5°$.

Figure 11.- Flow-field characteristics of swept-wing—fuselage combination at $y/\frac{b}{2} = -1.01$.

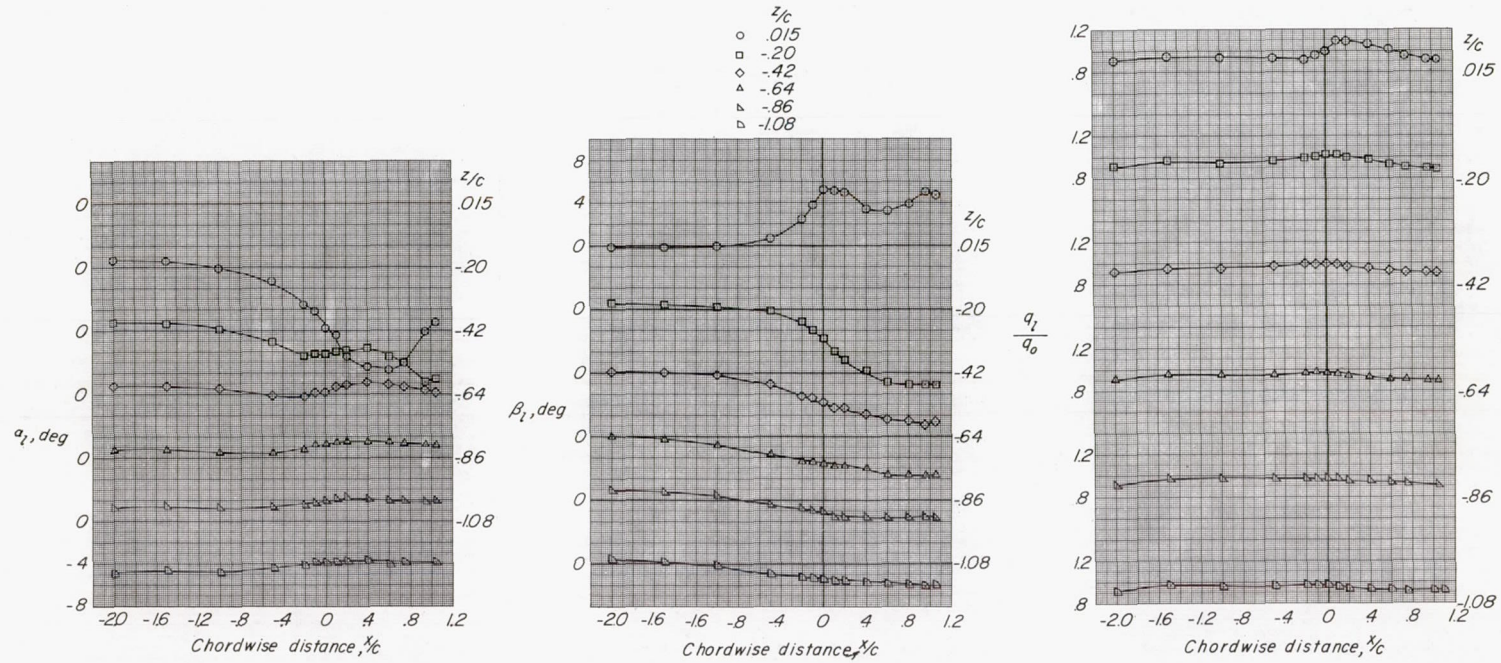

(b) $\alpha = -4.3^{\circ}$.

Figure 11.- Continued.

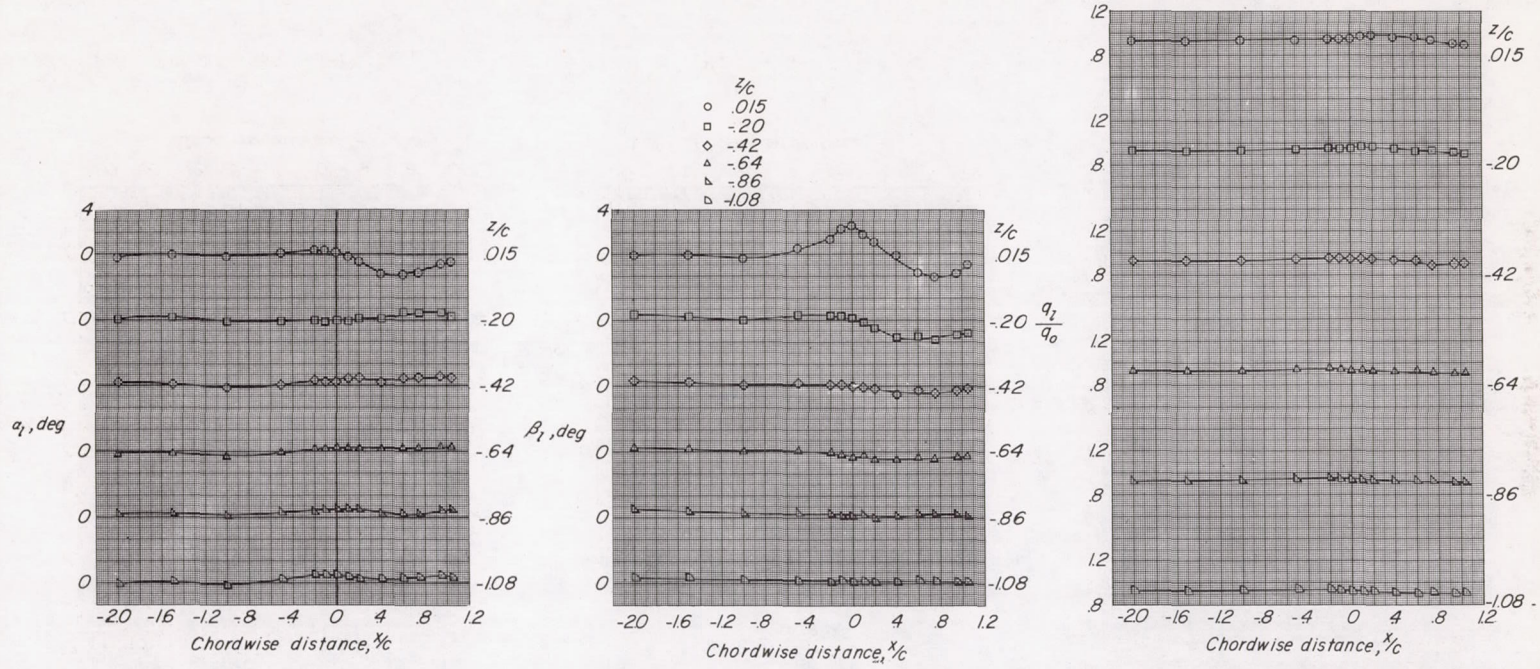

(c) $\alpha = -0.2^{\circ}$.

Figure 11.- Continued.

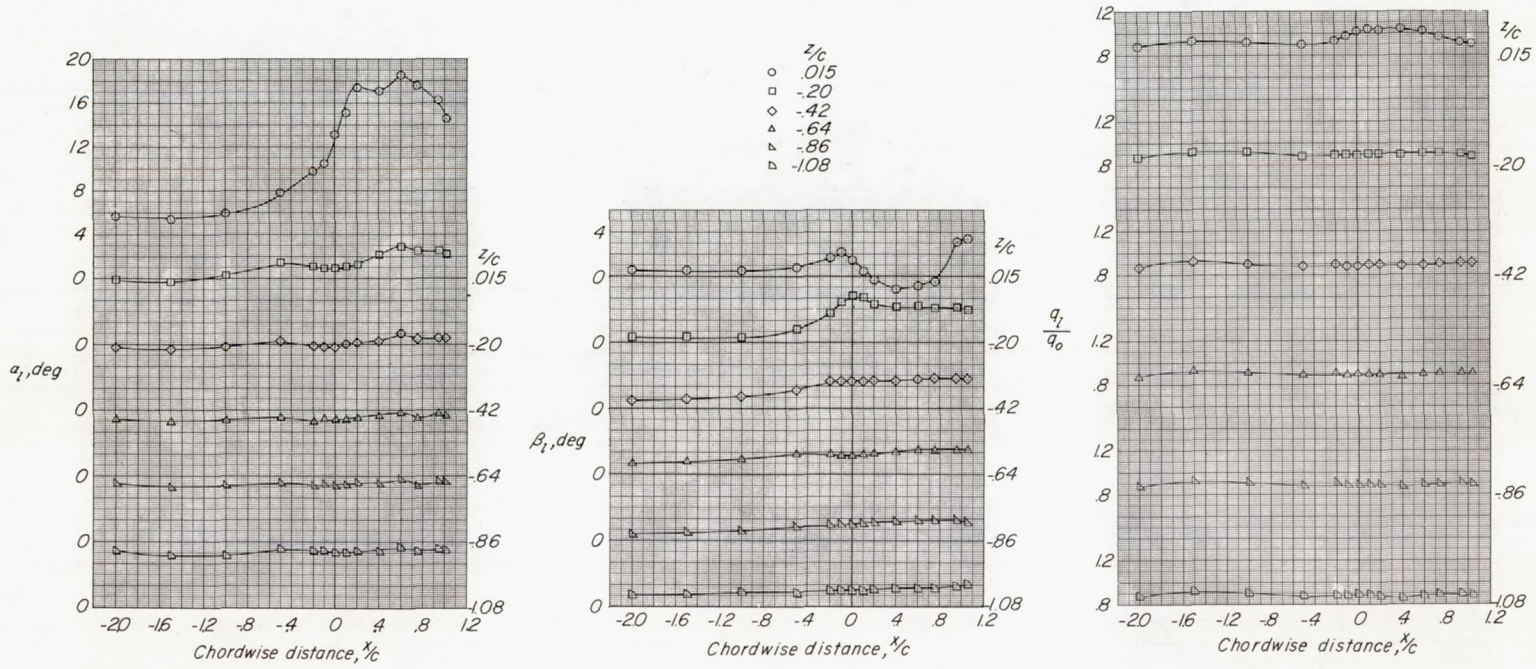

(d) $\alpha = 3.8^{\circ}$.

Figure 11.- Continued.

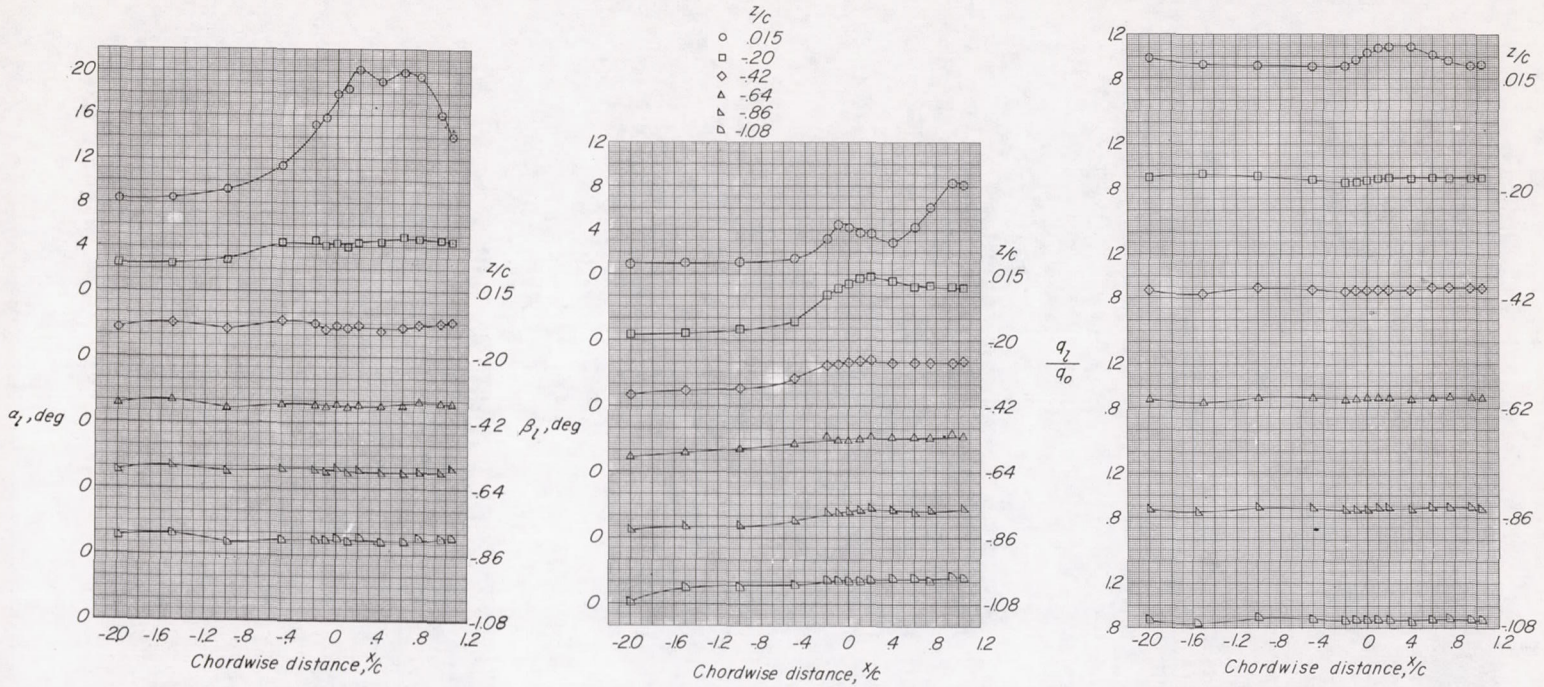

(e) $\alpha = 6.1^{\circ}$.

Figure 11.- Continued.

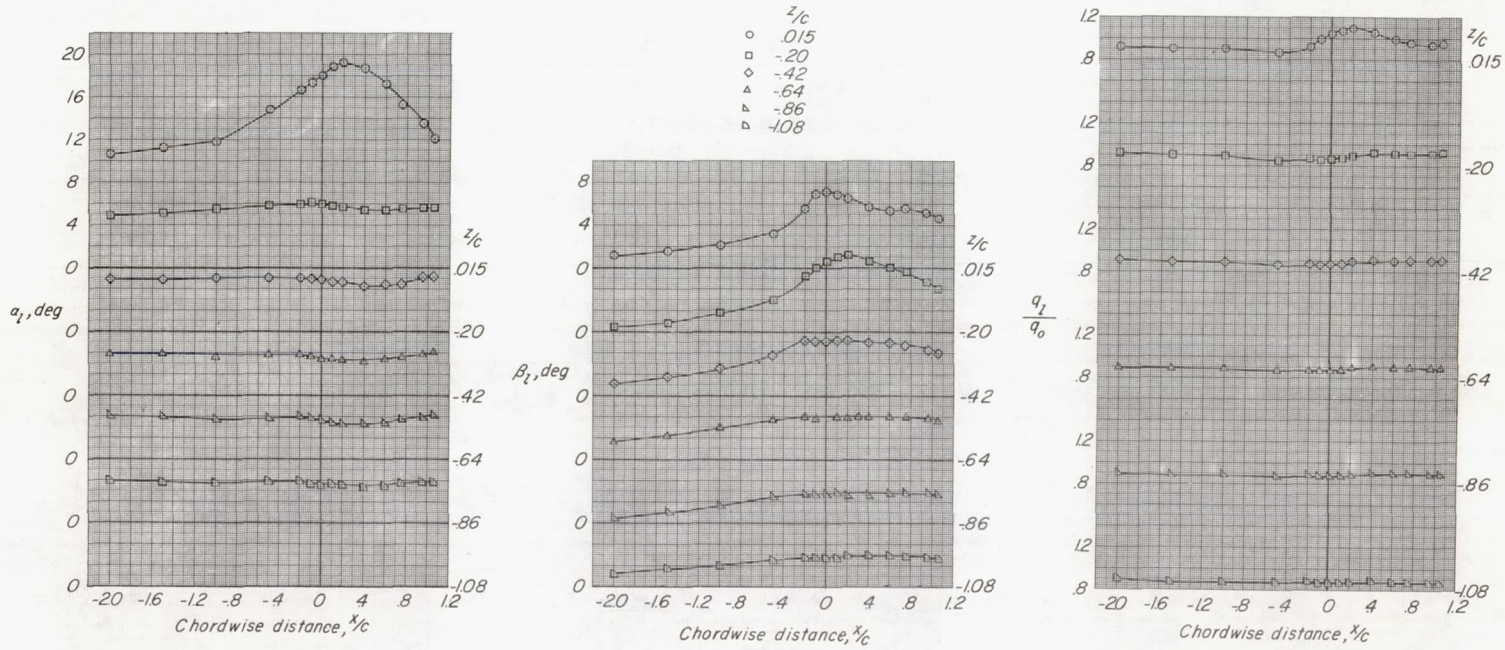

(f) $\alpha = 8.2^{\circ}$.

Figure 11.- Continued.

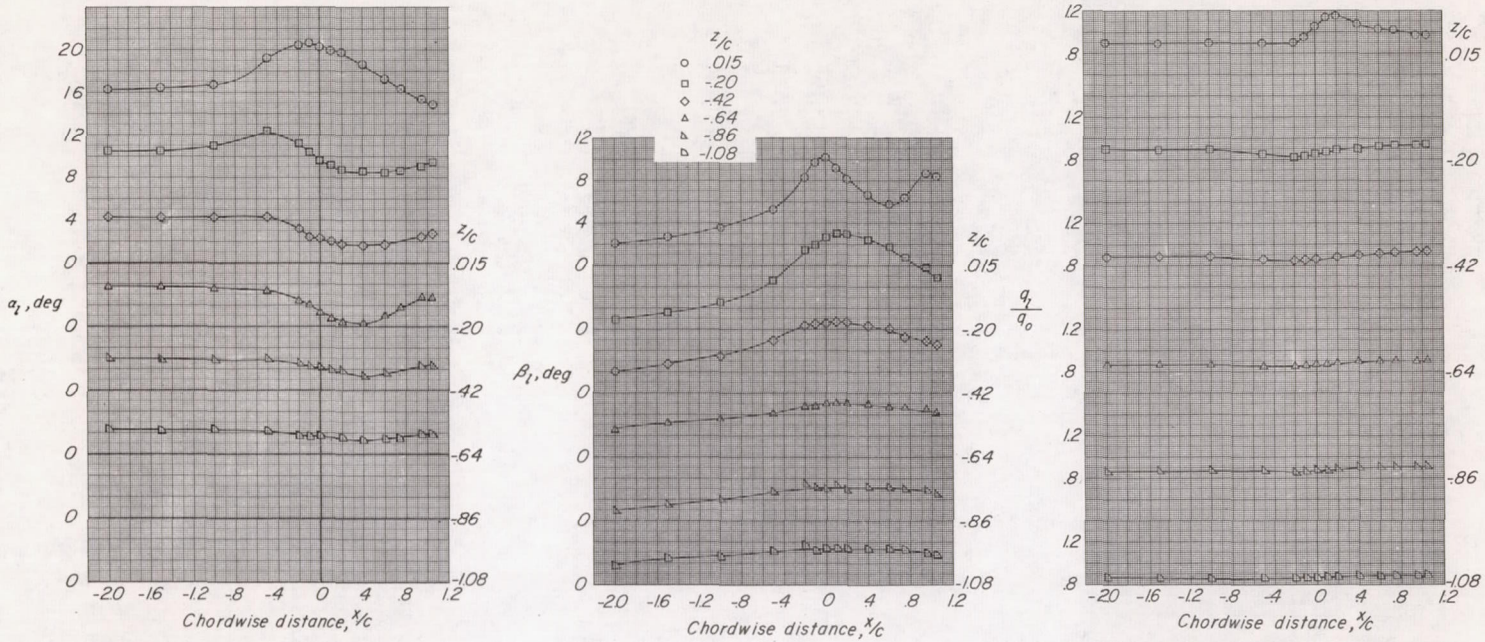

(g) $\alpha = 12.3^\circ$.

Figure 11.- Continued.

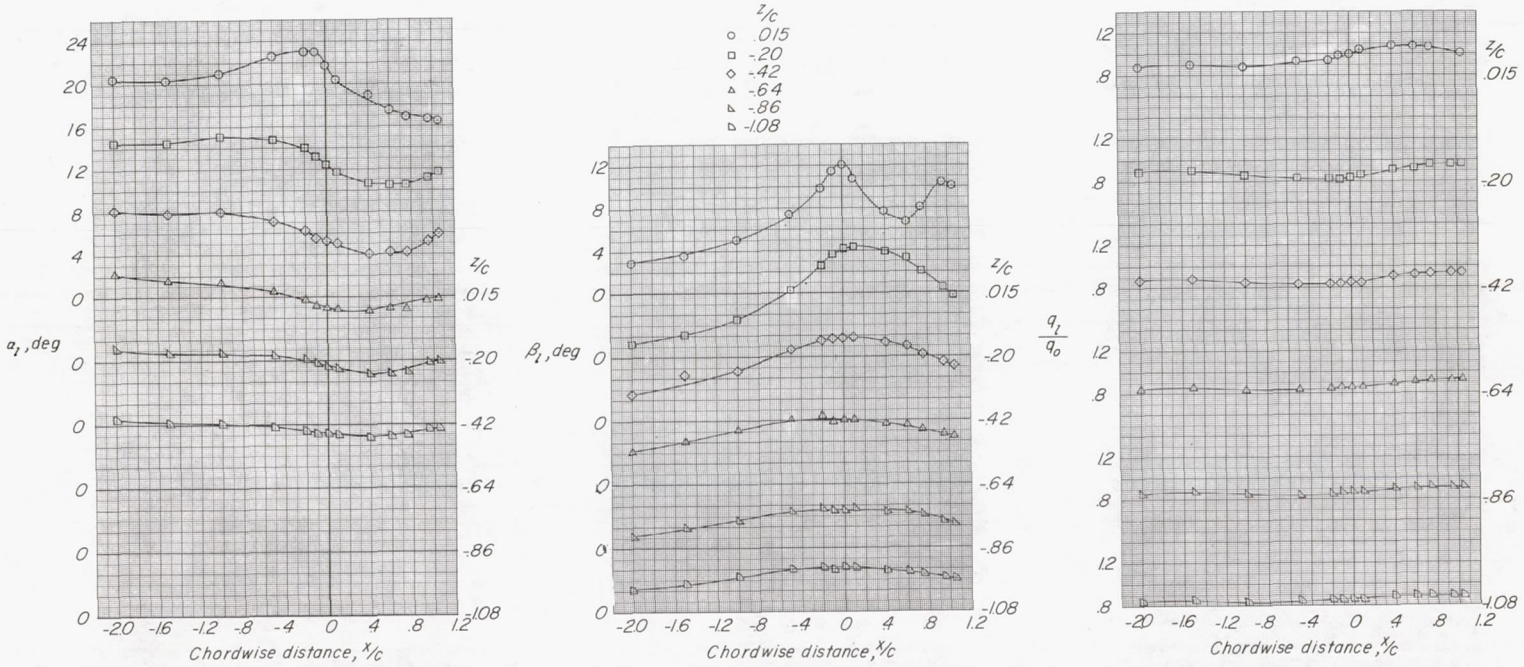

(h) $\alpha = 16.4^{\circ}$.

Figure 11.- Continued.

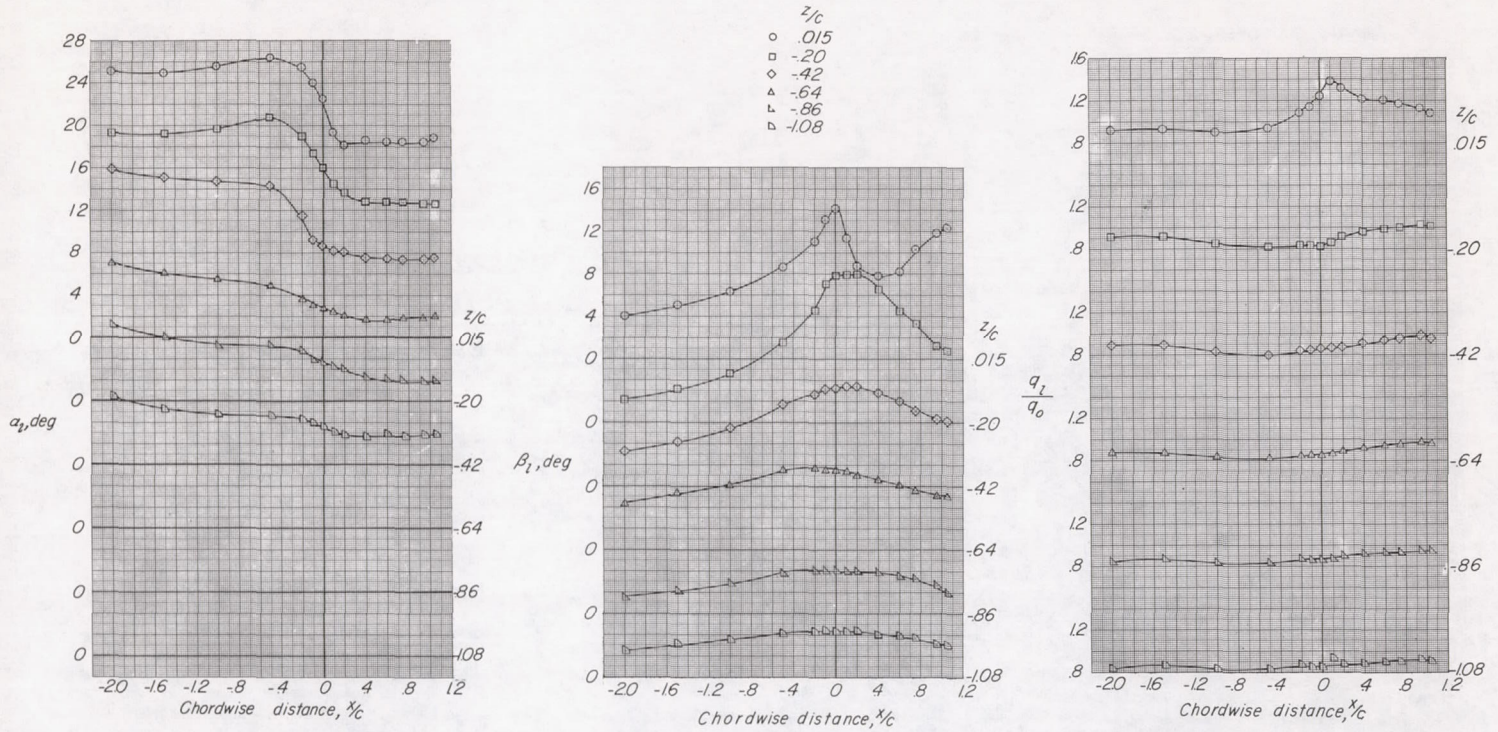

(i) $\alpha = 22.4^{\circ}$.

Figure 11.- Concluded.

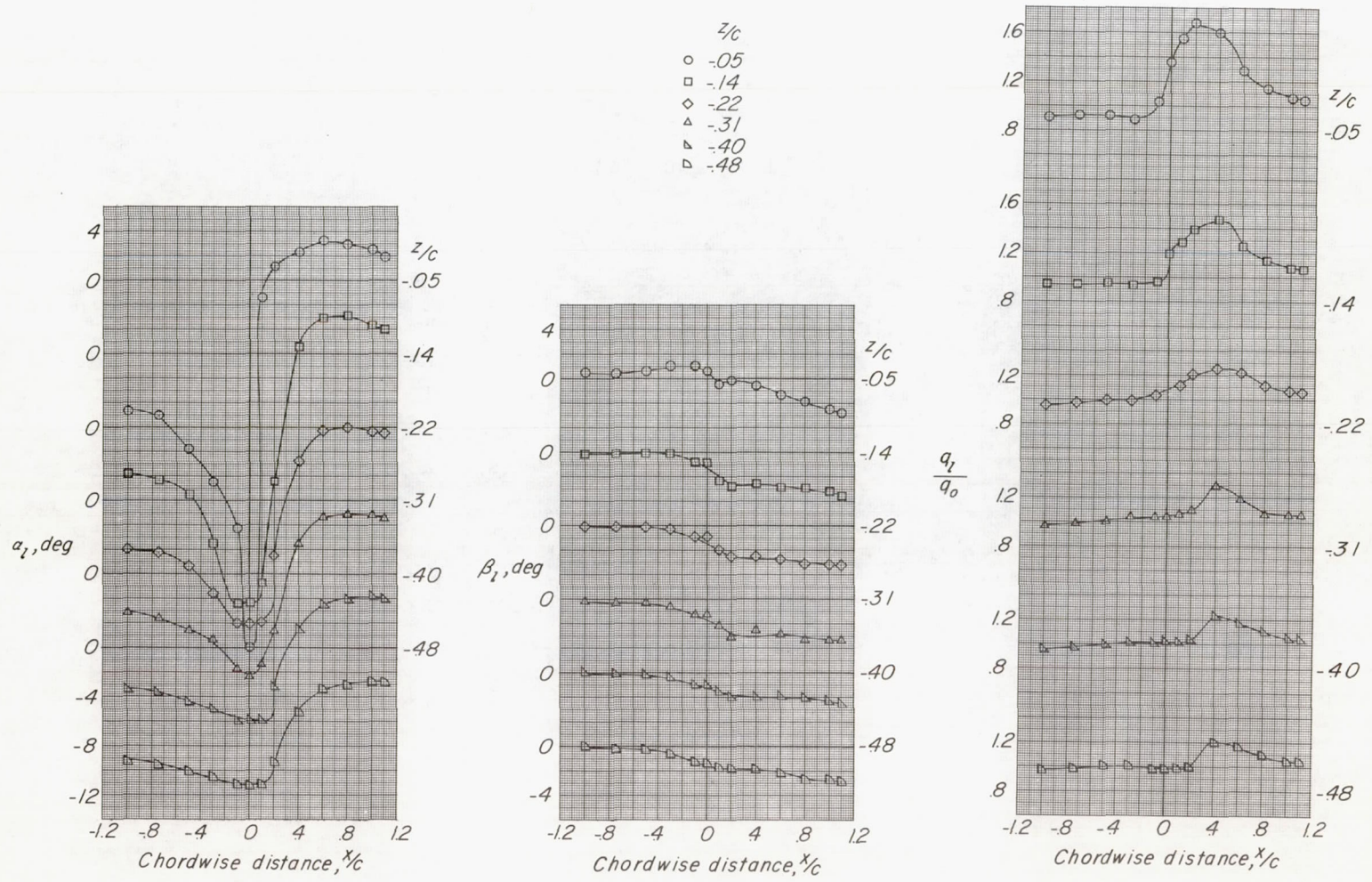

(a) $\alpha = -8.4^\circ$.

Figure 12.- Flow-field characteristics of unswept-wing—fuselage combination at $y/\frac{b}{2} = -0.50$.

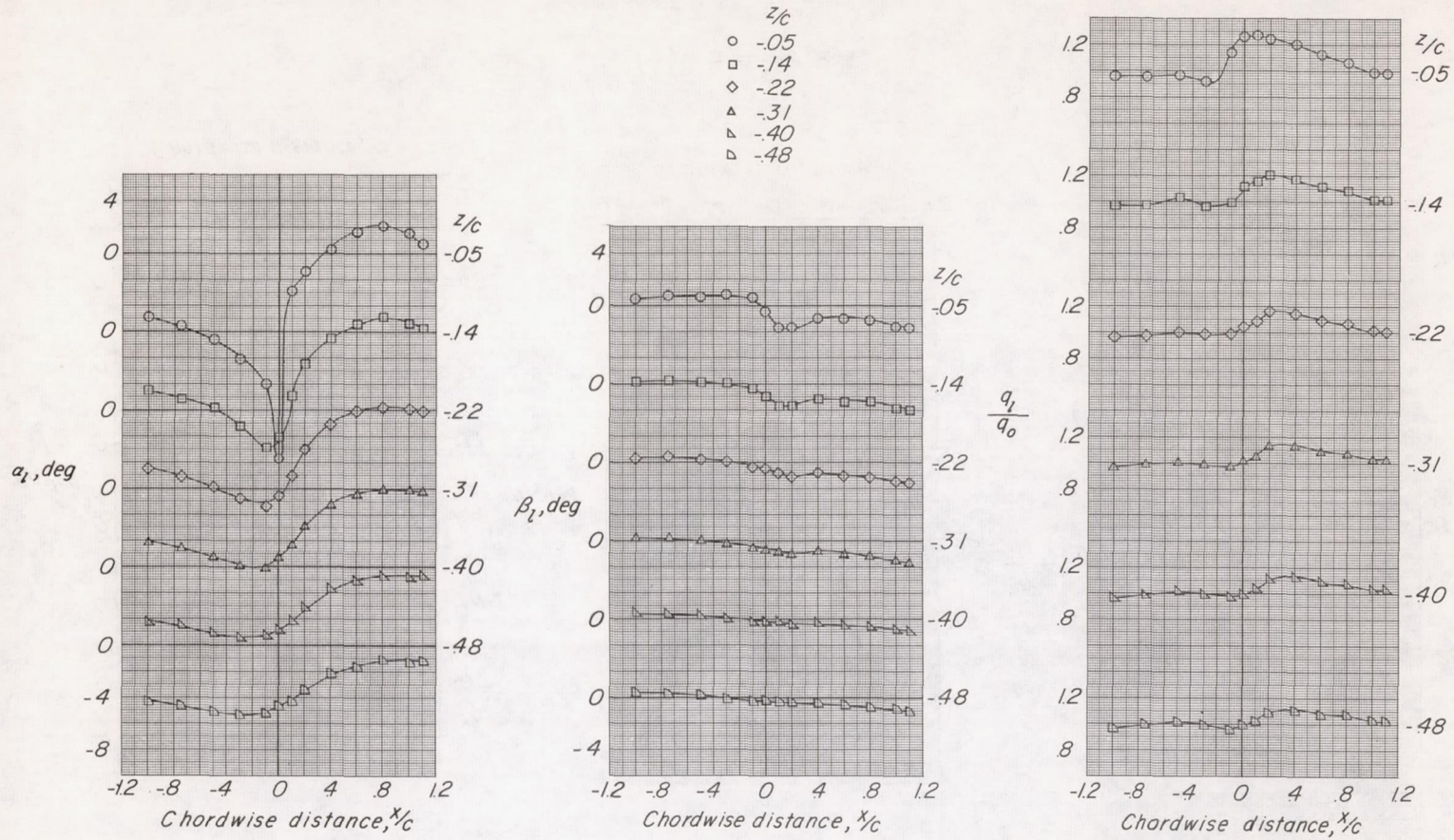

(b) $\alpha = -4.3^{\circ}$.

Figure 12.- Continued.

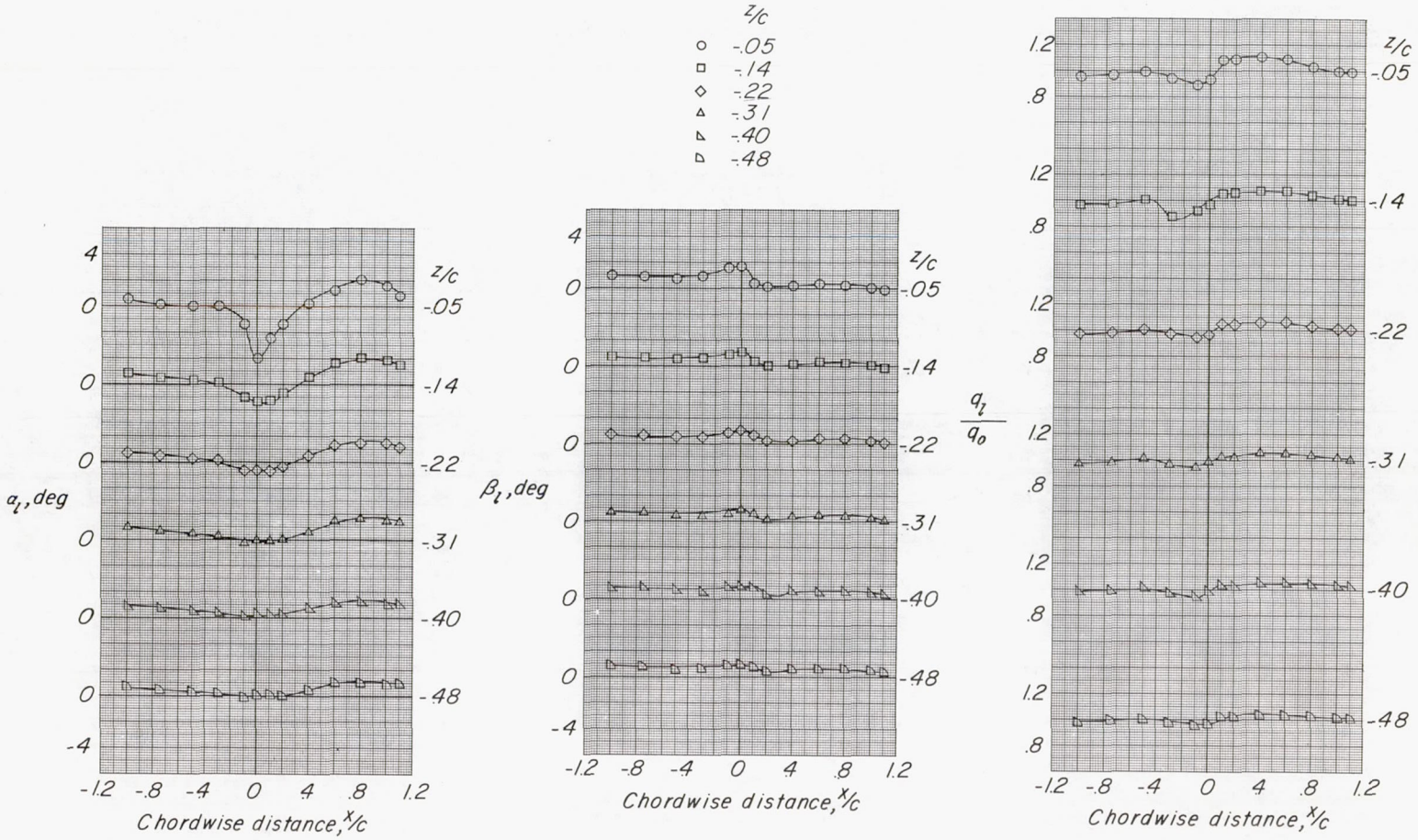

(c) $\alpha = -0.2^{\circ}$.

Figure 12.- Continued.

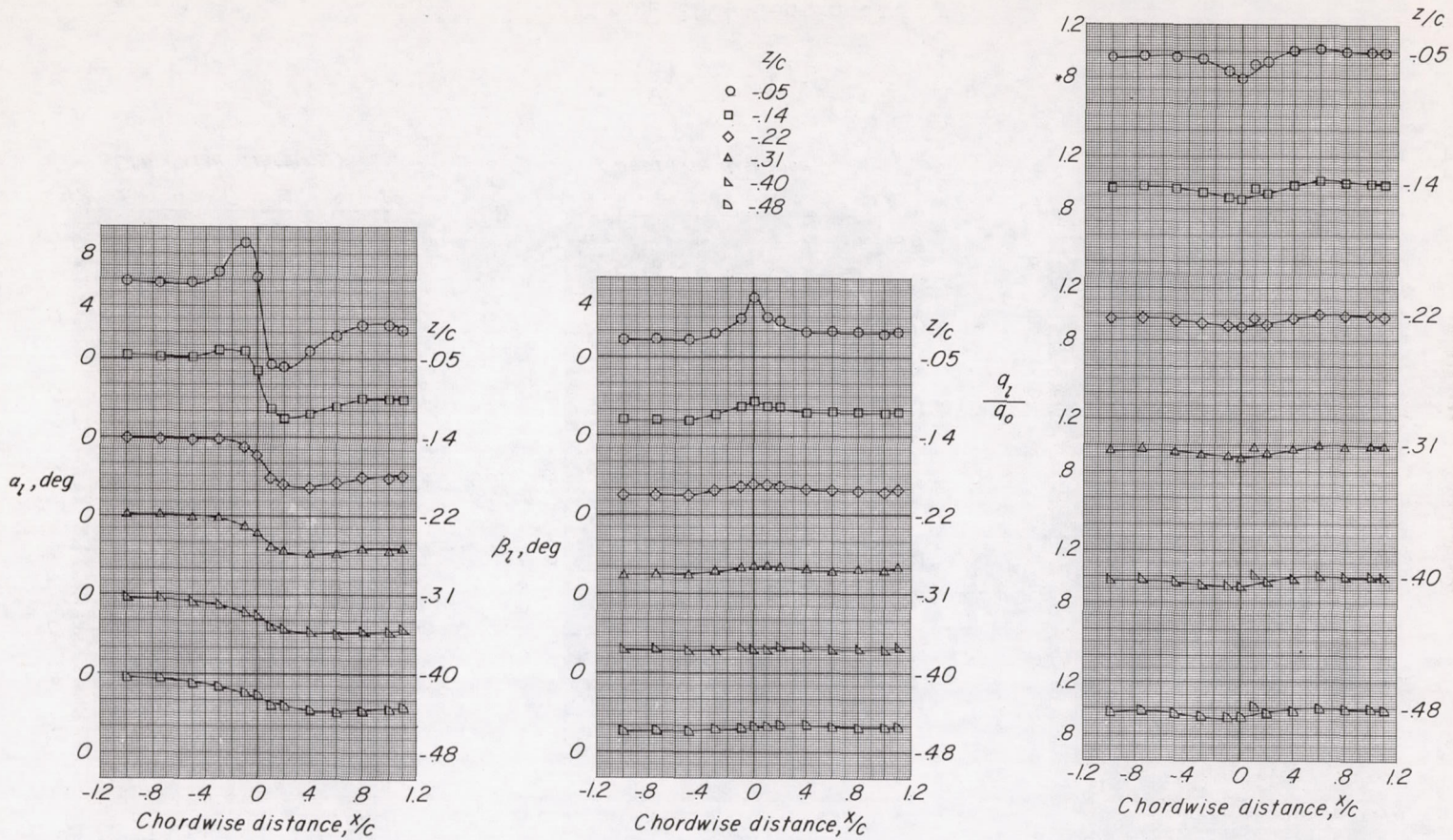

(d) $\alpha = 3.8^{\circ}$.

Figure 12.- Continued.

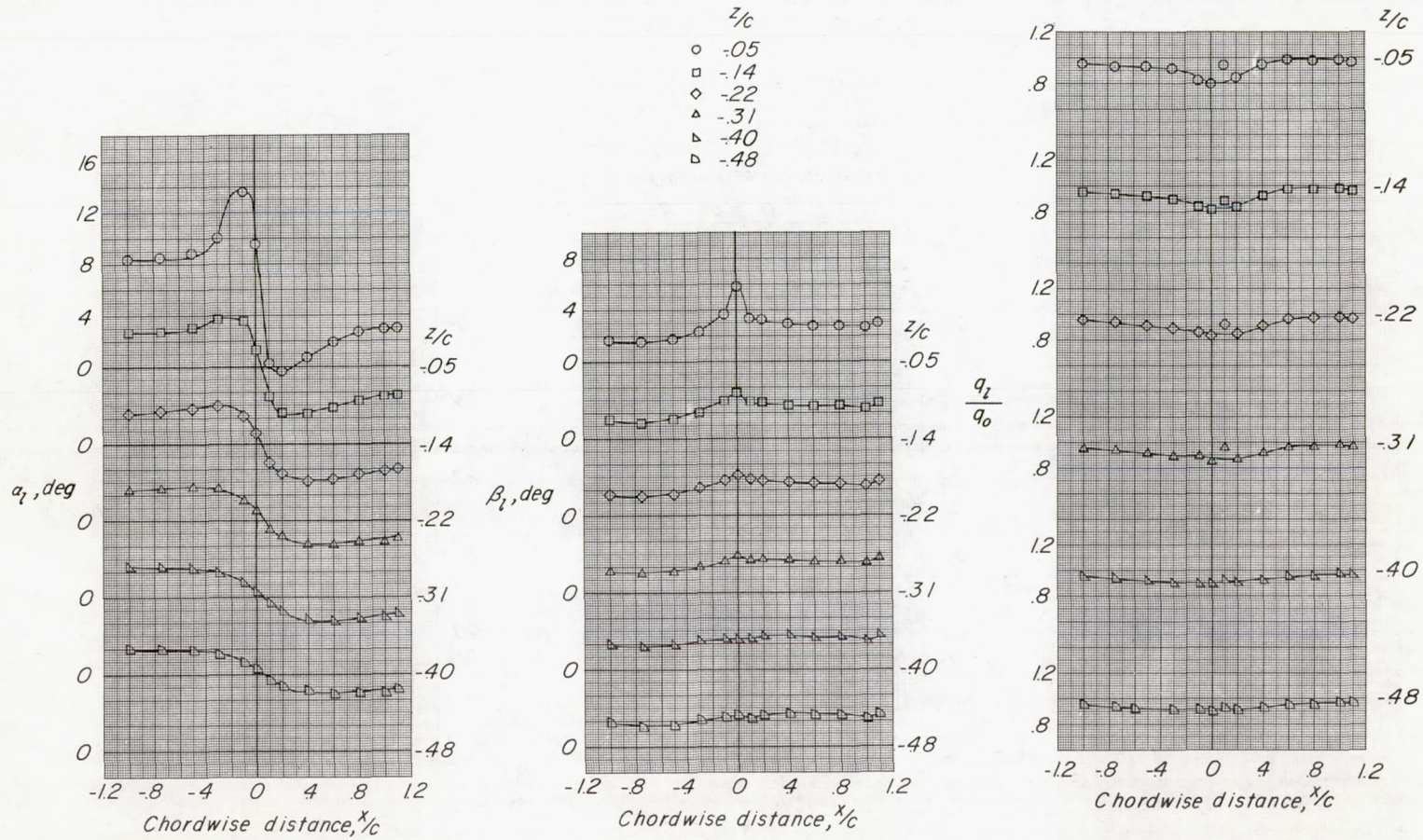

(e) $\alpha = 6.1^{\circ}$.

Figure 12.- Continued.

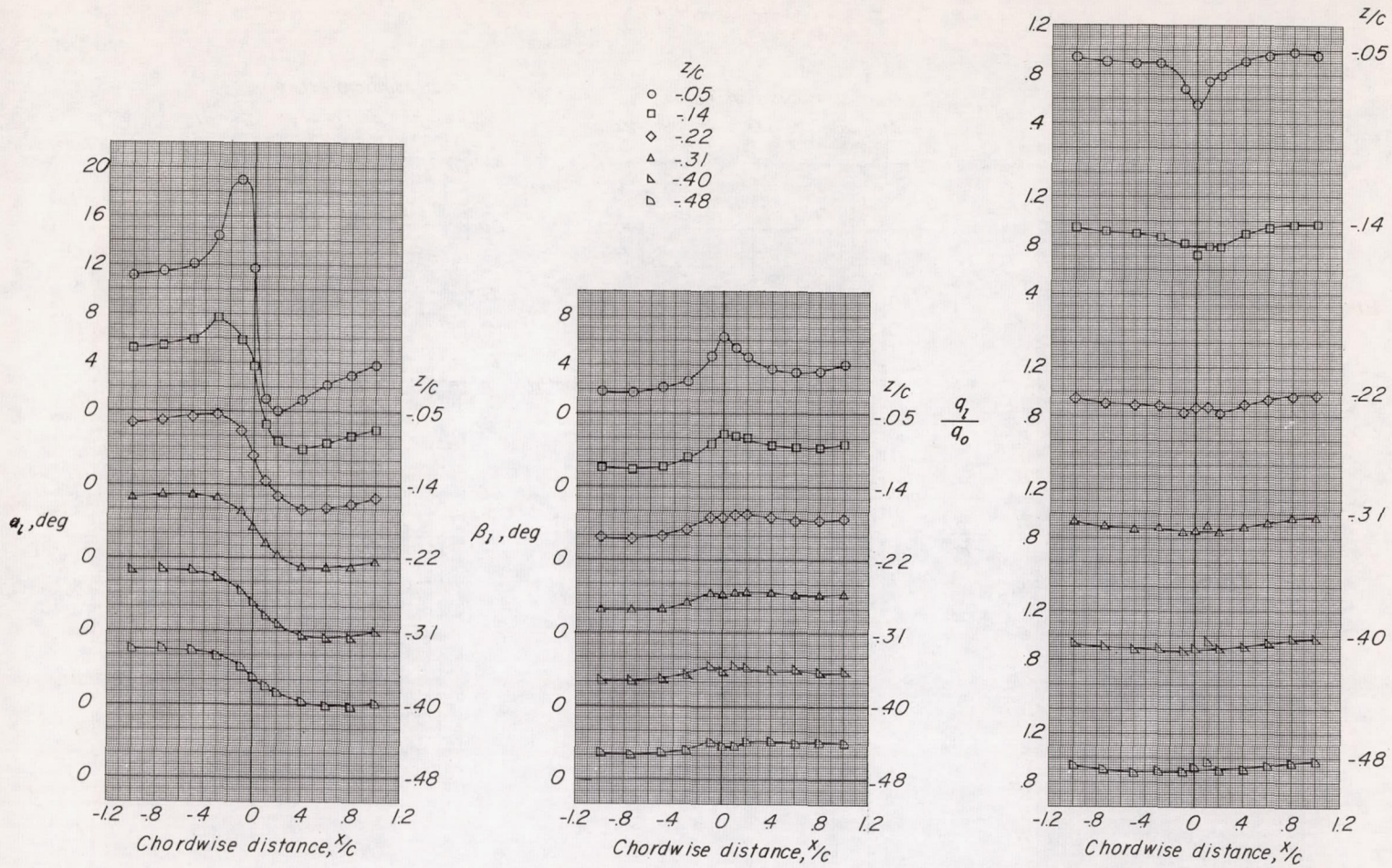

(f) $\alpha = 8.2^{\circ}$.

Figure 12.- Continued.

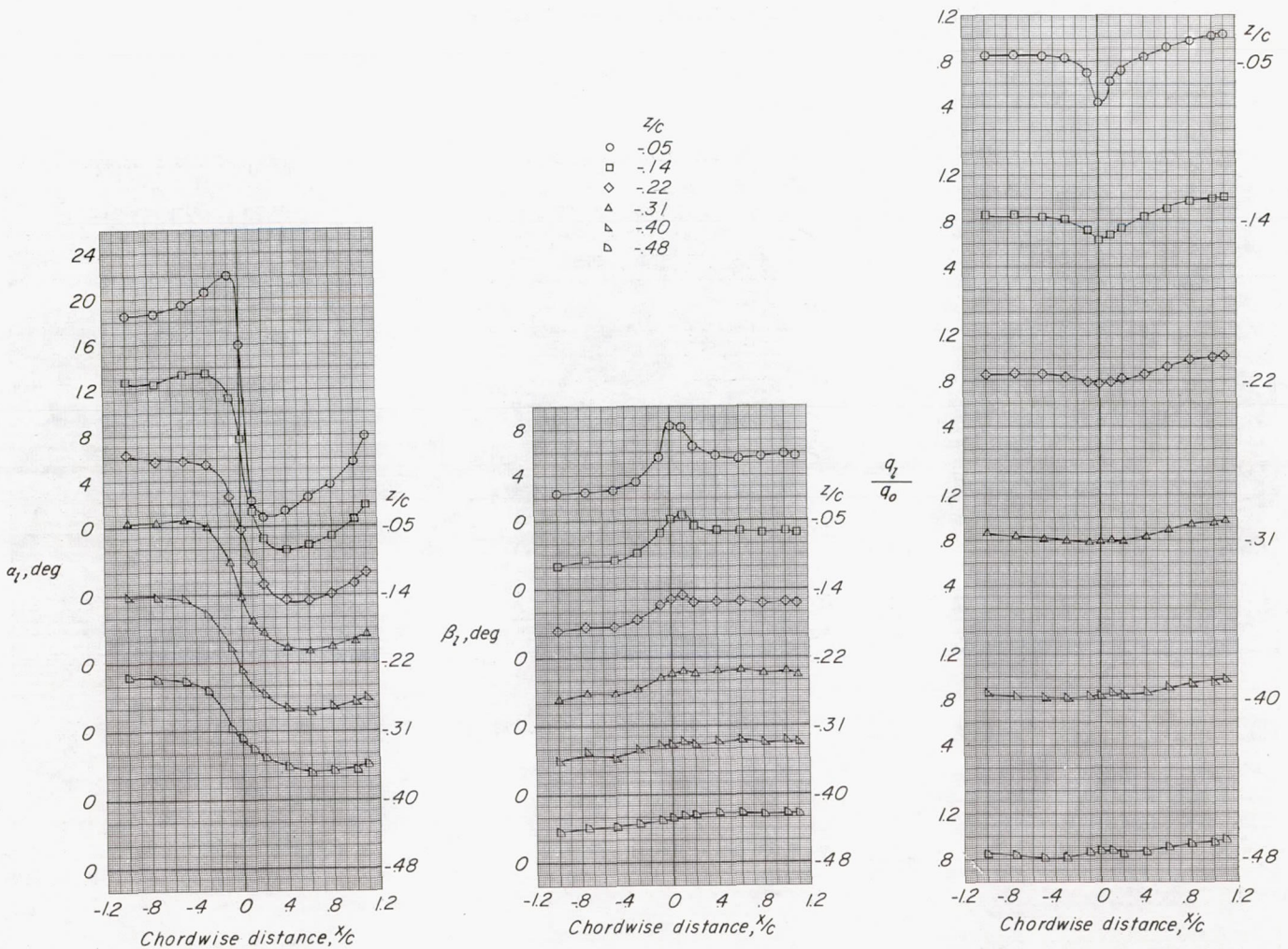

(g) $\alpha = 12.3^{\circ}$.

Figure 12.- Continued.

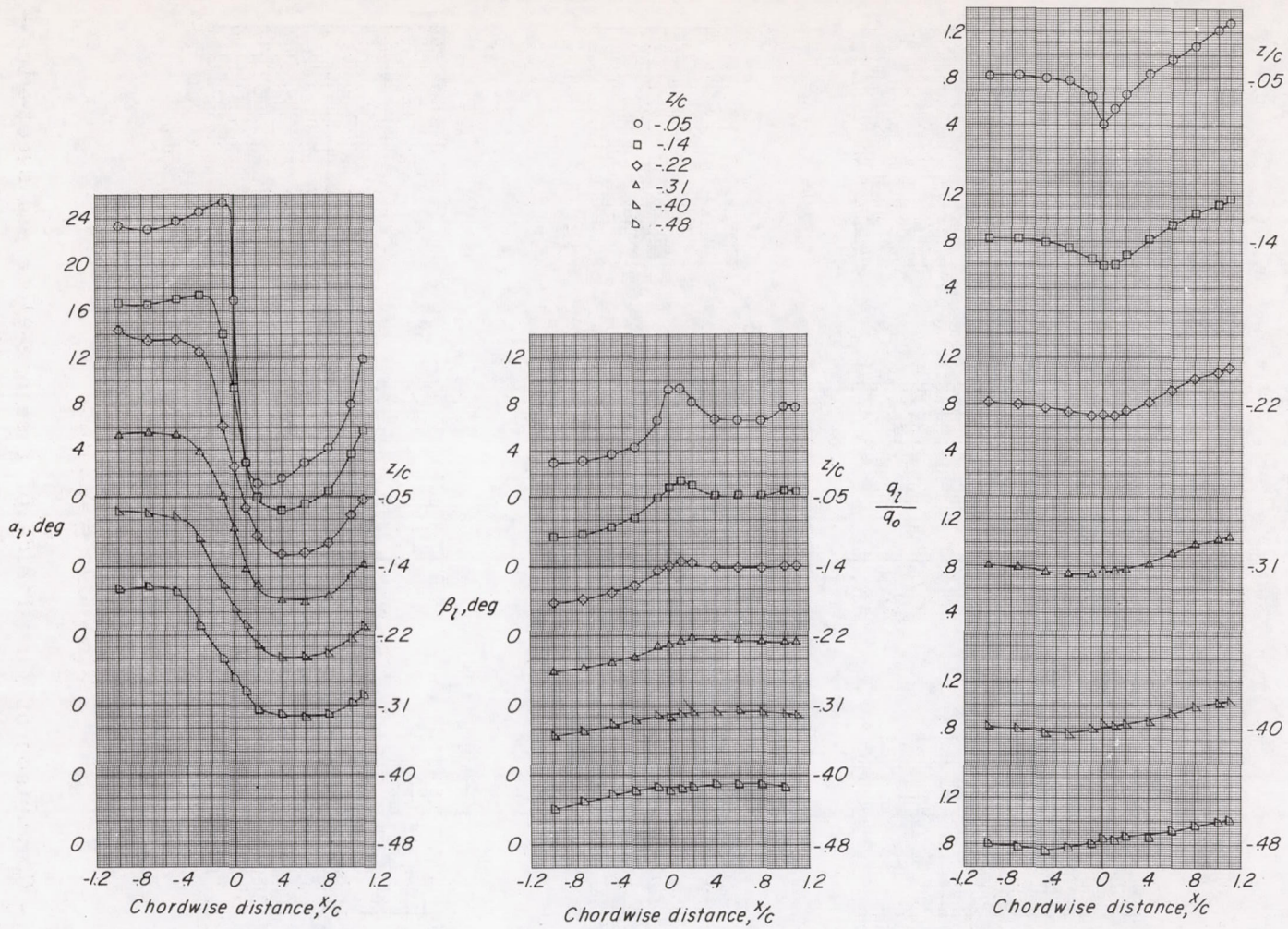

(h) $\alpha = 16.4^{\circ}$.

Figure 12.- Concluded.

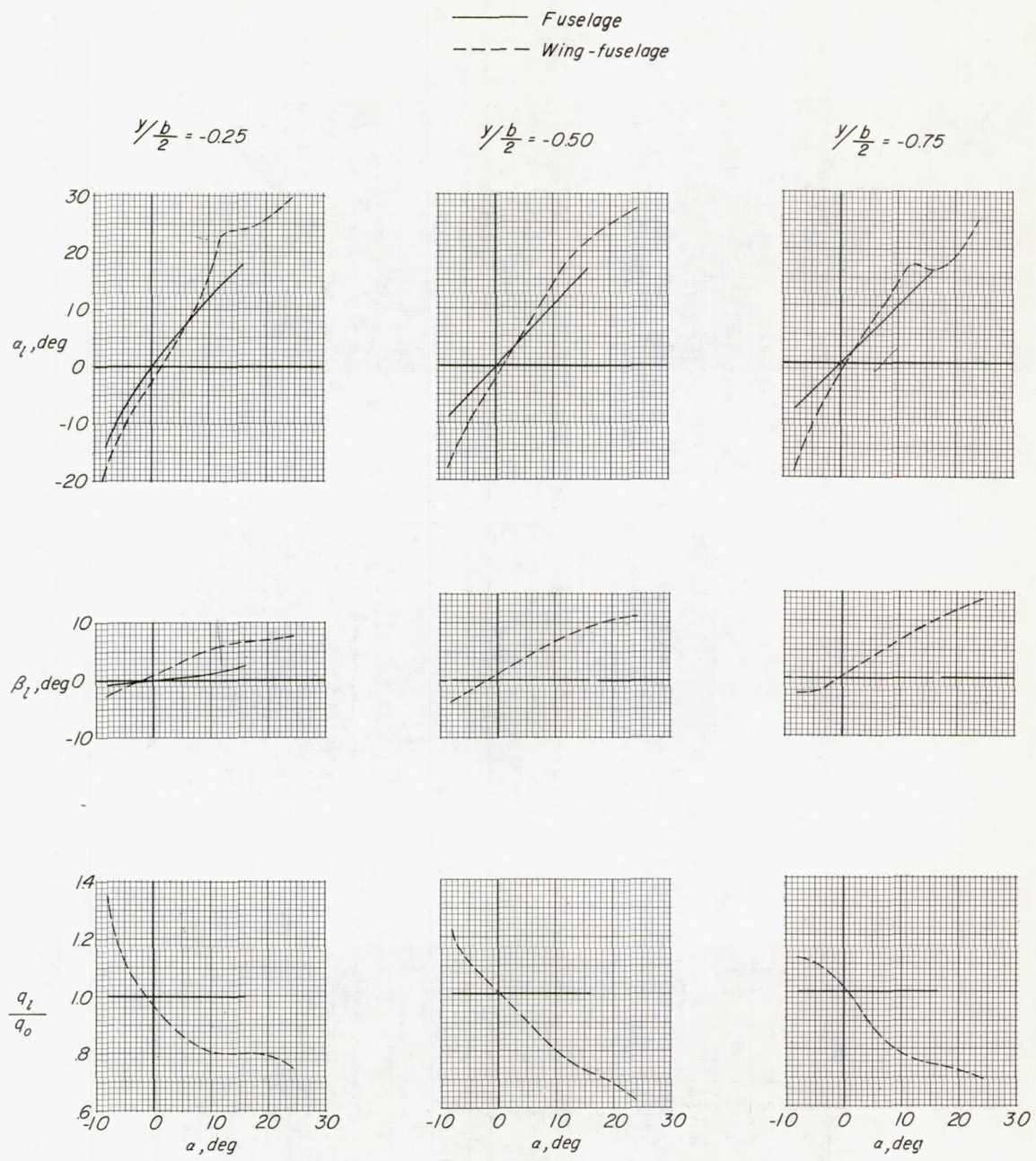

(a) x/c = -0.10.

Figure 13.- Comparison of flow-fields of fuselage-alone and swept-wing—fuselage combination; $z/\frac{b}{2} = -0.085$.

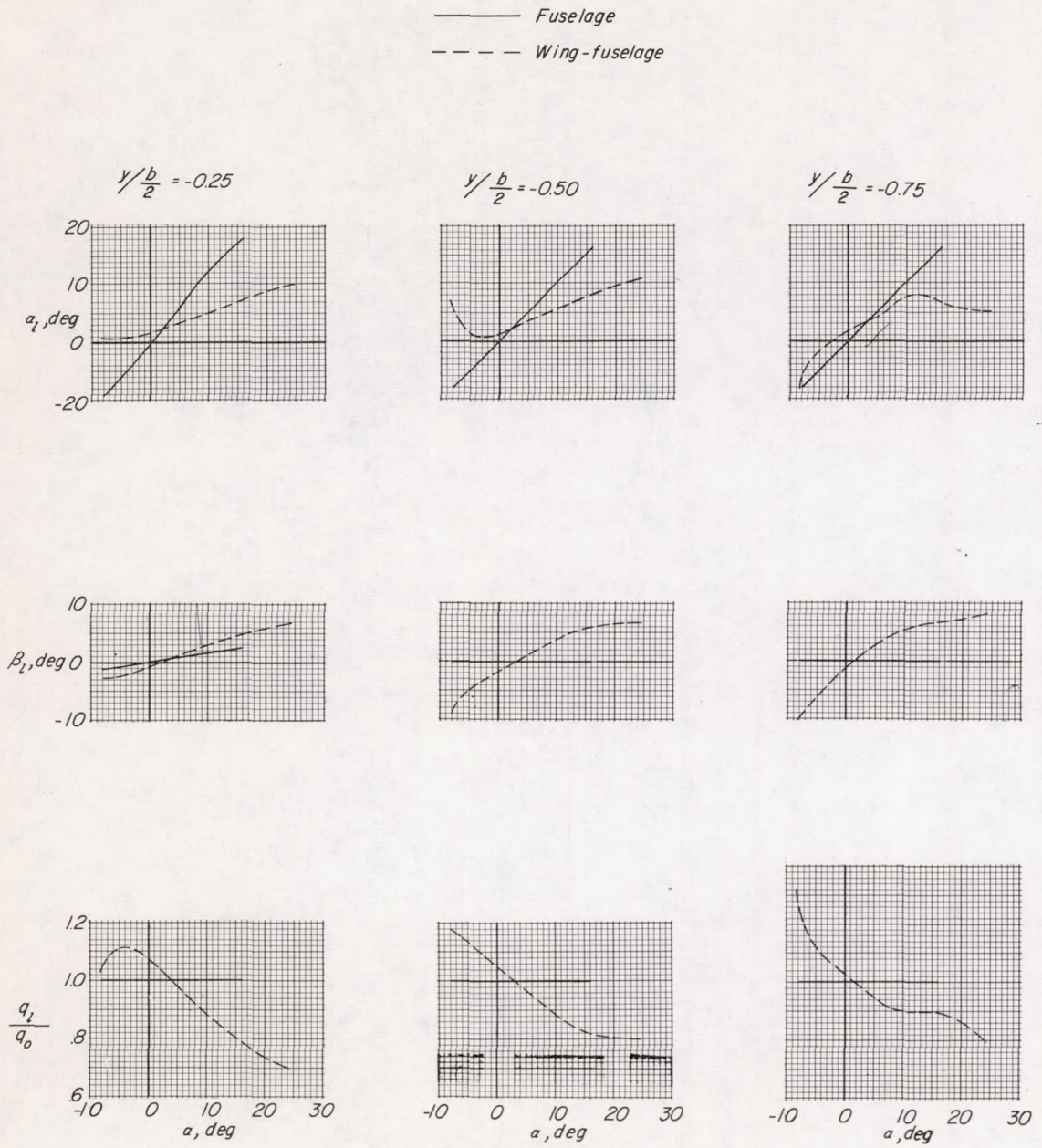

(b) x/c = 0.60.

Figure 13.- Concluded.